CLASSIFICATION OF HUMAN MOTION USING RADAR MICRO-DOPPLER SIGNATURES WITH HIDDEN MARKOV MODELS

A THESIS SUBMITTED TO
THE GRADUATE SCHOOL OF NATURAL AND APPLIED SCIENCES
OF
MIDDLE EAST TECHNICAL UNIVERSITY

BY

MEHMET ONUR PADAR

IN PARTIAL FULLFILLMENT OF THE REQUIREMENTS
FOR
THE DEGREE OF MASTER OF SCIENCE
IN
ELECTRICAL AND ELECTRONICS ENGINEERING

APRIL 2016

Approval of the thesis:

CLASSIFICATION OF HUMAN MOTION USING RADAR MICRO-DOPPLER SIGNATURES WITH HIDDEN MARKOV MODELS

submitted by **MEHMET ONUR PADAR** in partial fulfillment of the requirements for the degree of **Master of Science in Electrical and Electronics Engineering Department, Middle East Technical University** by,

Prof. Dr. Gülbin Dural Ünver
Dean, **Graduate School of Natural and Applied Sciences** _____

Prof. Dr. Gönül Turhan Sayan
Head of Department, **Electrical and Electronics Engineering** _____

Prof. Dr. Çağatay Candan
Supervisor, **Electrical and Electronics Engineering Dept., METU** _____

Examining Committee Members:

Prof. Dr. Sencer Koç
Electrical and Electronics Engineering Dept., METU _____

Prof. Dr. Çağatay Candan
Electrical and Electronics Engineering Dept., METU _____

Assoc. Prof. Dr. Umut Orguner
Electrical and Electronics Engineering Dept., METU _____

Assist. Prof. Dr. Sevinç Figen Öktem
Electrical and Electronics Engineering Dept., METU _____

Assist. Prof. Dr. Sevgi Zübeyde Gürbüz
Electrical and Electronics Engineering Dept., TOBB ETU _____

Date: _____

I hereby declare that all information in this document has been obtained and presented in accordance with academic rules and ethical conduct. I also declare that, as required by these rules and conduct, I have fully cited and referenced all material and results that are not original to this work.

Name, Last name : Mehmet Onur Padar

Signature :

ABSTRACT

CLASSIFICATION OF HUMAN MOTION USING RADAR MICRO-DOPPLER SIGNATURES WITH HIDDEN MARKOV MODELS

Padar, Mehmet Onur

M. S., Department of Electrical and Electronics Engineering

Supervisor: Prof. Dr. Çağatay Candan

April 2016, 116 pages

The detection and classification of a moving person is one of the important missions of a ground surveillance radar. Classification information gives the opportunity of announcing a warning message on the suspicious activity of detected person. The studies show that radar micro-Doppler signatures can be used to obtain the needed features to make the classification of different types of human motions. In general, spectrograms of micro-Doppler signals obtained from human in motion are used to analyze the necessary features to understand the type of the motion. However, most of the feature extraction methods are based on some image processing techniques on the spectrogram of the micro-Doppler signal that is the spectrogram is interpreted as an image. In this study, principal component analysis (PCA) is proposed to be used as a data-driven feature extraction method in order to capture time-varying information of the signal with a reduced dimension. Moreover, hidden Markov

models are used in classification to statistically track the time varying features of the micro-Doppler return signal. The experiments conducted during the study reveal that it is possible to make the classification of four different types of motions, namely walking, running, creeping and crawling, with a very high accuracy when training and test data sets are formed by different recordings of the same people. In addition, 90% accuracy is obtained when training and test data sets are formed by different recordings of different people.

Keywords: Micro-Doppler Signatures, Human Movement Classification, Feature Extraction, Principal Component Analysis, Hidden Markov Model.

ÖZ

İNSAN HAREKETLERİNİN RADAR MİKRO-DOPPLER İMZALARI VE GİZLİ MARKOV MODELLERİ İLE SINIFLANDIRILMASI

Padar, Mehmet Onur

Yüksek Lisans, Elektrik Elektronik Mühendisliği Bölümü

Tez Yöneticisi: Prof. Dr. Çağatay Candan

Nisan 2016, 116 sayfa

Hareket halindeki insanların tespiti kara gözetleme radarlarının en önemli görevlerinden biridir. Bununla birlikte, tespit edilen insanın yaptığı hareketin çeşidi ile ilgili bilgi üretebilme yeteneği de yine kara gözetleme radarları için önemli bir özelliktir. Hareket çeşidi bilgisi ile radar operatörlerine şüpheli insan hareketlerinin gözlenebilmesi imkanı tanınabilmektedir. Literatürdeki çalışmalar insan hareketlerinin sınıflandırılması konusunda çıkarılması gerekli öznitelikler için micro-Doppler imzaların kullanılabildiğini göstermektedir. Bu çalışmalarda, insan hareketlerinin ayrıştırılabilmesi için gerekli özniteliklerin analiz edilmesinde, genellikle micro-Doppler sinyallerin spektrogramı kullanılmaktadır. Ancak, bir çok öznitelik çıkarım çalışmalarında görüntü işleme teknikleriyle micro-Doppler sinyallerin spektrogramları incelenmektedir. Bu çalışmada, sinyal üzerindeki en önemli varyasyonların kapsanması ve çalışma boyutunun düşürülmesi için öznitelik çıkarım metodu olarak ana unsur analizi (PCA) kullanılmaktadır, Ayrıca, insan

hareketlerinin sınıflandırılması için sinyallerin anlık ve zamanla değişken özniteliklerini istatistiksel olarak modelleyen gizli Markov modelleri önerilmektedir. Çalışma boyunca yapılan deneyler göstermiştir ki, eğitim ve test veri serilerinin aynı insanların farklı kayıtlarından oluştuğu durumlarda insan hareketleri çok yüksek doğrulukla sınıflandırılabilmektedir. Bu çalışma kapsamında ayrıştırılan hareket çeşitleri, koşma, yürüme, emekleme ve sürünmedir. Buna ek olarak, eğitim ve test veri serilerinin farklı insanların farklı kayıtlarından oluştuğu durumlarda ise insan hareketleri % 90 başarı oranı ile sınıflandırılabildiği görülmüştür.

Anahtar Kelimeler: Mikro Doppler İmza, İnsan Hareketi Sınıflandırması, Öznitelik Çıkarımı, Ana Parça Analizi, Gizli Markov Modelleri.

To my beloved family and dear friends...

ACKNOWLEDGEMENTS

I would like to express that it was a great opportunity for me to study with Prof. Dr. Çağatay Candan and Dr. Ali Erdem Ertan (my unofficial co-advisor) during this study to improve myself in the sense of micro-Doppler signal processing on radar applications. I am grateful them for their very important guidance and enormous encouragements to me to complete the study.

Dr. Ali Erdem Ertan studied with me as playing a key role by advising new and unique ideas to solve the problems in the thesis. Although he was my co-advisor at the beginning of the thesis process, I could not officially state him as my co-advisor because of the new regulations. Still, he continued to motivate and help me a lot, as more than a co-advisor. I would like to express my endless gratitude to him hereby.

I would like to thank to my beloved family members, my mother Güngör Padar and my father Taner Padar for their continuous support during the period of study.

I would like to express my gratitude to my dear friends who helped me a lot to concentrate on my study both mentally and physically, Buse Altay, Anıl Karabeyli, Emre Koç, Ilgaz Kocatürk, Emrah Sekreter, İsmail Gökhan Dere, Gülesin Eren.

Finally, I would like to thank to TÜBİTAK and my company ASELSAN Inc. for the equipments and facilities I was provided with and my manager Yusuf Bora Kartal for his continuous support.

TABLE OF CONTENTS

LIST OF TABLES

TABLES

LIST OF FIGURES

FIGURES

LIST OF ABBREVIATIONS

HMM	:	HIDDEN MARKOV MODEL
STFT	:	SHORT TIME FOURIER TRANSFORM
FT	:	FOURIER TRANSFORM
RADAR	:	RADIO DETECTION AND RANGING
LADAR	:	LASER DETECTION AND RANGING
PRI	:	PULSE REPETITION INTERVAL
PRF	:	PULSE REPETITION FREQUENCY
PW	:	PULSE WIDTH
FMCW	:	FREQUENCY MODULATED CONTINUOUS WAVE
CPI	:	COHERENT PROCESSING INTERVAL
GSR	:	GROUND SURVEILLANCE RADAR
PCA	:	PRINCIPAL COMPONENT ANALYSIS
ANN	:	ARTIFICIAL NEURAL NETWORK
SVM	:	SUPPORT VECTOR MACHINE
GMM	:	GAUSSIAN MIXTURE MODEL
DTW	:	DYNAMIC TIME WARPING
K-NN	:	K NEAREST NEIGHBOR
DAC	:	DISCRIMINANT ANALYSIS CLASS
STSA	:	SYMBOLIC TIME SERIES ANALYSIS
MFCC	:	MEL-FREQUENCY CEPSTRAL COEFFICIENTS
LPC	:	LINEAR PREDICTION CODING
ML	:	MAXIMUM LIKELIHOOD
MV	:	MAJORITY VOTING
TVD	:	TIME VELOCITY DIAGRAM
CVD	:	CADENCE VELOCITY DIAGRAM

CHAPTER 1

INTRODUCTION

1.1 STATEMENT OF THE PROBLEM

Ground surveillance radars are widely used for both military and civilian purposes all around the world. These type of radars are able to detect pedestrians, light vehicles, tanks, convoys, Unmanned Aerial Vehicles (UAV) and low flying aircrafts. In addition, determining the motion type of the pedestrians (walking, running, creeping etc.) allows a law enforcement organization to observe suspicious activities remotely. Typical ground surveillance radars can work under almost all weather conditions and regardless of sunlight existence. This makes them crucial for surveillance activities.

Radar systems detect the targets by transmitting electromagnetic wave to the environment and processing the reflected signal from the target. Especially in coastal surveillance radars, cell-averaging constant false alarm rate (CA-CFAR) is applied to return signal obtained from a single pulse for target detection. In ground surveillance radars on the other hand, multiple pulses are transmitted within a CPI. The returned pulses are then processed together through a Doppler filter bank so that stationary clutter and targets in motion can be distinguished from each other. In addition, if the detected targets have moving or rotating parts, the reflected signal also has side frequency components around the main Doppler frequency. The signal with these time-varying frequency components are called as micro-Doppler signatures [2]. Since every type of motion has different mechanics, they also have distinct micro-Doppler signatures. Therefore, human motions can be classified by using the micro-Doppler signatures.

1.2 SCOPE OF THE THESIS

This thesis proposes a solution that is composed of data-driven feature extraction through principal component analysis (PCA) and stochastic modeling of instantaneous and time-varying variations in features through hidden Markov models (HMM). The motivation of choosing these methods is that Hidden Markov models is a stochastic modeling tool that can model the instantaneous and time-varying variations and variations across different people and needs a feature space as small as possible, and PCA is a data-driven approach that can capture most of the variations by reducing the workspace dimension. Four basic motions, walking, running, creeping and crawling are investigated for classification purpose in this thesis.

Since HMM models the time-varying nature of events in the signal, the features should be extracted by processing the signal frame-by-frame periodically. Moreover, it is important to reduce the dimension of the workspace to model the features, since smaller the feature space allows finding related statistics of the features more accurately from training data. In addition, the extracted features are desired to be uncorrelated to make the parameters in the model independent so that probability density functions can be modeled separately, which makes training of the system easier. Principal component analysis (PCA) is a feature extraction method that satisfies these objectives. In addition to feature selection, selecting the size of frame size from which features are estimated is also important. The frame should be as long as possible for having the best possible frequency resolution. On the other hand, the length should be selected such that the signal within the frame is always stationary.

The first step in this thesis is therefore to determine an optimal analysis window length. When a signal is processed by a linear transformation technique such as Fourier transform, it is assumed that the signal is stationary inside the analysis window. However, when the signal is not stationary during the analysis window, sharp frequency and magnitude variations in individual frequency components cause these frequency components smear into multiple frequency bins. Therefore, the analysis window length should also be short enough in order to make the signal stationary inside the frame. On the other hand, analysis window length is desired to

be as long as possible in order to have good frequency resolution. It is possible to observe all frequency components independently only when the frequency resolution is sufficient. Therefore, determination of analysis window length, which provides enough frequency resolution and does not cause frequency smearing for four types of motions investigated in this thesis, is studied in the first step of this thesis.

The four different human motions are modeled by hidden Markov models (HMM). However, the features used with HMM should satisfy two important properties for better and easier statistical modeling: The features should be uncorrelated so that they carry no redundant information for statistical modeling and the dimension should be as small as possible in order to reliably generate the joint probability density functions from a finite training data set. In addition, uncorrelated feature set makes reducing the dimension of the features straightforward. Fourier transform coefficients, which are used to generate spectrograms (and used in image based motion classification techniques), do not have uncorrelatedness property. They both are correlated and have large dimension to retain all information. Therefore, finding a proper transformation that meets the need of HMM is the second step of the proposed work.

Since human motion is periodic, the reflected signal from a person has a cyclic nature. However, every person does not execute the same motion identically. There are small variations in the same motion between different people. This study aims to model the instantaneous and time-varying variations in the features of different motions stochastically. Therefore, hidden Markov models, which consist of a number of states, probability of observations belonging to states and transition probabilities from one state to another in two successive observations, are used to model the micro-Doppler signals of a particular motion. The third contribution of the thesis is the application of hidden Markov models for statistically modeling the motions and use of the models to classify a given continuous wave (CW) signal as one of the four different types of human motion.

1.3 ORGANIZATION OF THE THESIS

The thesis is composed of six chapters. In the first chapter, statement of the problem and the scope of the study are discussed.

In the second chapter, background information about Doppler effect in the radar echo signal and micro-Doppler signatures are given. A literature review is presented on studies about feature extraction from micro-Doppler signals and classification of different human motions by various techniques.

Third chapter presents the experiments to determine a suitable analysis window length. The computer experiments are conducted using Victor Chen's human walking simulator [2]. The simulator is modified so that it could generate data similar to those generated by the ground surveillance radar which are used for this thesis studies. It is used to determine the proper analysis window length to be used in the rest of this study. Determination of analysis window length is important since the signal inside the frame should be stationary for feature extraction. During this chapter, movement in every segment of the human body (torso, head, should, hand etc.) is examined separately to find a common appropriate window size.

The fourth chapter presents the method to extract the uncorrelated and low dimension features of the echo signal. Principal component analysis (PCA) is applied to training data in this step and eigenvectors that form a basis for the transformation are calculated. Since the eigenvectors with small eigenvalues capture only small variations in the signal, they can be omitted. Thus, keeping only the eigenvectors with largest eigenvalues allows to capture the largest variations and at the same time yielding dimension reduction. The time domain signal is then frame-by-frame transformed into feature space using the eigenvectors. The sequence of uncorrelated and low dimension features is then used as the input to be modeled with the parameters in hidden Markov models (HMM).

In the fifth chapter, feature sequences for motions in a training set are used to train the models for four different types of human motions by deciding on the number of hidden states, and calculating probabilities of observations belonging to each state,

initial state probabilities and state transition probabilities between states. Through this way, instantaneous and time-varying variations in the motion of different people are modeled uniquely for each class. Once the models are obtained, feature sequences obtained from the test data are evaluated by calculating the similarity between the input feature sequence and the four models. Then, the model with the largest similarity is chosen as the classification outcome of the input test data. The classification experiment is conducted for both human dependent and human independent cases whose results are presented in Chapter 5.

Conclusive remarks about the thesis are presented in the sixth chapter. By examining the results in the fifth chapter, feasibility of applying these techniques to a real radar system is discussed.

CHAPTER 2

BACKGROUND

In this chapter, background information about Doppler effect, micro-Doppler phenomenon, feature extraction and classification methods are given. At the end of the chapter, techniques in literature and proposed solution in this thesis are compared.

2.1 DOPPLER EFFECT IN RADAR

Radar (Radio Detection and Ranging) is a system that uses electromagnetic waves to detect and locate the targets [1]. It works by radiating electromagnetic waves over the space and collecting the reflected signal (echo) from the environment The reflected signal not only provides information about presence of a target, but also includes information about distance when a target is present, which is determined by the time delay between the time of transmission and time of reception of the echo from the target. If the detected target is in motion, there occurs a frequency shift in the echo of the target. This frequency shift is called as "Doppler effect". As shown in [1], if we designate the distance from the radar to the target with R and wavelength of the electromagnetic wave with λ, the total number of wavelengths from the radar to the target and all the way back is $2R/\lambda$. If the target is not moving, the total number of angular excursion becomes $4\pi R/\lambda$ radians. However, when the targets detected by radar systems are in motion, the distance between the radar and the target, R, and phase of the returned signal, ϕ, changes while the targets is in motion. The change in the phase of the echo with respect to time is called the angular Doppler frequency and is it designated by Ω_d. The relationship is shown with the equation below [1];

$$\Omega_d = 2\pi f_d = \frac{\mathrm{d}\phi}{\mathrm{dt}} = \frac{4\pi dR}{\lambda dt} = \frac{4\pi v_r}{\lambda} \quad (1)$$

where f_d is the Doppler frequency shift in Hz and v_r is the radial velocity of the target towards to the radar system. After simplifying (1), the Doppler frequency shift can simply be obtained as;

$$f_d = \frac{2v_r}{\lambda} = \frac{2v_r f_0}{c} \quad (2)$$

where f_0 is the frequency of radar transmission and c is the velocity of electromagnetic wave propagation, which is approximately 3 x 10^8 m/sec. As it can easily be seen from the equations above, the Doppler frequency shift increases as the radial velocity of the target increases. In addition, if the frequency of transmission increases than the Doppler frequency shift increases as well.

2.2 RADAR MICRO-DOPPLER SIGNATURES

As in explained in Section 2.1, a moving subject generates a Doppler effect on the received signal whose frequency can be calculated from the difference between the frequencies of the transmitted signal and the received target echo. When the target has multiple moving parts, the return signal contains return from all parts of the target with different RCS and Doppler frequencies. Therefore, the targets with moving, vibrating or rotating parts cannot be considered as a single point target, which can have only a single Doppler component. In this case, several joints moving in coordination with the main target results in additional side frequency components around the main frequency shift. The research area that deals with analyzing the Doppler components in the signal is called micro-Doppler signal processing. Different types of motions lead different movements of body parts of the main target. Therefore, different motions result in different Doppler components. Summation of these Doppler frequency shifts and their change in time are called as the micro-Doppler signatures. As a result, different type of movements of a target with more than one moving parts generate different micro-Doppler signatures.

Micro-Doppler signal processing is still an active area of research. The studies show that different type of movement has different micro-Doppler signature in the frequency domain if the moving target has more than one moving parts [2], [3], [4]. The variations in micro-Doppler signatures for different movements are caused by variety of different motion, rotation or vibration of the joints of the main target [5], [6]. These movements and vibrations are a function of time; therefore, time-frequency analysis methods are often used to investigate such signals [4].

The micro-Doppler effect is first discussed in coherent laser radar systems [2]. These systems are called as LADAR (Laser detection and ranging) systems and use electromagnetic waves at optical frequencies. The reflected wave is received by the LADAR system in order to measure the range, velocity and other features by using the modulation in the laser beam. Amplitude, frequency, phase and polarization of the reflected signal are used for detecting the target. The target or any joint of the target illuminated by a LADAR (or a RADAR) system may have oscillatory motion. This motion is called as micro motion in [2]. Some examples for the oscillatory motion are rotating propeller of a fixed-wing aircraft, rotating rotor blades of a helicopter, rotating antenna of a radar and a walking person.

Chen examines the micro-Doppler effect in radar in [3]. Chen states that when a target is illuminated by a radar, it causes Doppler frequency shift in the return signal. If the illuminated target has micro motion dynamics like mechanical vibrations or rotations, these micro motion dynamics cause Doppler modulations on the returned signal. Chen calls these modulations as micro-Doppler effect around the main Doppler frequency [3]. An example of a micro-Doppler signature can be seen on Figure 1 as the spectrogram of the signal. Spectrogram is generated by taking short time Fourier transform of the time-domain signal inside an analysis window and computing the magnitude spectrum. The magnitude spectrum for each frame is then concatenated on time domain to complete forming the spectrogram. In the figure, the walking human body causes main Doppler frequency, and swinging and moving parts of the body cause micro-Doppler effect around the main Doppler shift.

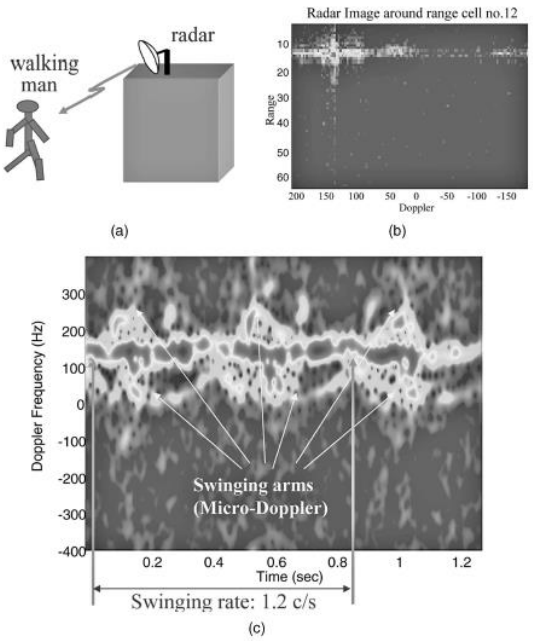

Figure 1: Micro-Doppler signature of a walking person in [3]

Chen in [4] explains that mechanical vibrating and rotating parts of a target can be used for target detection, classification and recognition. He states that moving, vibrating or rotating parts of the target cause micro-Doppler effect which changes in time. Doppler signature of the return signal can then be analyzed in joint time-frequency domain so that one can obtain useful information from the return signal for target detection, classification and recognition [4].

Micro-Doppler signature of the return signal can be observed in the frequency domain after taking the Fourier transform of the time domain signal [4]. Chen gives two reflectors example that can be seen on Figure 2. There are two reflectors away from the radar and while one of them is stable, the other one is vibrating. He shows the time-domain and Fourier domain signals in order to give insight into micro-Doppler effect. As can be seen from Figure 2, frequency component of the stable rotator is like a peak. However, frequency component of the vibrating rotator spreads in the range profile.

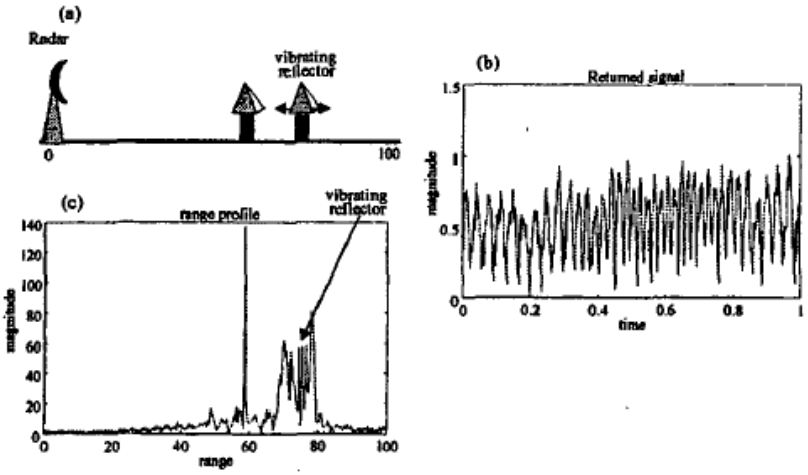

Figure 2: Micro-Doppler experiment: (a) Experiment setup, (b) time-domain return signal and (c) Fourier transform of the return signal [4]

Chen presents a brief analysis on micro-Doppler signature of human walk towards a radar system in [4]. He states that the main frequency component is generated by the motion of the whole body. He underlines that it is possible to observe the swinging arms effect by taking the time-frequency transform of the return signal. Since the arms are in opposite motion during walking motion, one arm has Doppler frequency below the main Doppler shift while the other has above [4]. The time-frequency transform of human walk can be seen on Figure 3.

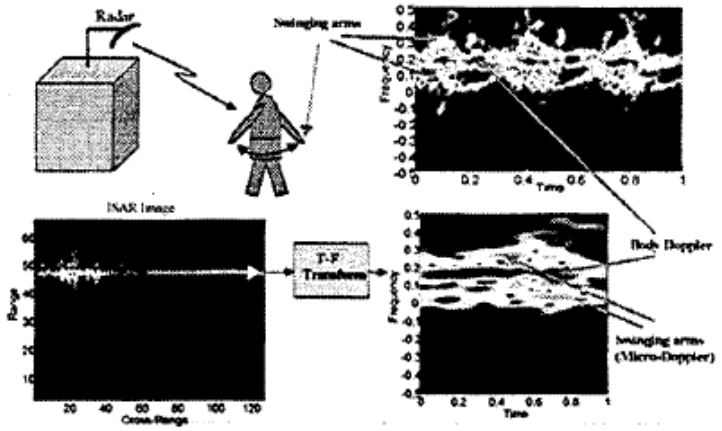

Figure 3: Micro-Doppler signature of a walking man with swinging arms [4]

The most comprehensive review in this research area is presented in [21]. The possible applications of micro-Doppler signal processing and possible sensor capabilities which can make use of micro Doppler signatures are summarized by Tahmoush. It is stated that air vehicle identification from micro-Doppler signatures is an important application since it can reduce the false alarms caused by birds by making classification between helicopters, UAVs, missiles and birds [21]. Birds are given as a confuser example for UAV detection and tracking. It is explained in the paper that it is possible to identify birds by using the Doppler spread of their wing flapping, which allows a system to distinguish between birds and UAVs. As another application, he discusses use of micro-Doppler signals for classification of human motion type. It is explained in [21] that every type of human motion has a different cyclic nature of gaits, and thus, has a different signature. So one can classify the human motions by using their micro-Doppler signatures. The most important use of this application is in border surveillance radars as animals can be an important source of false alarms. In particular, quadrupeds should be distinguished from humans in order to eliminate such false alarms. Micro-Doppler signatures can be used to solve this problem as well [21]. Another area micro-Doppler signatures can be used is health area. It is possible to observe and measure vital signs like heart-beat rate, pulse rate and breathing rate by processing the micro-Doppler returns. Finally, micro-Doppler signatures can be used with the through-the-wall radars for human detection. He states that, especially with low transmission frequencies, it is possible to detect humans beyond the wall by processing the micro-Doppler signatures of return signals. Tahmoush also proposes that the classification results can be improved by using multi-static radar sensors which would eliminate the problem with perpendicular aspect angle in which the Doppler signatures almost vanish [21].

2.3 FEATURE EXTRACTION AND CLASSIFICATION OF MICRO-DOPPLER SIGNATURES

There are two important steps for a recognition system; feature extraction and classification. The most desirable property of a feature space is to provide distinction among the classes, while a classifier is desired to easily differentiate between classes

by dividing the feature space for different classes properly. Therefore, selection of these two methods is very important in a classification system. It is possible to find a number of studies in the literature about Micro-Doppler signal processing in which features extraction and classification methods are discussed. In this section, a literature survey about human motion classification using micro-Doppler signatures will be presented.

Tahmoush examines the micro-Doppler signals obtained from a human in motion at long range for the purpose of target detection, target tracking and gait analysis. In his experiments, he uses indoor-recorded data, collected with a person moving towards the radar with zero degree aspect angle. Figure 4 presents the spectrogram of this motion, which is obtained by the short time Fourier transform of frames obtained from the radar return signal in regular intervals and by concatenating the magnitude spectrum of each frame. Tahmoush uses the stride rate as the feature for gait classification. The stride rate is extracted from the radar return signal in five steps: Target detection and range gating, clutter removal, torso detection in the spectrogram, eliminating everything in spectrogram except torso (torso filtering) and peak period extraction via Fourier transform of torso signature that gives the stride rate[6]. Torso line used for stride rate extraction can also be seen on the Figure 4. Figure 5 shows an example of stride rate from human walk. He uses this feature for motion classification in the article.

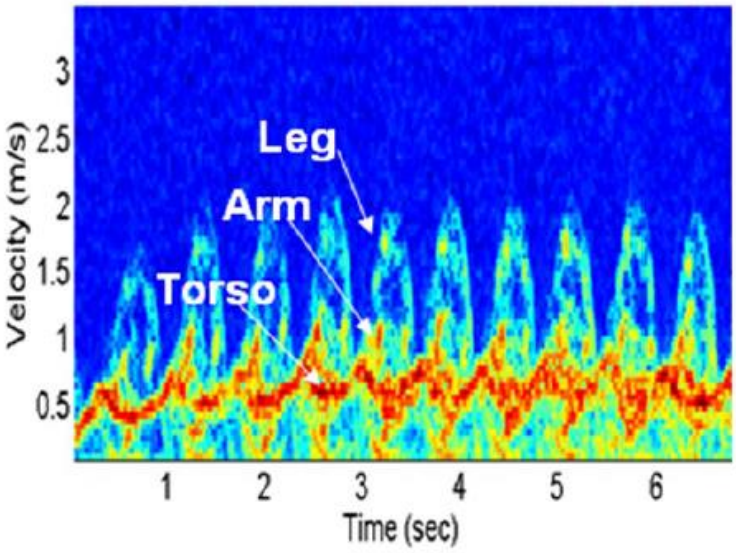

Figure 4: Measured Doppler motions of a walking man [6]

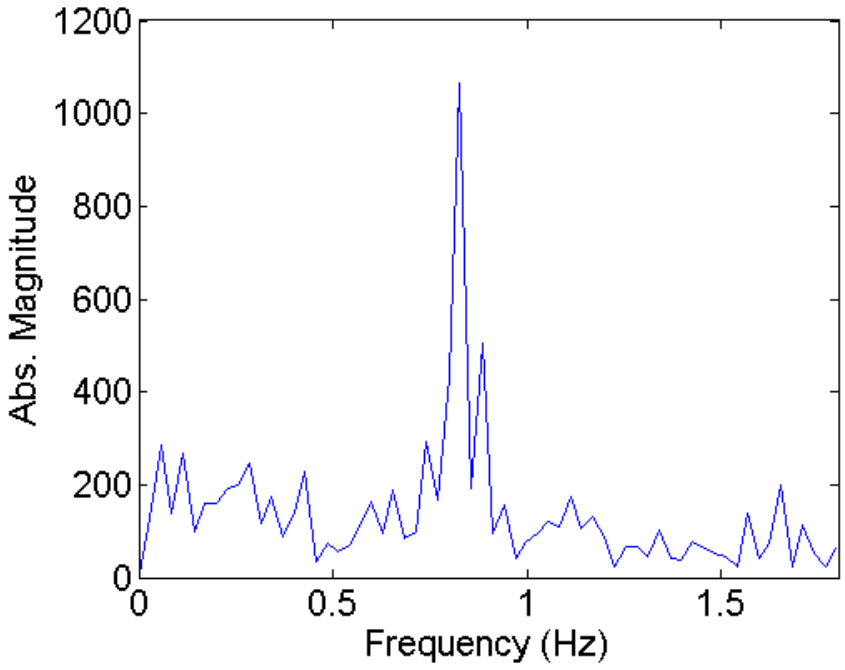

Figure 5: Stride rate extracted from the filtered torso line [6]

In another study, Otero uses a continuous wave (CW) radar in order to analyze the micro-Doppler signatures of walking human motion for detection and classification purposes [7]. Otero uses cadence frequency of legs, stride length and RCS ratio between appendage and torso as the features for classification purposes. He makes

the spectral analysis of the spectrogram so that it can be possible to obtain gait harmonics and signal strengths reflected from different parts of the body. In order to do that, he takes the Fourier transform of the spectrogram along time axis. The result can be seen in Figure 6 as spectral analysis of the spectrogram. The fundamental gait cadence in Figure 6 represents the cadence frequency of legs as the first feature. Second, torso velocity is obtained from Figure 6 and stride length is calculated by dividing the torso velocity to cadence frequency of the legs. Third, the ratio between appendage and torso is calculated by dividing the amplitude of the torso peak to the summation of amplitudes of the other harmonics [7], which can be seen on Figure 6. A simple binary classifier whose class limits for features are determined by Otero is used to make the decision about presence of a human. It is stated in the article that the decision can be made by 88% success rate.

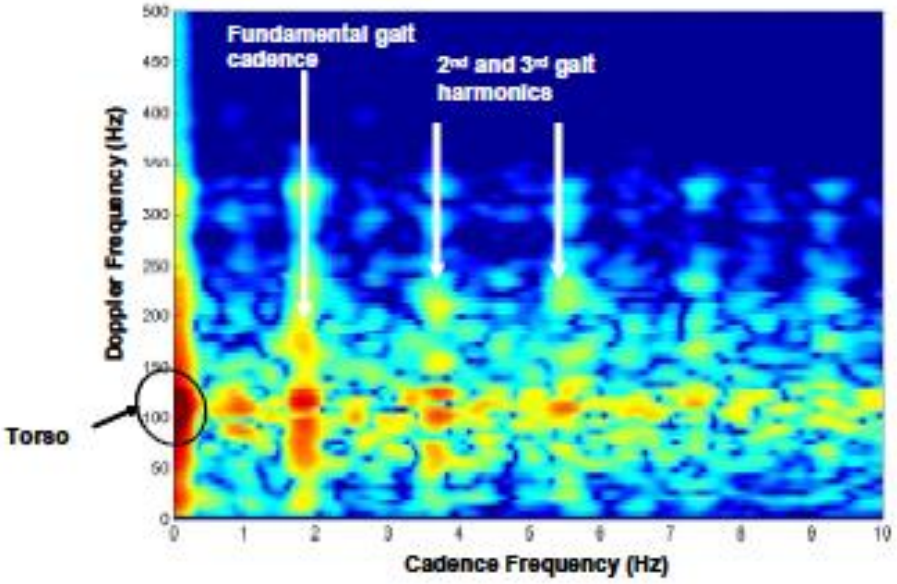

Figure 6: Spectral analysis of the spectrogram [7]

Vignaud explains in [8] that micro-Doppler effects are observed as sidebands around the main Doppler frequency. He states that unlike CW radars, which examines only Doppler of the target, it is possible to observe motion of the target by taking snapshots of the range-Doppler map if a radar that can transmit coherent pulses is used. A range-Doppler map that contains only the returns from the target can then be

generated periodically in short time intervals so that a movie can be obtained for classification purpose. Vignaud makes his analyses in two different ways. He first applies short time Fourier transform (STFT) to time-domain return signal and generates the spectrogram of the motion. He extracts periodicity of the motion from the spectrogram as the first feature. Second, he makes a range-Doppler movie analysis in which he observes the images successively. His purpose is to extract information about the position of the reflectors from the body as the second feature. Figure 7 shows the experimental spectrogram of human walk he used for periodicity extraction while Figure 8 presents a snapshot of the range-Doppler view from the movie that gives information about position of the reflectors [8]. He proposes that these images can be used to classify a walking human, running human and walking multiple people.

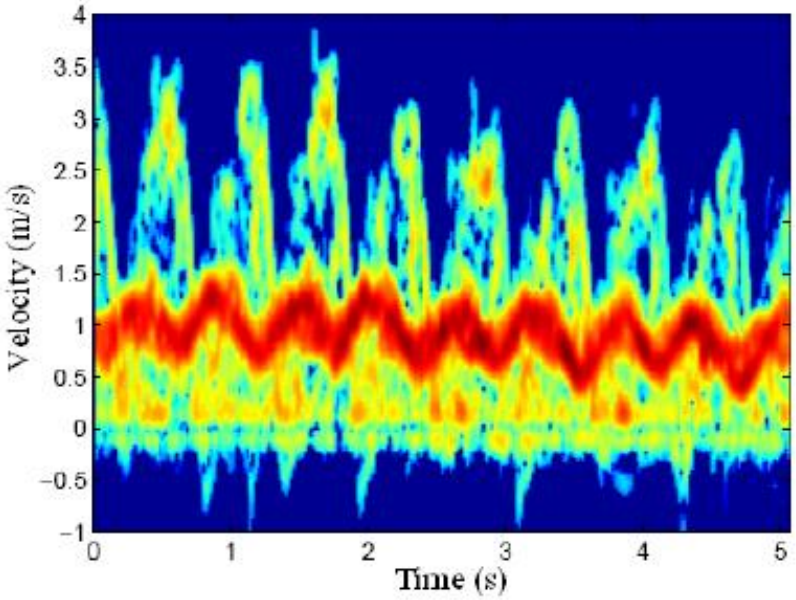

Figure 7: Experimental data of human walk [8]

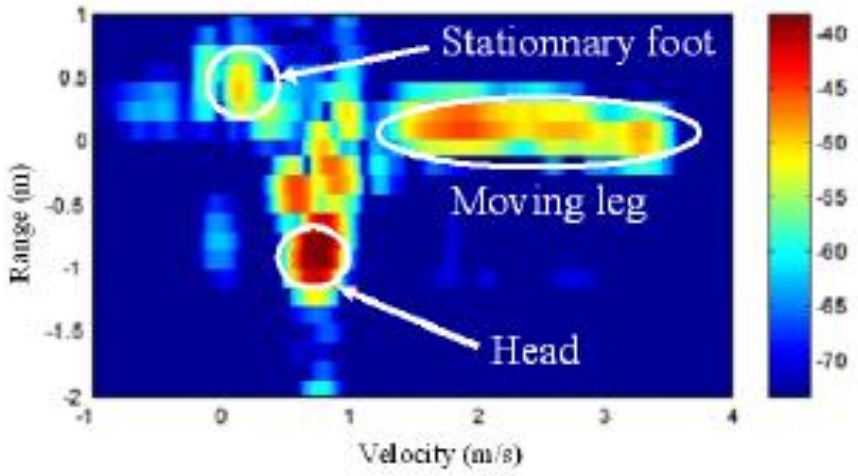

Figure 8: Experimental range-Doppler image of the walk [8]

Youngwook proposes to apply artificial neural network (ANN) for micro-Doppler signature based human motion classification in his article [9]. For this purpose, he proposes six features extracted from the spectrogram of the human motion data and uses these features in an ANN for classification. The features extracted from the spectrogram are the torso Doppler frequency, the total bandwidth (BW) of the Doppler signal, the offset of the total Doppler, the bandwidth without micro-Doppler, the normalized standard deviation of the Doppler signal strength and the period of the limb motion [9]. He gives an illustration of these features on Figure 9. He reports that ANN has less classification error compared to other methods like Fisher linear discriminator and Bayesian decision method [9]. Youngwook explains in his paper that he collected the experimental data using a Doppler radar from twelve people for seven different types of motion. Spectrograms of six of the motions can be seen on Figure 10. He reports that motion classification success with ANN is 82.7% and 87.8% for two different validation scenarios that use one-quarter of the test set.

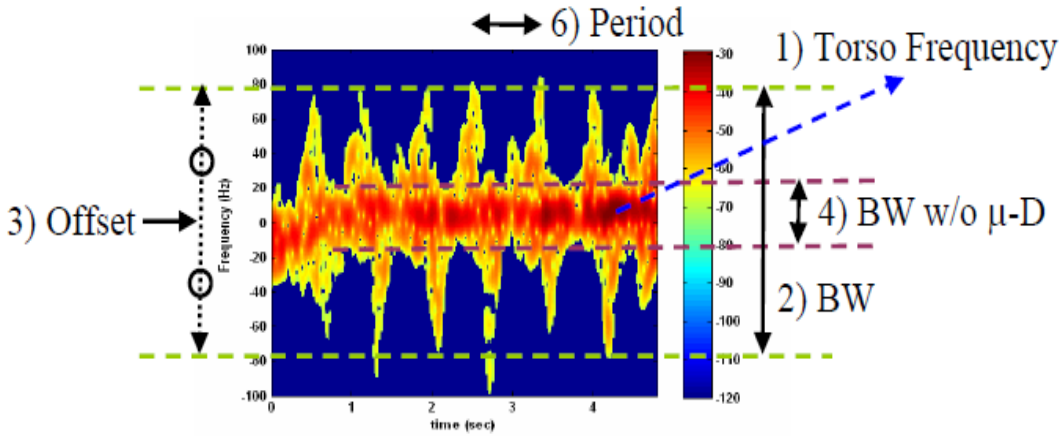

Figure 9: Micro-Doppler features in Youngwook's study [9]

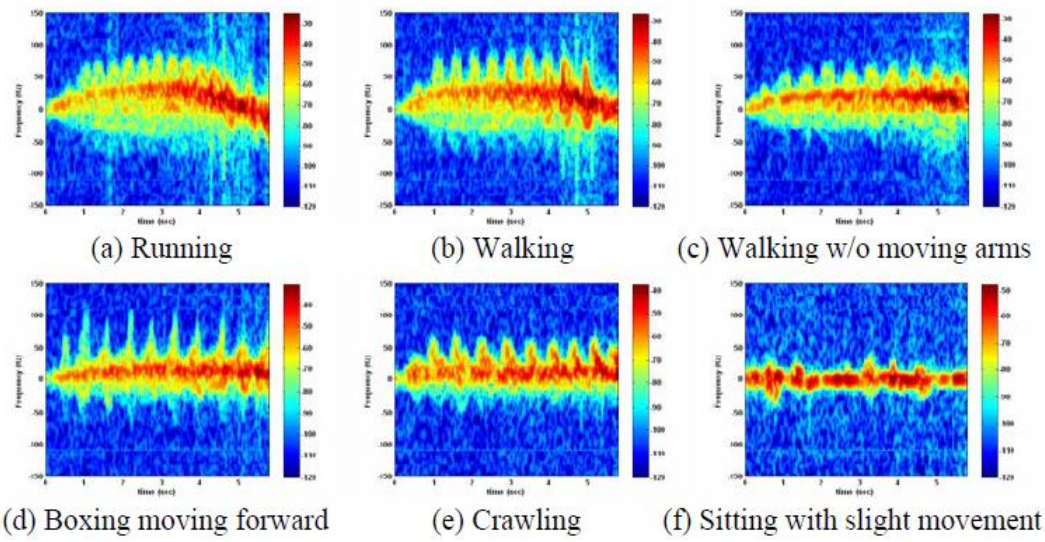

Figure 10: Micro-Doppler signatures of six motions in Youngwook's study [9]

In Dorp's study [10], Boulic's model for human walking is used for feature extraction from human motion spectrogram. The model describes human motion with a number of parameters. One of these parameters is the personification information obtained by estimating the leg and torso parameters [10]. Leg and torso parameters are calculated by using the temporal minimum, maximum and center velocity of the motion distribution. Moreover, by using the velocity slices on the spectrogram of a return signal, motion repetition frequency can be estimated as another feature. The mapping between body parts and features on spectrogram can be seen on Figure 11. The figure

presents torso reflections that has the features of average torso speed, torso cycle frequency and torso deviation. The spectrogram also shows the average leg speed, leg cycle and leg amplitude. These information are extracted as the parameters of Boulic model and form a basis for the construction of the walking model through formulating the human limbs as global equations [10]. Dorp uses the features for parameter estimation of human walking in his article, but not for classification purposes. After that, he investigates the radar recordings for human walk and controls the estimated parameters by comparing with the experimental data.

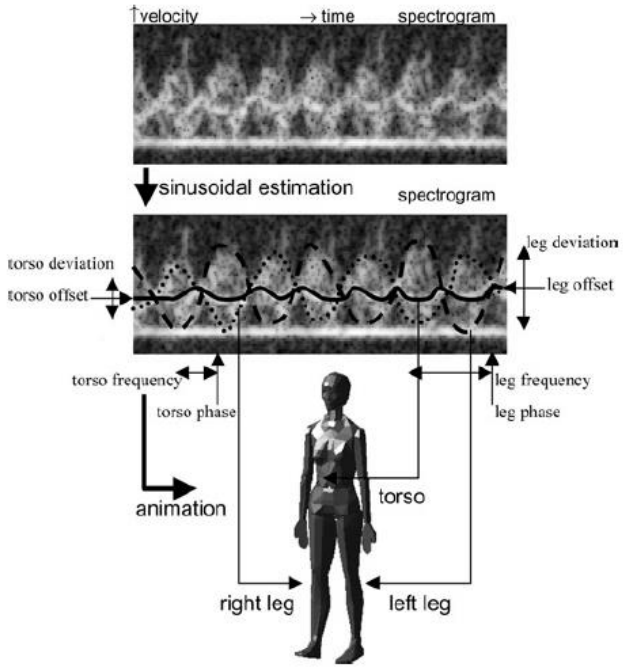

Figure 11: Illustration of Dorp's method [10]

Pan discusses in [11] that feature extraction can be performed by a transformation method to reduce the dimension of the input data. The reduction process is perceived to be beneficial, since it reduces the computational complexity and improves the accuracy of the classifier by eliminating the irrelevant and correlated features. He sums up that the principal component analysis (PCA), linear discriminant analysis (LDA) and maximum margin criterion (MMC) are such feature extraction methods for dimension reduction. In his paper, Pan proposes a novel feature extraction

algorithm called K-nearest neighbor (K-NN) local margin maximization that is applied to the raw data. He evaluates the success of his algorithm by the making comparison with the PCA, LDA and MMC methods. Although there is no exact information about the type of the classifier, it is presented that classification results for the proposed method is around 70% which is very similar to those of other feature extraction methods [11].

Youngwook uses SVM for human activity classification based on micro-Doppler signatures in [14]. Support vector machine is a supervised learning model based on Kernel methods, which requires only a similarity function over pairs of data points in raw representation, are widely used for various classification problems in machine learning [14]. By training SVM, a decision boundary is generated so that the classifier can decide which class the input data belongs. Youngwook uses the data from [9] that include data from twelve different people for seven different human motions. The same six features reported in [9] are used to train support vector machine (SVM). Since SVM is a binary classifier, he implements a multiclass classification for discrimination of seven motions by using a decision tree structure as seen in Figure 12 [14]. He divides the target set into classes so that one or more motion types can be eliminated at every node. Youngwook finds the optimal parameters for the SVM such as kernel and penalty parameters by trial-and-error and concludes that it is possible to classify the human activity with 90 % accuracy by using SVM as the classifier.

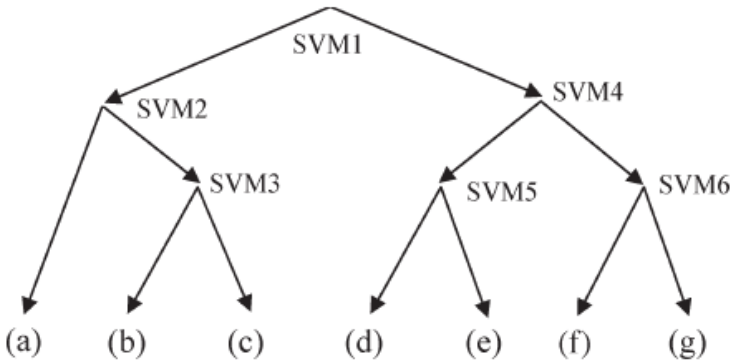

Figure 12: Decision tree used in [14]

Lei proposes a Gabor filtering method for the feature extraction of micro-Doppler signatures in [15]. The dimension of the features obtained by Gabor filtering is reduced by principal component analysis (PCA). After that step, three different classifiers using those features, Bayes linear classifier, k-nearest neighbor classifier and support vector machine (SVM), are trained with simulated data. In order to do that, Gabor filter is applied to the image (spectrogram of the motion) in four different directions as shown in Figure 13. The capitals A, B, C, D represent four different motions; vibrating, rotating, coning and tumbling respectively. After filtering, size of the images is reduced through PCA. The compressed features are then fed into the classifiers for decision making process. Lei concluded that Gabor features are robust for discriminating the micro-Doppler effects of different human activities and support vector machine (SVM) gives the best classification results with 92% success rate among the three classifiers [15]. In the experiments, the highest performance of Bayes linear classifier and k-NN are reported as 78% and 84%, respectively.

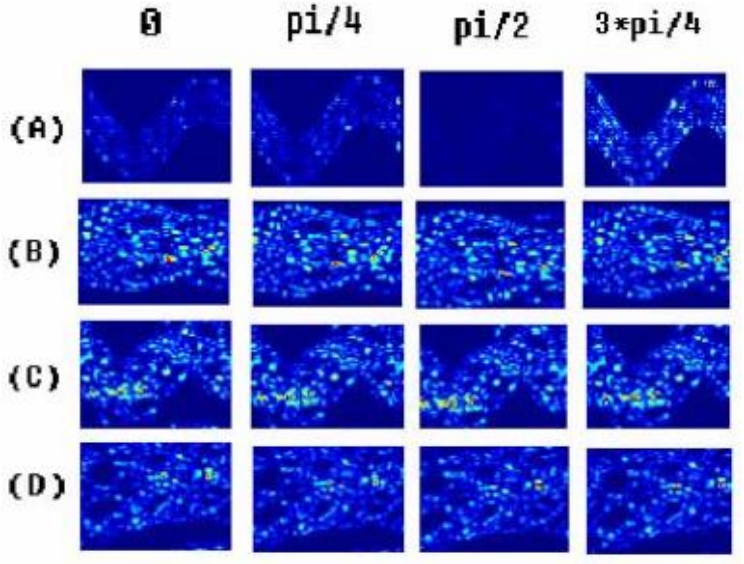

Figure 13: Gabor filtered images in [15]

In another study, Smith claims that when a radar on the field can provide Doppler tone of the target, it is also possible to classify the target by acoustic signature of the motion from Doppler tone [16]. The article then proposes a solution using dynamic

time warping of features (DTW), a speech recognition technique, before classification [16]. The algorithm simply calculates the distance between two series of measurements. Each of the series is composed of feature vectors. DTW initially computes sum of the distance, Euclidean in general, between the feature vectors. After that, a mapping process is made between the features whose distance are the shortest (The green line in Figure 14). The features are then normalized on time in order to compensate the differences caused by different speed of the same motion. Figure 14 presents an example of the method. The reference signal has increasing frequency and the test signal has a constant frequency. The figure shows the distances between the points of the signals and the optimal warping line. The same thing is done using time-velocity diagram (spectrogram) of tracked vehicle, wheeled vehicle and walking person. Smith concludes that this method gives the opportunity of classifying the target as vehicle or human with the success rate of 86.5%.

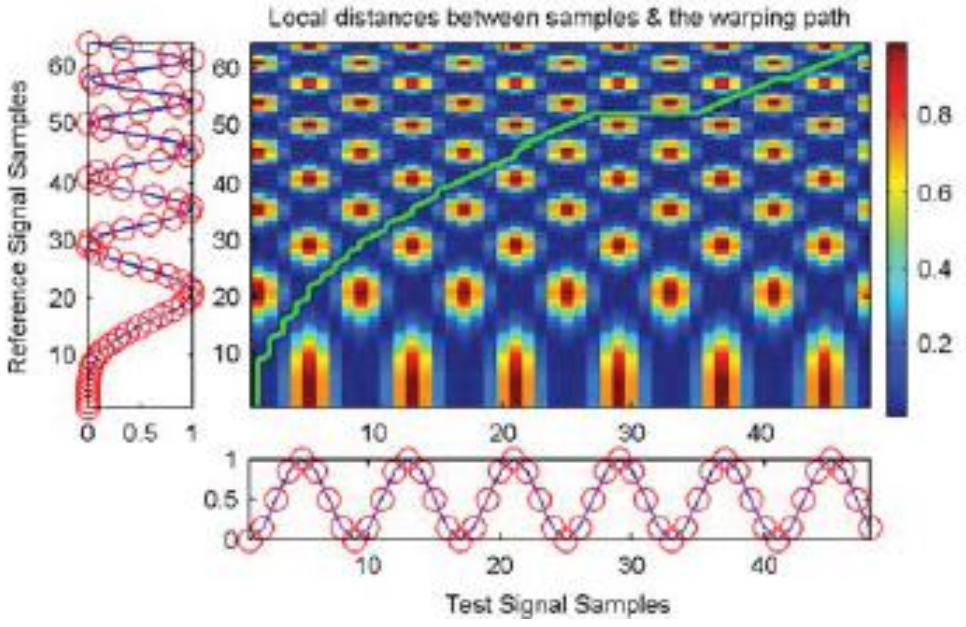

Figure 14: Optimal warping path between two series found by DTW in [16]

Li presents another method for human motion classification in [17]. For the experiments in the article, a frequency modulated continuous wave (FMCW) radar is used to illuminate the target and STFT is used to transform the time-domain signal into frequency domain so that the spectrogram of the signal can be observed [17].

After that step, principal component analysis (PCA) and linear discriminant analysis (LDA) are applied to the spectrogram for feature extraction and dimension reduction. Support vector machine (SVM) is used for human motion classification by using the data-driven features for the different types of human motion. The motion types in the experiments are normal walking, walking while carrying one object with one hand and walking while carrying one object with two hands. There are seven subjects and each subject repeats the movement for three times. After that, three-fold-cross validation is applied for evaluation of the classification performance. It is reported in the article that the average classification rate is 92%.

Alemdaroğlu also uses the micro-Doppler signatures of different human motions for feature extraction and classification purposes in [20]. Before feature extraction step, she applies short time Fourier transform (STFT) and Wigner-Ville distribution (WVD) as time-frequency transformation methods to obtain spectrograms. STFT is chosen as the transformation method, since the radar return signal is a multi-component signal and WVD causes cross-term interferences for these types of signals. She also uses the same six features as Youngwook reported in [9]. Classification is made on clustering the features of four different motions. These motions are walking, running, creeping and crawling. There is no exact classifier used in the study, but plots of the features gives an insight about numeric range of features for different types of motion as seen on Figure 15. It can be seen that the motions can be differentiated even by selecting only two features like torso frequency and offset, or torso frequency and bandwidth, or standard deviation and period, etc. It is also reported in [20] that even if the motion types can be classified easily at zero degree aspect angle, it gets increasingly difficult when aspect angle starts to increase.

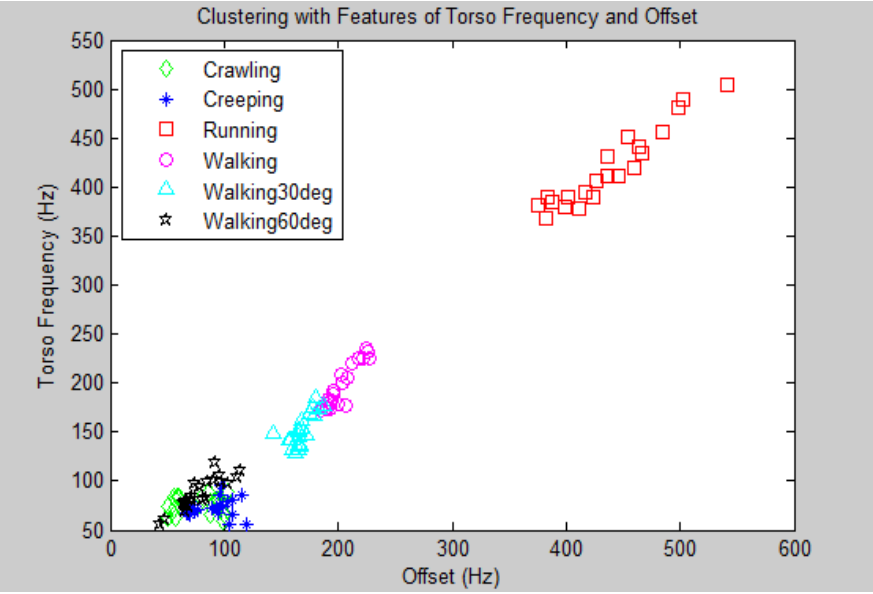

Figure 15: Clustering of features; torso frequency vs offset [20]

Björklund investigates time-velocity diagram (TVD) and cadence velocity diagram (CVD) for feature extraction of micro-Doppler signatures in [22]. For this purpose, he first applies STFT to the time domain echo and obtains the time-velocity diagram (Doppler shift in spectrogram is proportional to the target's velocity) of the signal. After that, cadence-velocity diagram is obtained by taking the absolute value of the Fourier transform of the time-velocity diagram along time. Björklund extracts features both from TVD and CVD. The features he extracts from the TVD are the same features in [9]. He defines these features as the time-velocity features. Velocity profiles and cadence frequencies of the echo are calculated by using the CVD, and peak velocities and frequencies are used as the features obtained from the CVD. Figure 16 shows an example about the cadence-velocity features [22]. Björklund uses TV and CV features separately for classification of human motion by SVM. He finds the cost parameter and Kernel function that provides the best classification results. The motions he examines are walking, running, creeping, crawling and jogging. There are three subjects and all of them repeats the motion for ten times in order to obtain test and training sequence database. "Leave-one-sequence-out" cross validation process is used to test the classification performance. It is stated in the

article that these five motions can be classified accurately with 87% using the TV features and 91% using the CV features alone.

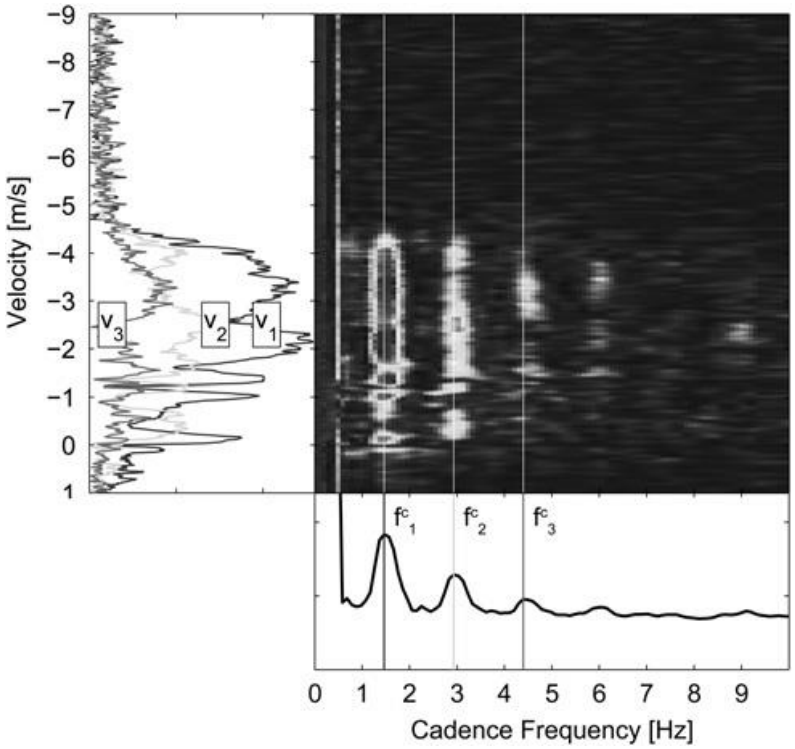

Figure 16: CV based feature extraction (cadence frequencies and velocity profiles)[22]

In Balleri's article [23], personnel targets are classified by using acoustic sensors. He collects his data using an ultrasound system operating at 80 kHz and with radar principles. Micro-Doppler signatures of the motions walking, running, walking while carrying an object with one hand, walking while carrying an object with two hands and walking with a heavy backpack on the shoulders are recorded. He proposes principal component analysis (PCA), cepstrum and mel-cepstrum for feature extraction of these micro-Doppler signals. The features are then used in Bayesian classifier and k-NN classifier for classification purpose. Bayesian classifier assumes that the elements of the feature vector are statistically independent and Gaussian distributed. Probability density functions of features are then calculated for each motion from training data set. Classification with Bayesian classifier is done based

on the computation of probability density functions (pdf) of features for given input and the motion with most similar pdf is determined. It is explained in the article that the five motions can be classified with 90% success rate using Bayesian classifier. K-NN which calculates the Euclidean distance between test feature vector and all training vectors is investigated as the second classifier. It is reported in the article that k-NN could classify the five motions with 80% success rate [23].

Liu examines micro-Doppler signatures in order to detect falling motion of elderly people in [24]. He proposes that a Doppler radar-based fall detection system can be developed for such problem. In the article, mel-frequency cepstral coefficients (MFCC) are used for feature extraction of various human activities like walking, bending and falling. In order to do that, spectrogram of the time-domain return signal is calculated as the first step. After that, energy burst curve is obtained from the spectrogram as shown in Figure 17. Mel-frequency cepstral coefficients are calculated inside a window around the peak point of the burst curve. Then, SVM and k-NN using those features are used to detect falls. In this work, the purpose is only to classify the motion as fall or not-fall. It is reported in the article that k-NN classifies the fall motion with 96% success rate while SVM classifies with 92% success rate [24].

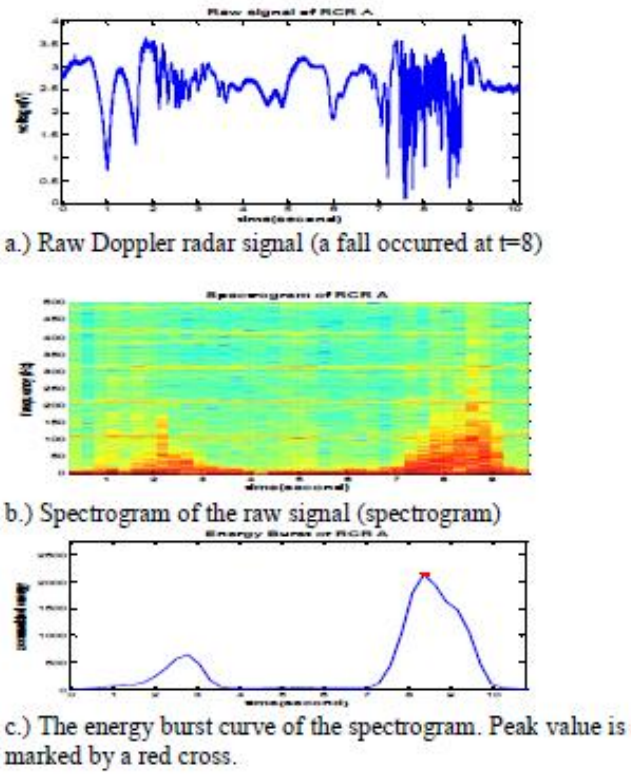

a.) Raw Doppler radar signal (a fall occurred at t=8)

b.) Spectrogram of the raw signal (spectrogram)

c.) The energy burst curve of the spectrogram. Peak value is marked by a red cross.

Figure 17: Three signal processing steps of the echo [24]

In another work, Harmanny uses micro-Doppler signatures to discriminate birds and small Unmanned Aerial Vehicles (UAVs) [25]. In the article, Harmanny mentions human eye can make a quick distinction between man-made objects and bio-life. Therefore, he proposes various features can be extracted from both spectrogram and cepstrogram. First, short time Fourier transform (STFT) is periodically applied to the return signal and spectrogram is obtained. Radar cross section, main velocity component, spectrogram periodicity, spectrum width and spectrogram symmetry are proposed to be used as features for classification. After that, cepstrogram of the return signal is calculated to obtain quefrency by taking the inverse of it which gives the periodicity of the micro-Doppler signature. An example of spectrogram and cepstrogram of an UAV with two rotors can be seen on Figure 18. Cesptrogram gives the quefrency values of the rotors so that rotation rate can be calculated. It is concluded in the article that human eye can make classification between birds and

UAVs with spectrogram and cepstrogram information [25]. No actual classification algorithm is proposed in the study.

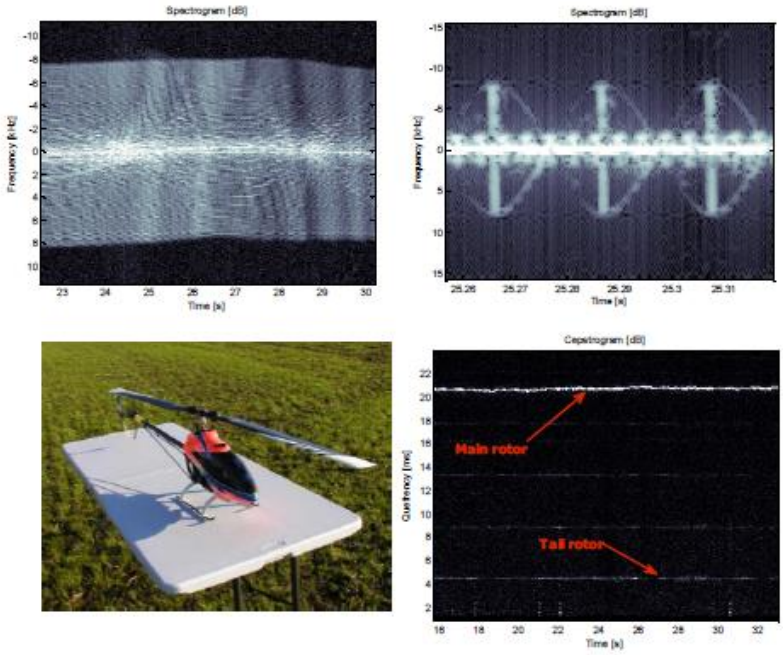

Figure 18: Long and short integration interval spectrograms (top) of an helicopter shown bottom left. The cepstrogram is shown bottom right [25]

Molchanov explains two novel methods to classify ground moving targets using the features related to the radial velocity of the targets in [26]. He investigates eight classes for classification. These classes are human walking toward/away the radar, truck, clutter, wheeled, human running, human crawling, a group of people walking and a group of people running. Molchanov proposes two features: For the first feature, he takes Fourier transform of the spectrogram along the time axis, computes logarithm and forms projections into frequency and time domain. As the second feature, he finds the singular value decomposition of the spectrogram of the echo signal and Fourier transform of the left singular matrix is computed as the second feature for classification. SVM and Gaussian mixture model (GMM) are used as the classification methods. It is reported in the article that both classification methods can classify the eight classes with up to 95% success rate [26].

McDonald explains in [27] that performance of airborne radars is often limited by false alarms caused by imperfect elimination of clutter reflections. However, an airborne radar is supposed to detect only presence of a human. In his work, it is proposed that micro-Doppler signatures can be used to address this problem. In the article, FM modulation index, AM modulation index, FM angular modulation frequency, AM angular modulation frequency and amplitude of the signal are determined as the features of the echo signal that discriminates human walk signature from clutter. These features are then used in discriminant analysis classifier (DAC), k-NN and SVM for classification. Different SNR values and dwell times are also investigated and it is reported that human walk can be classified with 80% success rate using any of the three classifiers [27].

Bar-Shalom uses principal component analysis as a feature extraction method for classification based on micro-Doppler signatures in [36]. He takes the radar recordings of one person crawling, one person walking, one person running, group of people walking and group of people running. After that, STFT is applied to the raw data to obtain the spectrogram of the echo signals. PCA is applied to the spectrogram, not to the raw data, in order to extract the features of the motions separately. Then, SVM is used for classification of the five different recordings. It is stated in the article that classification rate can be improved up to 95% by changing the principal component numbers and acquisition length [36].

Fioranelli uses a multistatik radar system to collect the experimental data for classification of unarmed and potentially armed personnel walking along different trajectories in [37]. Four empirical features, which are bandwidth, mean period, Doppler offset and radar cross-section ratio of limbs and body, are extracted using the spectrogram that is obtained by applying STFT to the radar return signal. In addition, singular value decomposition (SVD) is proposed to extract features while reducing the dimension of the workspace. The classification is made using a Naïve Bayes classifier and it is concluded that unarmed and armed personnel can be classified with 97% accuracy when SVD-based features and 91% accuracy when four empirical features are used [37].

Finally, Bilik develops an automatic target recognition algorithm based on Gaussian mixture model (GMM) in [28]. In his work, his target set is composed of walking person, tracked vehicle, wheeled vehicle, animals and clutter. Linear prediction coding (LPC) and cepstrum coefficients are used as features, extracted from the micro-Doppler signals. After feature extraction, the parameters of GMM used for statistical modeling of the feature distributions are calculated. Using GMM, models of the target set are generated and maximum-likelihood and majority voting decision methods are applied to the models for classification. Fourteen people are used as subjects and each motion is recorded at least three times. It is reported in the article that correct classification rate of maximum likelihood is 88% while correct classification rate of majority voting decision is 96% [28].

2.4 MOTIVATION IN CHOOSING FEATURES AND CLASSIFICATION METHODS IN THE THESIS

The purpose of this thesis is to classify four different human motions: walking, running, creeping and crawling. Different instances during a movement cycle can be defined as states and these states are interconnected to each other. Hence, all variations in a particular motion among different people should be modeled through states and the transitions between states. Moreover, states of the movement cycle is not observable, yet the observations are statistically related to the states. Therefore, hidden Markov models (HMM) is chosen as the method to model these variations in the micro-Doppler signal. In addition, it is also desirable that observation space dimension should be small so that the probability density functions can be obtained from training data reliably. Hence, principal component analysis (PCA) is chosen as the feature extraction method since it gives the opportunity of generating uncorrelated features using the basis vectors obtained by PCA and dimension of workspace can be reduced by eliminating the dimensions with less variations. Through this way, both estimation of state observation statistics is easier (covariance matrix is diagonal) and a feature space with less dimension can be used. As the features obtained through PCA satisfies these properties by transforming the time-domain signal into another domain where the features are uncorrelated, PCA is an

excellent choice for our purpose. In addition, a time-varying observation sequence is needed for HMM, which results in feature extraction on a frame-by-frame basis. Therefore, selection of frame length is also important and optimal frame length is determined in this thesis as well.

To the best of our knowledge, the application of PCA for feature generation and HMM based classifier to the micro-Doppler problem is not investigated elsewhere in the literature. A conference paper on our findings is to be presented in IEEE International Radar Conference 2016 [34].

CHAPTER 3

DETERMINATION OF OPTIMUM ANALYSIS WINDOW LENGTH FOR MICRO-DOPPLER SIGNALS OF HUMAN MOTION

Spectrogram of the radar return signals is investigated for feature extraction and classification of micro-Doppler signatures in many studies as discussed in Chapter 2 [6-9]. Radar return signal is periodically divided into overlapped frames and short time Fourier transform is applied as the transformation method in these studies. Outcomes of the transformation are concatenated in a sequence to form the spectrogram. Linear transformation techniques such as Fourier transform assume that the signal inside the analysis window is stationary. However, if the length of the analysis window is not selected properly, this would not be the case and a single frequency component may smear into multiple FFT bins because of the rapid change of frequency within a frame. This situation is caused by sharp frequency and magnitude changes of the signal within analysis window. On the other hand, the analysis window is desired to be as long as possible, as frequency resolution increases with increasing analysis window length. High frequency resolution is important, because it gives the opportunity of observing low frequency components and resolving close frequency components of the investigated signal. Therefore, a proper analysis window length, which is as long as possible, and at the same time providing stationarity and avoiding frequency smearing, should be determined.

In this chapter, a stationarity analysis method is proposed and an optimal analysis window length is determined for micro-Doppler signal of human motion. The analysis is conducted for different limbs of human in walking motion by using a human walking simulator known as Victor Chen's human walking simulator. The simulator can generate Doppler frequency components of the limbs and produce the

micro-Doppler signature of human walk through the use of Boulic model and radar equations.

3.1 VICTOR CHEN'S HUMAN WALKING SIMULATOR

Shape of the human body can change while in motion and distance between two distinct limbs of human body can vary in time [2]. Radar return signal from human body can be modeled as combination of rigid limbs and motion of this non-rigid body can be analyzed as motion of multiple rigid segments [2]. The motion of these segments can be characterized as a periodic motion, since the nature of human motion is also periodic. To illustrate, a human walking motion cycle can be decomposed into two phases, which are stance and swing phases.

Human walk is a periodic motion with opposite positions of feet, swinging arms and legs, and body center movement of up and down. Although general characteristics of a walking cycle do not change from one person to another, everyone maintains his/her own unique motion characteristics. Moreover, motion characteristics of a person may change according to his/her daily mood. As an example, motion of a happy person is different from motion of a depressed person in general [2].

Human motion can be formed by using kinematic method whose parameters are changing dynamically. Kinematic method is applied easily to calculate the positions of human body limbs using joint angles, if the motion is generated without involving the forces from outside. Inverse kinematics is applied to calculate joint angles by using the positions of human limbs [2]. Kinematic parameters of human motion are linear position, linear velocity, linear acceleration, angular position, angular velocity and angular acceleration of limbs. First three of these parameters are called as linear parameters while the rest is called as angular parameters. Angular and linear motion of body segments are characterized by these parameters.

The human walk can be modeled based on both mathematical and empirical models. Boulic proposes to estimate kinematic parameters of human body segments by using a global human walking model generated by collecting a large number of experimental data and empirical mathematical parameterization. Spatial positions

and orientations of body segments are intended to be supplied in Cartesian coordinates. The motion is described by 12 trajectories and 14 rotations and this corresponds to one cycle of the motion. The trajectories are; translational trajectories which are vertical translation, lateral translation and translation forward/backward, rotational trajectories which are rotation forward/backward, rotation left/right, torsion rotation and flexing trajectories in the upper and lower body which are flexing at the hip, flexing at the knee, flexing at the ankle, motion of the thorax, flexing at the shoulder and flexing at the elbow [2]. Translational trajectories are described in distance versus cycle time while other trajectories are described in angle versus cycle time. Locations of the 17 reference points (head, neck, base of spine, left and right shoulders, left and right elbows, left and right hands, left and right hips, left and right knees, left and right ankles, left and right toes) that can be seen on Figure 19 are calculated by using the information on these 12 trajectories. Finally, position and orientation of body segments are obtained under the light of the location of 17 reference points [2].

In Chen's human walking simulator, this global human walking model is used to compute the position and velocity of the rigid limbs, and then, Doppler return signal is calculated as if the model is illuminated by a CW radar. Relative length of a cycle, relative velocity of the motion, number of cycle, height of the person in simulation, radar transmission wavelength and radar location can be adjusted as inputs to the human walking simulator. The simulator calculates the return signal from all body segments and generates the micro-Doppler signature of human walk as seen on Figure 20.

Figure 19: Simulation of global human walk [2]

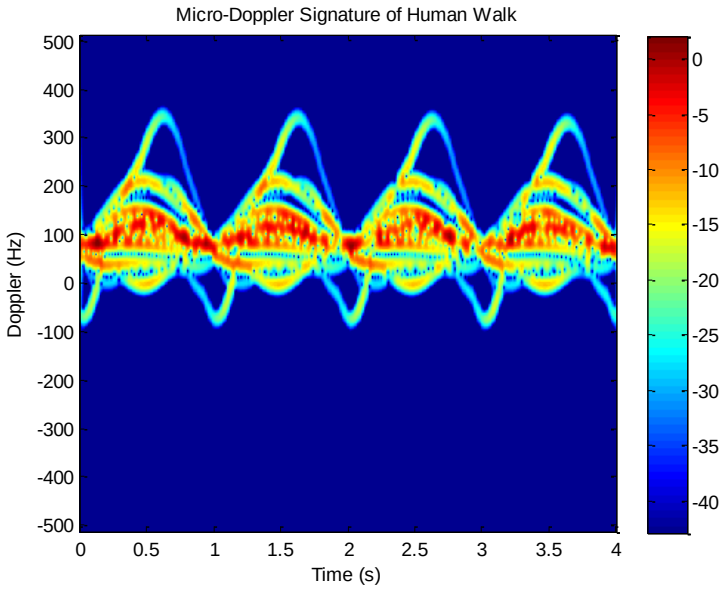

Figure 20: Spectrogram of simulated micro-Doppler signature of human walk [2]

3.2 STATIONARITY ANALYSIS FOR SIMULATED MICRO-DOPPLER SIGNALS

As discussed before, analysis window length is desired to be as long as possible to satisfy better frequency resolution. However, if there occurs a rapid change in frequency inside the analysis window, frequency components of the investigated signal smear into multiple frequency bins after STFT. Therefore, the analysis window length should be chosen properly to guarantee that low frequency components of the motion are observable, and at the same time, there is no frequency smearing in the spectrum. In addition, even if a frequency does not smear into multiple frequency bins because of a change in frequency inside the analysis window, this could still affect the magnitude of the component at the closest frequency bin. Therefore, the analysis window length should be selected so that the magnitude of the slowly varying frequency component at the closest frequency bin should not be significantly different when compared to the magnitude of a completely stationary mean frequency at the same closest frequency bin.

For this purpose, two tests are defined to control stationarity of the signal inside an analysis window. Maximum frequency change of the signal in the analysis window and its difference with frequency resolution is controlled in the first test. Effect of the time-varying signal after STFT to the magnitude change at the nearest frequency bin is controlled in the second experiment. As Victor Chen's human walking simulator generates Doppler frequencies of all body parts as a function of time [2], and input signal to the STFT analysis can be generated with this simulator, it is used to perform both tests to determine the optimum analysis window length.

For the first stationarity test, the frequency change of the signal inside an analysis window is extracted. For this purpose, Doppler frequencies of all body segments are generated as a function of time by using Chen's human walking simulator [2]. Example of Doppler frequency for upper leg can be seen on Figure 21. In the experiment, aspect angle is chosen as zero degree and radar transmission frequency is in Ku-band. Doppler frequency graphs of other limbs are given in Appendix A. In this test, for each candidate window length, the frequency change inside an analysis window from the motion of all body limbs is calculated on a frame-by-frame basis by sliding window of one sample. As a result, for every limb and every window size ranging from 2.5 milliseconds to 100 milliseconds, maximum frequency change for every sample inside the analysis window is calculated and compared with the frequency resolution, which itself is determined by the analysis window length. Ideally, no smearing is desired, but this means very short analysis window and bad frequency resolution. Therefore, a limit of 5% is set for the percentage of sequences in which an individual frequency is allowed to smear into multiple frequency bins inside the analysis window. Since shorter window length improves low frequency resolution, 5% of the sequences smearing to multiple FFT bin inside the analysis window seems to be a good compromise for the first test.

Figure 21: Simulated Doppler shift of upper leg

The window length analysis is performed for seven different window lengths ranging from 2.5 milliseconds to 100 milliseconds as shown between Table 1 and Table 8. This experiment reveals maximum frequency change and percentage of the sequences in which frequency change is less than frequency resolution inside the seven different windows for all body segments during the walking motion. The results can be seen in "Max Frequency Variation" and "FFT Bin Test" columns in tables between Table 1 and Table 8 for eight different limbs. In this test, it is observed that analysis window length of 20 milliseconds avoids smearing for all limbs, and 30 milliseconds window avoids smearing for four of the eight limbs. As the frequency resolution should also be as high as possible, it is desirable to use 20 milliseconds window with smearing only in 5% of the entire sequence and only in four of the limbs. Therefore, 20 milliseconds of analysis window is selected as the best common length derived from the first test.

The effect of the frequency change to the magnitude of the nearest FFT bin is investigated as the second stationarity test. This effect is desired to be under the limit of 1 dB in magnitude. For this purpose, two signals are generated for each analysis

window. The first signal is generated with the time-varying frequency, while the second signal is generated with a constant frequency which is the average of the time-varying frequency within the analysis window. Then, Fourier transform of both signals are taken, and magnitudes of the FFT bin closest to the time-varying component for both signals are recorded, and their difference is calculated. Analysis window lengths which limits the magnitude change by 1 dB in at least 90% of the sequences is considered as stationary for the signals to be examined. The outcomes of the experiments can be seen in "dB Test" columns on Table 1-8 for eight parts of human body. The results present that 20 milliseconds of analysis window length is a good choice for all eight limbs, while 30 milliseconds is good for five and 45 milliseconds is only good for two limbs. Therefore, as in the first test, 20 milliseconds of analysis window is determined to be the best length for human walk analysis in case of magnitude test.

Table 1: Window size calculations for head

SEGMENT (RCS m^2)	WINDOW LENGTH	MAXIMUM FREQUENCY DIFFERENCE (Hz)	FFT BIN TEST	dB TEST
HEAD (0.0407-0.0425)	2.5 ms 20 sample	0.26193	0: %100 1: %0	<0.5: %100 >0.5 & <1: %0 >1: %0
	5 ms 40 sample	0.53761	0: %100 1: %0	<0.5: %100 >0.5 & <1: %0 >1: %0
	10 ms 80 sample	1.0888	0: %100 1: %0	<0.5: %100 >0.5 & <1: %0 >1: %0
	20 ms 160 sample	2.1902	0: %100 1: %0	<0.5: %100 >0.5 & <1: %0 >1: %0
	30 ms 240 sample	3.2874	0: %100 1: %0	<0.5: %61.8 >0.5 & <1: %35.2 >1: %3
	45 ms 360 sample	4.8991	0: %91.11 1: %8.89	<0.5: %64.4 >0.5 & <1: %27.3 >1: %8.3
	100 ms 800 sample	10.7946	0: %45 1: %55	<0.5: %10 >0.5 & <1: %47.8 >1: %42.2

Table 2: Window size calculations for hand

SEGMENT (RCS m^2)	WINDOW LENGTH	MAXIMUM FREQUENCY DIFFERENCE (Hz)	FFT BIN TEST	dB TEST
HAND (0.0014-0.0532)	2.5 ms 20 sample	0.87287	0: %99.76 1: %0.24	<0.5: %100 >0.5 & <1: %0 >1: %0
	5 ms 40 sample	1.7821	0: %99.51 1: %0.49	<0.5: %100 >0.5 & <1: %0 >1: %0
	10 ms 80 sample	3.5699	0: %98.04 1: %1.96	<0.5: %89.2 >0.5 & <1: %10.8 >1: %0
	20 ms 160 sample	7.0129	0: %95.42 1: %4.58	<0.5: %50.9 >0.5 & <1: %42.4 >1: %6.7
	30 ms 240 sample	10.4487	0: %82.35 1: %17.65	<0.5: %25 >0.5 & <1: %55 >1: %20
	45 ms 360 sample	15.0274	0: %62.2 1: %37.8	<0.5: %8.9 >0.5 & <1: %49.1 >1: %42
	100 ms 800 sample	33.56	0: %10 1: %25 >1: %65	<0.5: %15 >0.5 & <1: %45 >1: %40

Table 3: Window size calculations for leg

SEGMENT (RCS m^2)	WINDOW LENGTH	MAXIMUM FREQUENCY DIFFERENCE (Hz)	FFT BIN TEST	dB TEST
LEG (0.0128-0.3054)	2.5 ms 20 sample	0.8709	0: %99.76 1: %0.14	<0.5: %100 >0.5 & <1: %0 >1: %0
	5 ms 40 sample	1.7875	0: %99.5 1: %0.5	<0.5: %100 >0.5 & <1: %0 >1: %0
	10 ms 80 sample	3.6206	0: %99.02 1: %0.98	<0.5: %98.53 >0.5 & <1: %1.47 >1: %0
	20 ms 160 sample	7.257	0: %96.08 1: %3.92	<0.5: %86.3 >0.5 & <1: %13.7 >1: %0
	30 ms 240 sample	10.7684	0: %88.24 1: %11.76	<0.5: %64.7 >0.5 & <1: %25.7 >1: %9.6
	45 ms 360 sample	16.2625	0: %77.8 1: %22.2	<0.5: %51.1 >0.5 & <1: %34.8 >1: %14.1
	100 ms 800 sample	31.1043	0: %35 1: %35 >1: %30	<0.5: %25 >0.5 & <1: %45 >1: %30

Table 4: Window size calculations for hip

SEGMENT (RCS m^2)	WINDOW LENGTH	MAXIMUM FREQUENCY DIFFERENCE (Hz)	FFT BIN TEST	dB TEST
HIP (0.0226-0.0232)	2.5 ms 20 sample	0.24483	0: %100 1: %0	<0.5: %100 >0.5 & <1: %0 >1: %0
	5 ms 40 sample	0.50251	0: %100 1: %0	<0.5: %100 >0.5 & <1: %0 >1: %0
	10 ms 80 sample	1.0176	0: %100 1: %0	<0.5: %100 >0.5 & <1: %0 >1: %0
	20 ms 160 sample	2.0448	0: %100 1: %0	<0.5: %100 >0.5 & <1: %0 >1: %0
	30 ms 240 sample	3.0654	0: %97.06 1: %2.94	<0.5: %86.8 >0.5 & <1: %13.2 >1: %0
	45 ms 360 sample	4.609	0: %91.1 1: %8.9	<0.5: %46.7 >0.5 & <1: %33.4 >1: %19.9
	100 ms 800 sample	10.1263	0: %60 1: %40	<0.5: %15 >0.5 & <1: %40 >1: %45

Table 5: Window size calculations for shoulder

SEGMENT (RCS m^2)	WINDOW LENGTH	MAXIMUM FREQUENCY DIFFERENCE (Hz)	FFT BIN TEST	dB TEST
SHOULDER (0.0412-0.0427)	2.5 ms 20 sample	0.29227	0: %100 1: %0	<0.5: %100 >0.5 & <1: %0 >1: %0
	5 ms 40 sample	0.59898	0: %100 1: %0	<0.5: %100 >0.5 & <1: %0 >1: %0
	10 ms 80 sample	1.2092	0: %100 1: %0	<0.5: %100 >0.5 & <1: %0 >1: %0
	20 ms 160 sample	2.3731	0: %100 1: %0	<0.5: %100 >0.5 & <1: %0 >1: %0
	30 ms 240 sample	3.5975	0: %97.06 1: %2.94	<0.5: %88.2 >0.5 & <1: %11.8 >1: %0
	45 ms 360 sample	5.0004	0: %91.11 1: %8.89	<0.5: %53.3 >0.5 & <1: %36.8 >1: %9.9
	100 ms 800 sample	10.7664	0: %50 1: %50	<0.5: %20 >0.5 & <1: %50 >1: %30

Table 6: Window size calculations for foot

SEGMENT (RCS m^2)	WINDOW LENGTH	MAXIMUM FREQUENCY DIFFERENCE (Hz)	FFT BIN TEST	dB TEST
FOOT (0.0012-0.0520)	2.5 ms 20 sample	2.8389	0: %99.76 1: %0.24	<0.5: %100 >0.5 & <1: %0 >1: %0
	5 ms 40 sample	5.7384	0: %98.53 1: %1.47	<0.5: %94.86 >0.5 & <1: %5.14 >1: %0
	10 ms 80 sample	11.3414	0: %97.07 1: %2.93	<0.5: %91.8 >0.5 & <1: %9.2 >1: %0
	20 ms 160 sample	22.7256	0: %95.07 1: %4.93	<0.5: %89.8 >0.5 & <1: %10.2 >1: %0
	30 ms 240 sample	32.3989	0: %64.7 1: %35.3	<0.5: %41.2 >0.5 & <1: %48.6 >1: %10.2
	45 ms 360 sample	46.7031	0: %46.7 1: %35.5 >1: %17.8	<0.5: %46.7 >0.5 & <1: %40.5 >1: %12.8
	100 ms 800 sample	83.6432	0: %20 1: %10 >1: %70	<0.5: %25 >0.5 & <1: %55 >1: %20

Table 7: Window size calculations for arm

SEGMENT (RCS m^2)	WINDOW LENGTH	MAXIMUM FREQUENCY DIFFERENCE (Hz)	FFT BIN TEST	dB TEST
ARM (0.0078-0.1487)	2.5 ms 20 sample	0.39086	0: %100 1: %0	<0.5: %100 >0.5 & <1: %0 >1: %0
	5 ms 40 sample	0.80224	0: %100 1: %0	<0.5: %100 >0.5 & <1: %0 >1: %0
	10 ms 80 sample	1.625	0: %100 1: %0	<0.5: %100 >0.5 & <1: %0 >1: %0
	20 ms 160 sample	3.2687	0: %96.07 1: %3.93	<0.5: %79.4 >0.5 & <1: %18.2 >1: %2.4
	30 ms 240 sample	4.9068	0: %94.11 1: %5.89	<0.5: %66.17 >0.5 & <1: %20.5 >1: %13.33
	45 ms 360 sample	7.3711	0: %86.7 1: %13.3	<0.5: %37.8 >0.5 & <1: %29.1 >1: %33.1
	100 ms 800 sample	16.2824	0: %35 1: %55 >1: %10	<0.5: %20 >0.5 & <1: %40 >1: %40

Table 8: Window size calculations for torso

SEGMENT (RCS m^2)	WINDOW LENGTH	MAXIMUM FREQUENCY DIFFERENCE (Hz)	FFT BIN TEST	dB TEST
TORSO (0.1378-0.1862)	2.5 ms 20 sample	0.21392	0: %100 1: %0	<0.5: %100 >0.5 & <1: %0 >1: %0
	5 ms 40 sample	0.43905	0: %100 1: %0	<0.5: %100 >0.5 & <1: %0 >1: %0
	10 ms 80 sample	0.88927	0: %100 1: %0	<0.5: %100 >0.5 & <1: %0 >1: %0
	20 ms 160 sample	1.7872	0: %100 1: %0	<0.5: %100 >0.5 & <1: %0 >1: %0
	30 ms 240 sample	2.6839	0: %100 1: %0	<0.5: %100 >0.5 & <1: %0 >1: %0
	45 ms 360 sample	4.0243	0: %91.1 1: %8.9	<0.5: %55.6 >0.5 & <1: %30.2 >1: %14.2
	100 ms 800 sample	8.6629	0: %60 1: %40	<0.5: %30 >0.5 & <1: %50 >1: %20

The results show that an analysis window length of 20 milliseconds satisfies both constraints for stationarity. In addition, 20 milliseconds window length provides a frequency resolution of 50 Hertz, which is expected to be sufficient for capturing low frequency components while avoiding frequency smearing for a Ku band radar which is the most common band used for ground surveillance radars. As the motions investigated in this study are walking, running, creeping and crawling, selection of

this window size is expected to give also good results for the motions slower than walking such as creeping and crawling. Although there may be a problem for running motion, 20 ms window length is still a good compromise for a common frame length for examining all of these four types of human motion.

It should also be noted that these results would change depending on RF transmission frequency of the radar. This is because of the fact that Doppler frequencies for the radars with shorter wavelength are larger and spread more. As a result, these signals can be examined with shorter analysis windows with less frequency smearing. The radars with shorter wavelengths have therefore an advantage compared to radars with longer wavelengths for obtaining micro-Doppler signatures of the signals.

CHAPTER 4

DATA GENERATION AND FEATURE EXTRACTION

Feature extraction is one of the two most important aspects of a good classification system (the other classifier itself). Each feature is desired to have unique information so that all relevant information is captured in as few dimensions as possible. This also allows estimating probability distribution function of features from available training data more reliably for probability based classifiers. The features with these properties can be obtained by applying a data-driven method like principal component analysis (PCA). Since PCA is a linear transformation method, it assumes that the signal inside the analysis window is stationary. As analysis window length of 20 milliseconds satisfies stationarity requirement as discussed in Chapter 2, this window size is used in principal component analysis of micro-Doppler signals. For classification experiments, radar data for four different types of motions, walking, running, creeping and crawling, are experimentally collected using a ground surveillance radar from five subjects. This data is also used to find basis vectors that decorrelate input space through PCA.

In this chapter, background information about principal component analysis method is given in the first section. Then, experimental setup in which all the data were collected is explained. In the third section, pre-processing of data before feature extraction is presented. Finally, analysis of PCA basis vectors obtained with real micro-Doppler signals is presented.

4.1 BACKGROUND INFORMATION ABOUT PRINCIPAL COMPONENT ANALYSIS

Principal component analysis is a data decorrelation method through computing orthogonal basis vectors for training data. In addition, signal variation for each PCA

basis vector can be calculated as the eigenvalues of the eigenvectors, and eigenvectors with less variation can be eliminated for dimension reduction. Xiao presents in [12] that PCA can be used as a feature extraction method from a series of images. Since PCA is a good way to extract relevant data from a large amount of data set, it is useful for compression and classification purposes [12]. Therefore, the method is used in a large variety of fields like image processing, image compression and pattern recognition. Xiao uses singular value decomposition method for PCA in his paper in order to obtain uncorrelated eigenvectors of the data. After that, features of the images are extracted via transformation so that they can be processed for detection and classification.

Principal component analysis is a beneficial method for image processing purposes like pattern identification and image compression [13]. It gives the chance for identifying patterns in data and representing it in a way to highlight the differences and similarities as expressed in [13]. The tool is effective especially when low dimension of data with uncorrelated features are required.

For making PCA, three methods are proposed in [29]. Eigenvalue decomposition and singular value decomposition are explained as two of the methods for PCA. Expectation Maximization (EM) algorithm is also discussed as another method for PCA. The formulas to find the eigenvalues of the input data for PCA are given below for eigenvalue decomposition and singular value decomposition respectively.

$$\boldsymbol{R} = \boldsymbol{E\lambda E^H} \tag{3}$$

$$\boldsymbol{R} = \boldsymbol{USV^H} \tag{4}$$

where $\boldsymbol{R}$ is the covariance of the input, $\boldsymbol{E}$ is the eigenvector matrix, $\boldsymbol{\lambda}$ is the eigenvalue matrix, columns of $\boldsymbol{U}$ are the eigenvectors of $\boldsymbol{R}$ and singular values in $\boldsymbol{S}$ are the magnitudes of eigenvalues of $\boldsymbol{R}$. Since $\boldsymbol{R}$ matrix is symmetric and positive semidefinite, two decompositions (PCA and SVD) are identical. In this case, $\boldsymbol{V}$ matrix is composed of the eigenvectors of $\boldsymbol{R}$ matrix. It is stated that PCA with SVD is more stable and robust, but complexity is higher than eigenvalue decomposition

[29]. Therefore, eigenvalue decomposition is more advantageous in terms of computational complexity when the input dimension is large.

Eigenvalues of the covariance matrix are defined to be the principal components of the input data. The first component has the largest variation in the signal. The principal components are orthogonal to each other and the variations in the signal determine the direction of the components. An example for first two principal components of a data is given in Figure 22. The principal components are orthogonal to each other and they form an orthogonal basis for transformation of the input signal.

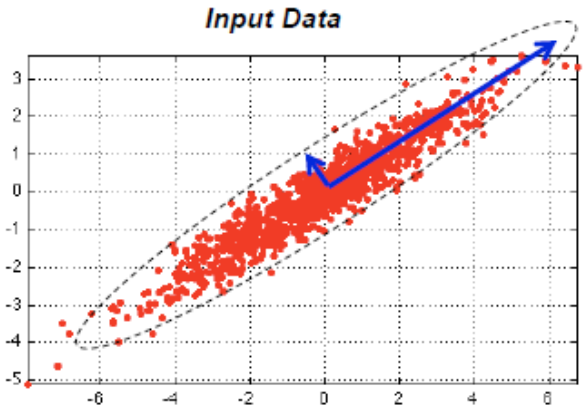

Figure 22: An example of principal component [29]

Eigenvectors matrix is used as the transformation matrix for PCA. It decorrelates the signal and transforms the input signal to uncorrelated, low dimension feature vectors. Mathematical representation of the transformation is given below, where $\boldsymbol{a}$ is the column vector that includes a frame of the input signal, $\boldsymbol{W}$ is the transformation matrix that includes the eigenvectors and $\boldsymbol{t}$ is the feature vector as a column vector. Figure 23 shows an example for transformation of the input by PCA.

$$\boldsymbol{t} = \boldsymbol{W}^{\boldsymbol{H}}\boldsymbol{a} \tag{5}$$

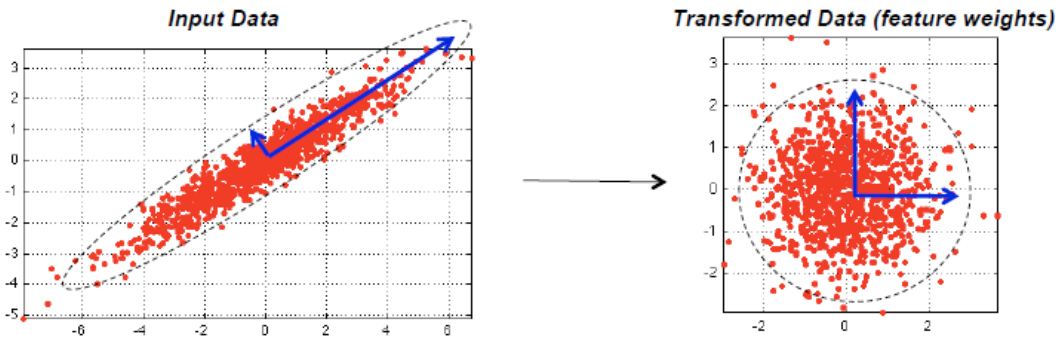

Figure 23: An example of transformation by PCA [29]

The PCA has also some optimality properties from the context of information theory. As discussed in [35], if we consider that the random vectors are Gaussian random vectors, that is the entries of the random vector are jointly Gaussian distributed; then the mutual information between the random vector $\boldsymbol{x}$ and its dimension reduced version, that is $\boldsymbol{y} = \boldsymbol{W}^H \boldsymbol{x}$, can be expressed as

$$I(\boldsymbol{x}; \boldsymbol{y}) = H(\boldsymbol{y}) - H(\boldsymbol{y}|\boldsymbol{x}) \tag{6}$$

where $H(\boldsymbol{x})$ and $H(\boldsymbol{x}|\boldsymbol{y})$ are entropy and conditional entropy functions, respectively. The mutual information is a measure relating the statistical dependency of its arguments. In a communication setting, the mutual information between input and output of a channel is critically important; since it is known that the amount of information (say in bits), that can be reliably transferred with a single utilization of this channel is limited by the maximum mutual information between channel input and output.

As discussed in [35], the mutual information maximizing dimension reduction transformation is the PCA (Furthermore, in the presence of observation noise, the optimal transformation is the generalized eigenvectors of signal and noise space covariance matrix). The optimality of PCA (the case without the observation noise) is rather easy to show.

It can be noted that $H(\boldsymbol{y}|\boldsymbol{x}) = 0$, since the vector $\boldsymbol{y}$ is deterministically related to the vector $\boldsymbol{x}$ via the relation $\boldsymbol{y} = \boldsymbol{W}^H\boldsymbol{x}$. Then, equation (6) reduces to $I(\boldsymbol{x};\boldsymbol{y}) = H(\boldsymbol{y}) - H(\boldsymbol{y}|\boldsymbol{x}) = H(\boldsymbol{y})$. The entropy for Gaussian random vector is simply

$$H(\boldsymbol{y}) = \frac{1}{2}\ln\{(2\pi e)^N \det(\mathbf{C}_y)\} \tag{7}$$

where $\mathbf{C}_y$ denotes the covariance matrix of the random vector $\boldsymbol{y}$.

Let's assume that $y = \boldsymbol{e_1^H x}$, that is the random vector $\boldsymbol{x}$ is projected to a one dimensional space. For this case, $H(y)$ becomes

$$H(y) = \frac{1}{2}\ln\{2\pi e\sigma_y^2\} \tag{8}$$

where σ_y^2 is the variance of the random variable y formed after projection. From the development of PCA given earlier, we know that the dominant eigenvector of $\mathbf{C}_y$ maximizes σ_y^2 among all unit norm vectors. Hence, the optimal one dimensional space, from the viewpoint of mutual information preservation, is the dominant eigenvector of $\mathbf{C}_y$. For higher dimensional spaces, the same argument can be repeatedly applied to formalize the optimality of PCA in the sense of mutual information preservation.

Roweis presents expectation-maximization (EM) algorithm for principal component analysis in [30]. He states that eigenvectors should be extracted from a large amount of data in general. He claims that his novel approach for PCA is the best fit to find eigenvectors when the data set is very large. Sometimes, it is very difficult to find eigenvectors of covariance matrix of the input due to high computational complexity. Roweis states that EM method for PCA does not require calculating covariance matrix to find the principal components of the signal [30]. Therefore, it is possible to extract eigenvectors of data with very high dimension easier compared to eigenvalue decomposition and singular value decomposition methods in case of computational cost.

4.2 EXPERIMENTAL SETUP

For human motion micro-Doppler signature studies, a pulsed-Doppler ground surveillance radar was used to collect the experimental data. The data were collected in June 2015 in an area suitable for collecting micro-Doppler data. The weather was sunny and the temperature was around 30 degrees Celsius. It was a clear day and there was no wind. The subjects of the experiment, completed the four motions by coming towards the radar starting from a range about 150 meters. The four types of motions were walking, running, creeping and crawling. From each person, three recordings were collected for walking and running and two recordings were collected for creeping and crawling. Information about the people whose radar signals were recorded is given in Table 9.

Table 9: Physical properties of subjects of the experiment

Person #	Gender	Age	Height (cm)
Person 1	Female	35-45	160-170
Person 2	Male	25-30	160-170
Person 3	Male	30-40	170-180
Person 4	Male	25-30	180-190
Person 5	Male	30-40	180-190

4.3 DATA PRE-PROCESSING FOR FEATURE EXTRACTION AND CLASSIFICATION EXPERIMENTS

Pulsed radar systems use multiple CPIs with different PRFs in order to solve ambiguities both in range and Doppler. In addition, this type of systems process the echo signal in the same range bin from all coherent pulses inside a single CPI in order to differentiate moving targets with radial velocities from stationary clutter.

Every target with different Doppler is the output of different Doppler filters so that targets can be differentiated from the stationary clutter. Stationary clutter is the output of the zero Doppler filter.

Obtaining data for micro-Doppler signatures from pulsed radars is more difficult compared to continuous wave radars. It is because of the fact that the return signal in CW radars is continuous Doppler signal while pulsed radars receives return echo energy in a number of range cells from a number of pulses. Therefore, in a pulsed radar, the required data is extracted by accumulating and processing echo return in each pulse of the CPI in the same range bin. However, since there are multiple CPIs with different PRFs in a typical pulsed ground surveillance radar, the echo in each CPI must be resampled to a fixed PRF that should be close to all CPI's PRFs. The resampling procedure in terms of PRI conversion can be seen on Figure 24. Radar return signal has same number of samples inside a CPI; however every CPI has different number of samples after resampling process. Still, since the CPIs are concatenated after resampling, this does not cause a problem for the next processing steps. As an example, Figure 25 and Figure 26 show the original and resampled raw data spectrograms of human walking motion. It can be seen on the spectrograms that there are some vertical spikes spread on frequency axis before resampling process. This is because of the discontinuities between the CPIs with different PRFs. In order to solve this problem, resampling is applied to the radar return signal. Original and resampled raw data spectrograms of the other three motion types, running, creeping and crawling, can be seen at Appendix B.

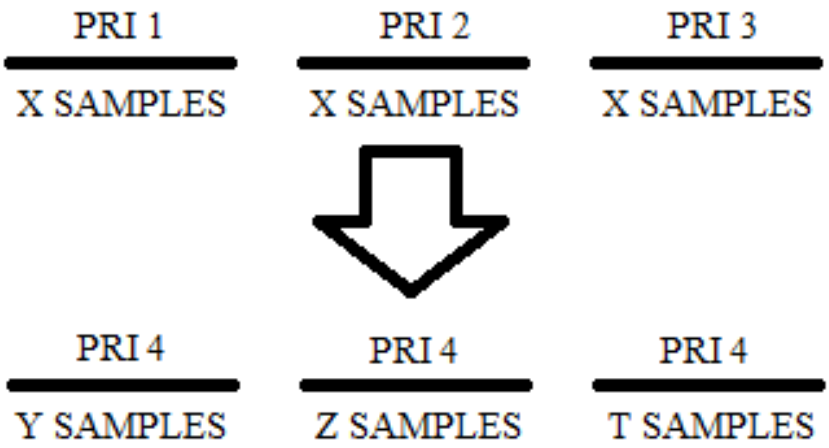

Figure 24: PRI conversion of radar data

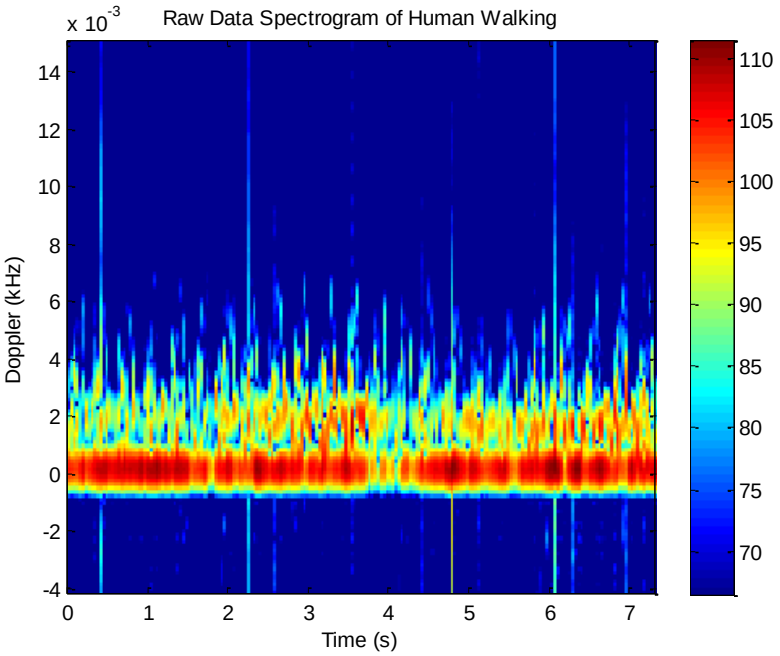

Figure 25: Original raw data spectrogram of walking

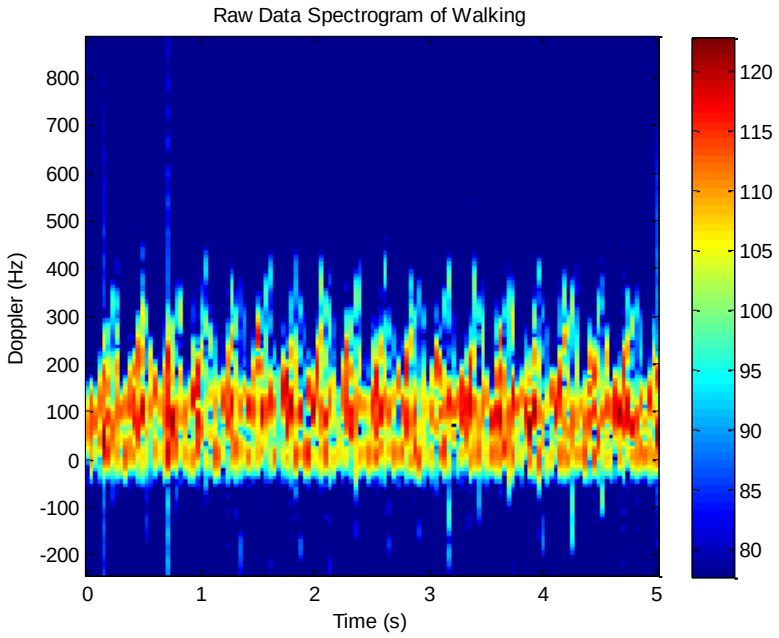

Figure 26: Resampled raw data spectrogram of walking with a constant PRF

After PRF conversion of consecutive CPIs, the pulses in each CPI are concatenated and filtered with a high pass filter in order to eliminate the stationary clutter in the signal. The high pass filter removes the signal content around zero Doppler frequency. Figure 27 shows the magnitude response of the high pass filter used for the processing. The cut-off frequency of the filter is 50 Hz. Since our frequency resolution due to the analysis window length is 50 Hz, removal of the frequency components below 50 Hz is not a problem. After clutter removal, signal vectors are extracted on a frame-by-frame basis with an analysis window of length 20 milliseconds and with a sliding window of one sample for data-driven feature extraction using PCA, and with a sliding window of 5 milliseconds for hidden Markov models experiments. The formula for extraction is given as:

$$\mathbf{x_k} = \left[x[(k-1)*M+1]\; x[(k-1)*M+2]\; x[(k-1)*M+3] \ldots\; x[(k-1)*M+L]\right]^T \qquad (9)$$

where M is the length of the sliding window (1 sample for data-driven feature extraction, 5 milliseconds for HMM), L is the length of the analysis window (20 milliseconds for PCA experiments), $\boldsymbol{x}[\boldsymbol{n}]$ is the high-pass filtered radar echo signal

and $\boldsymbol{x_k}$ is the signal vector for the k[th] frame. The extracted vectors are then written as the columns of a matrix $\boldsymbol{X}$. The matrix is then used for the data-driven feature extraction and classification purposes. $\boldsymbol{X}$ is obtained as;

$$\mathbf{X} = [\mathbf{x_1}\ \mathbf{x_2}\ \mathbf{x_3}\ \ldots \mathbf{x_N}] \tag{10}$$

where $\boldsymbol{N}$ is the total number of frames in all training sequences.

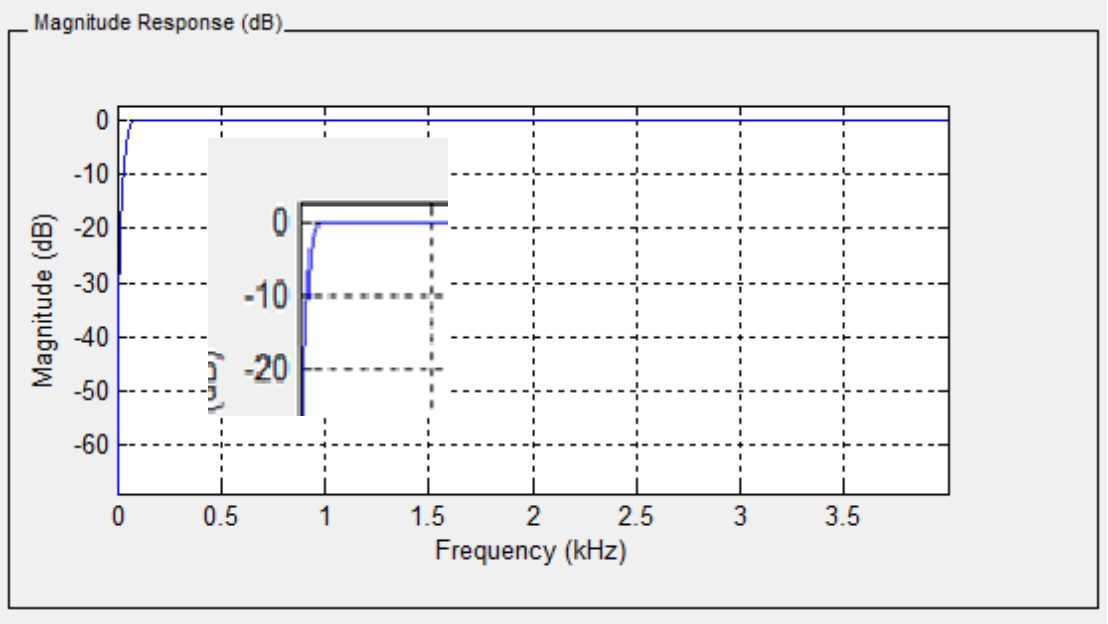

Figure 27: High pass filter used for clutter removal

For this experiment, 50 recordings from five different people are used for four types of human motion.

4.4 PRINCIPAL COMPONENT ANALYSIS FOR HUMAN MOTION MICRO-DOPPLER SIGNATURES

As it is discussed in the introduction, most of the studies on micro-Doppler signal processing are based on Fourier transform and investigation of spectrograms of different human movements [2-6]. In these studies, the features are extracted from spectrograms by various image based feature extraction methods [9], [17], [20]. In order to obtain spectrograms, STFT is used in these studies as the linear

transformation method. However, hidden Markov models (HMM) desires a number of uncorrelated features from the input signal with low dimension so that the joint probability density of the features can be modeled reliably. Therefore, Fourier coefficients are not the best features for HMM, since the coefficients are correlated and a large dimension is required to capture all important information of the input signal. As a result, basis vectors of PCA are calculated in order to generate the uncorrelated features of the input signal, which in turn allows reducing the workspace dimension.

Covariance matrix of the input signal is calculated as:

$$\boldsymbol{C} = \boldsymbol{X}\boldsymbol{X}^{\boldsymbol{H}} \tag{11}$$

After forming the covariance matrix, PCA generates eigenvectors with corresponding eigenvalues as discussed in Section 4.2 [29, 30]. Total energy of the eigenvalues is equal to the total energy of the vectors in $\boldsymbol{X}$. It is common knowledge that capturing at least 95% of the energy of the input signal is sufficient for classification purposes. Therefore, number of eigenvectors needed to capture highest variations of the input signal is determined by measuring the energy content of the eigenvalues. The eigenvalues are sorted from highest value to the lowest. Total number of largest eigenvalues, which covers 95% of the signal energy, is found. After the eigenvectors corresponding to selected eigenvalues are determined, these eigenvectors are written into a transformation matrix as the columns ($\boldsymbol{W}$ in (5)) for feature extraction. Total number of eigenvectors determines the dimension of the transformation, and hence dimension of the features.

PCA is initially applied to data from four different types of human motions separately. Energy percentage coverage using the accumulated largest eigenvalues vs. number of the accumulated eigenvalues is given between Figure 28 and Figure 31 for walking, running, creeping and crawling. It can be concluded from the figures that it is possible to cover at least 95% energy with six eigenvectors for running and walking, but with twenty eigenvectors for creeping and crawling. Hence, it is concluded that features of the input signal should be extracted by using twenty

eigenvectors with the largest eigenvalues of the covariance matrix. The eigenvectors are obtained by application of PCA to the data that includes all four types of human motion altogether.

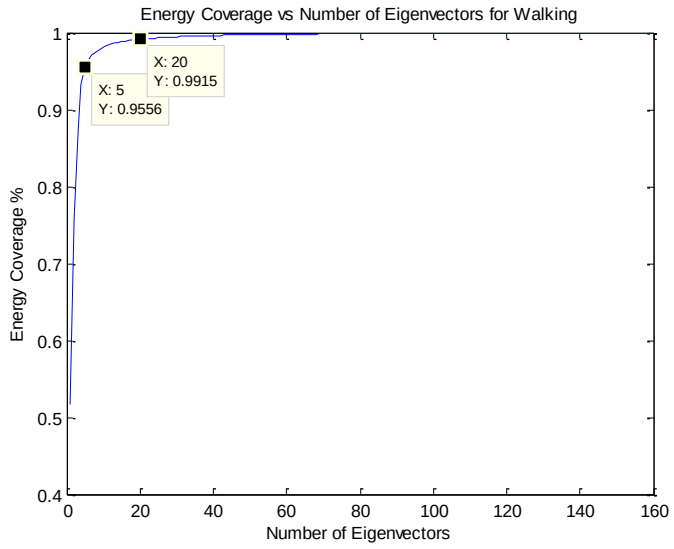

(a)

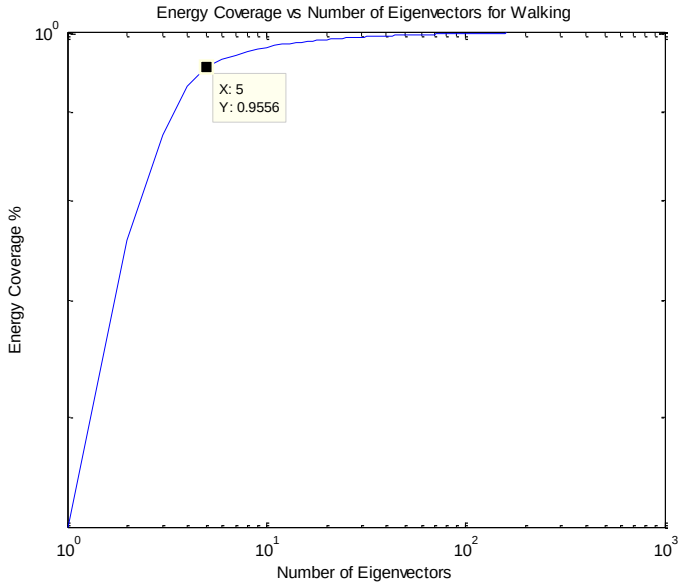

(b)

Figure 28: Energy coverage of eigenvectors for walking in linear scale (a) and log scale (b)

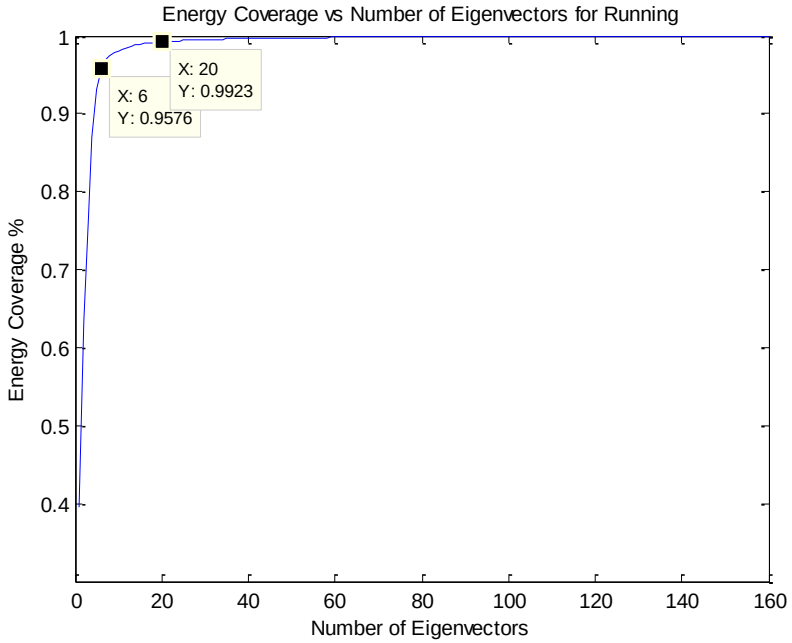

(a)

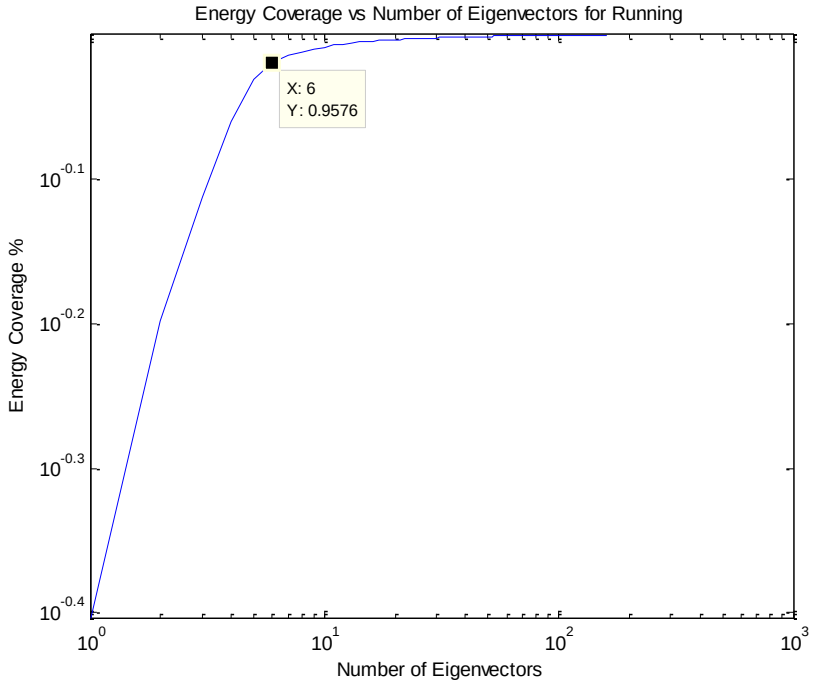

(b)

Figure 29: Energy coverage of eigenvectors for running in linear scale (a) and log scale (b)

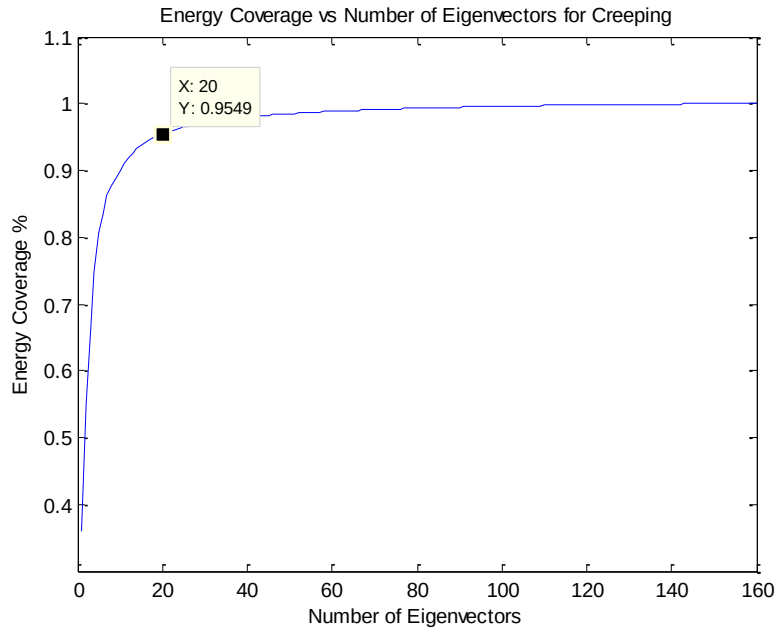

(a)

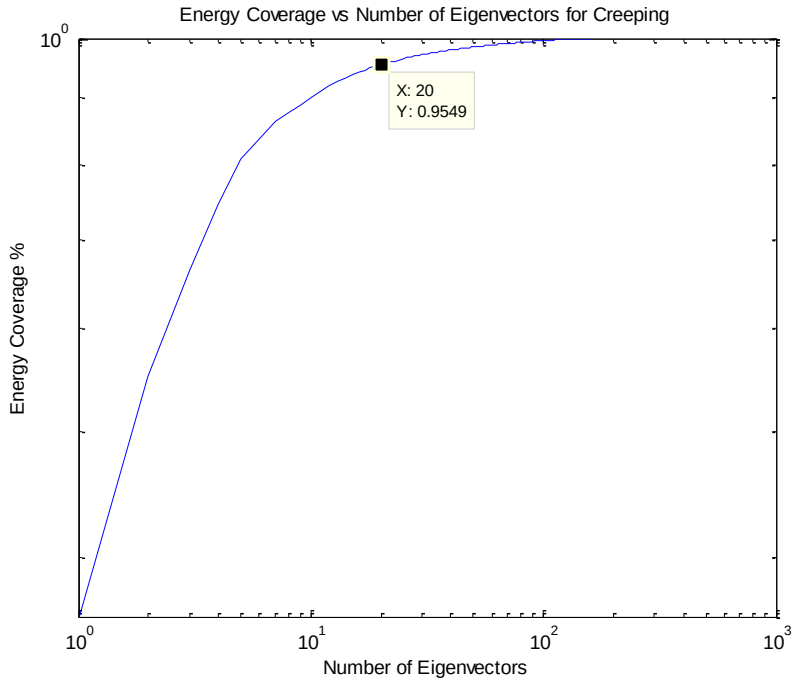

(b)

Figure 30: Energy coverage of eigenvectors for creeping in linear scale (a) and log scale (b)

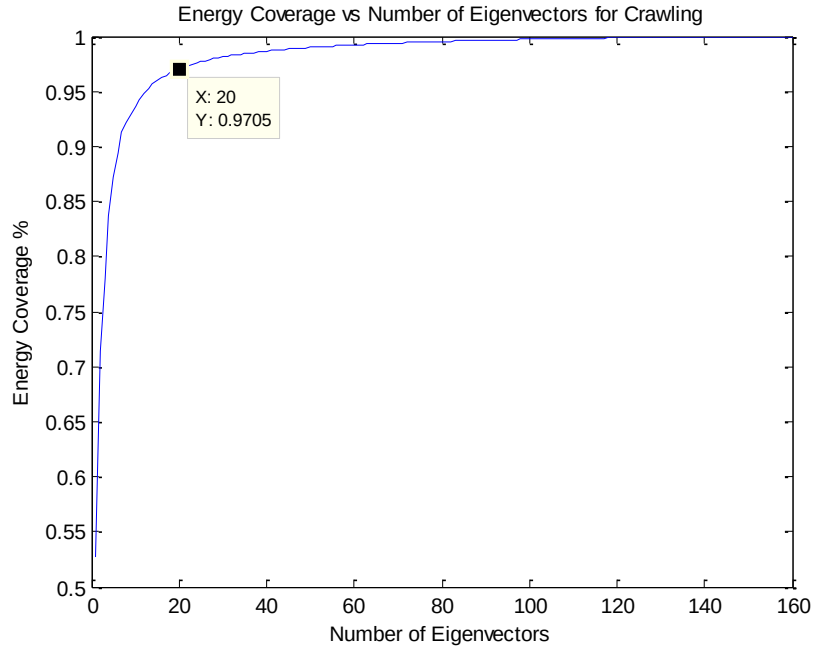

(a)

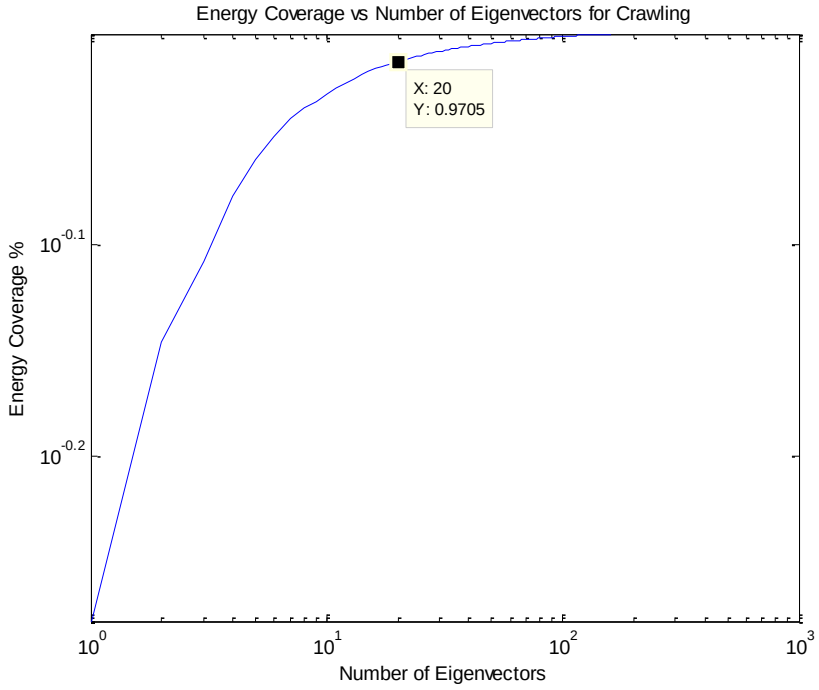

(b)

Figure 31: Energy coverage of eigenvectors for crawling in linear scale (a) and log scale (b)

After determining the number of eigenvectors, which corresponds to feature space dimension in other words, covariance matrix and eigenvectors through PCA are calculated for feature extraction. Figures 32-37 compare the DFTs of a Fourier Transform basis vector and the first three basis vector obtained by PCA. Figures that compares the fourth and fifth basis vectors are given in Appendix C. It can be concluded from the figures that PCA basis vectors covers multiple frequency components, while Fourier transform basis vectors cover only one frequency component as intended. That is why it is possible to capture highest variations of the input signal with a small number of dimensions using principal component analysis (PCA).

In order to obtain transformed coefficients for each frame, twenty eigenvectors with the largest eigenvalues are written into an eigenvector matrix **E** as columns. After that, the feature vectors to be used in HMM are extracted by projecting input frames onto the twenty eigenvectors as:

$$\hat{\boldsymbol{x}}_{\boldsymbol{k}} = \boldsymbol{E}^{\boldsymbol{T}}\boldsymbol{x}_{\boldsymbol{k}} \tag{12}$$

where $\boldsymbol{x}_{\boldsymbol{k}}$ is the k^{th} frame of the input signal and $\boldsymbol{E}$ is the matrix with twenty eigenvectors. Feature vectors for four different types of motions are determined separately.

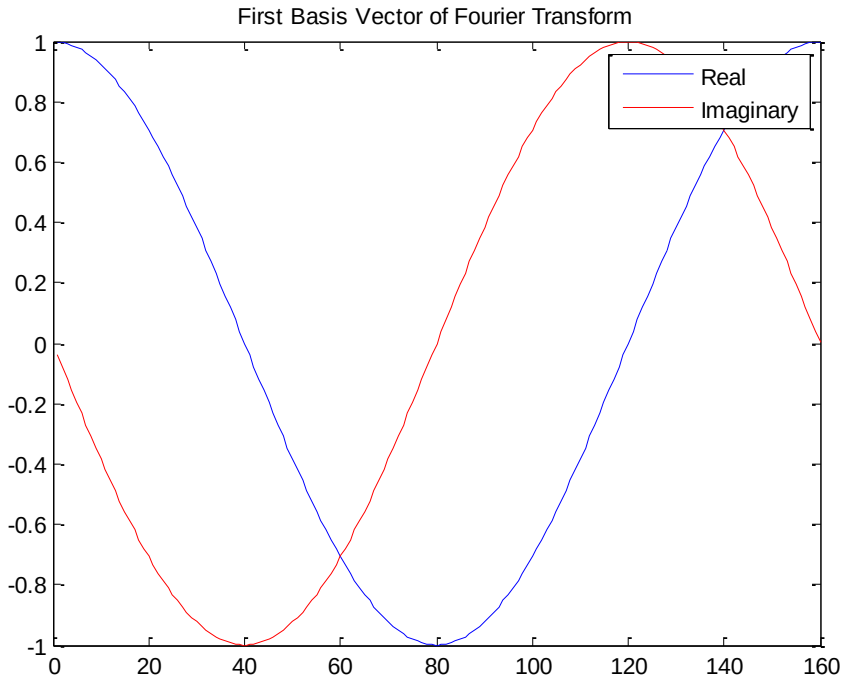

Figure 32: First basis vector of Fourier transform (time-domain)

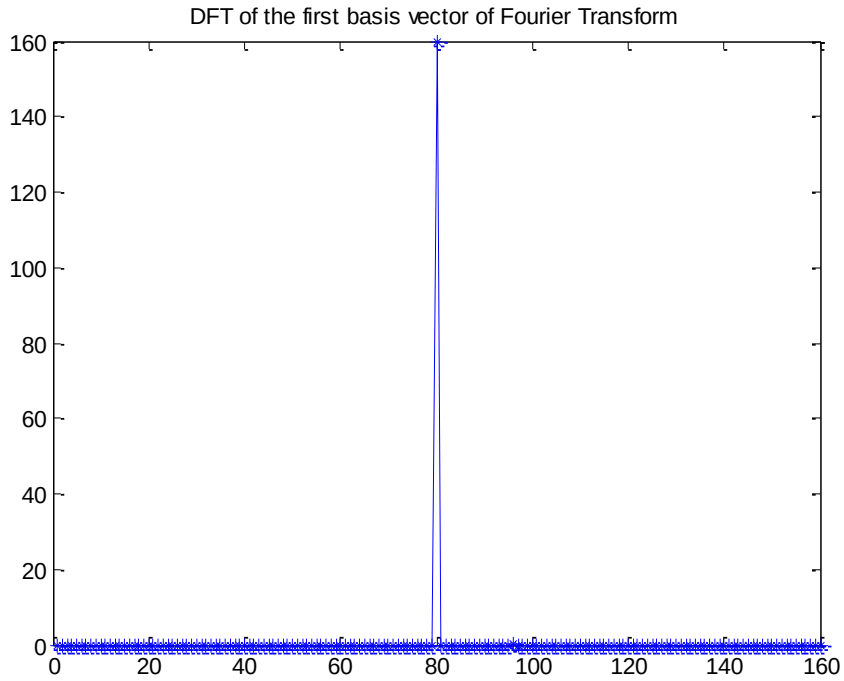

Figure 33: DFT of the first basis vector of Fourier transform

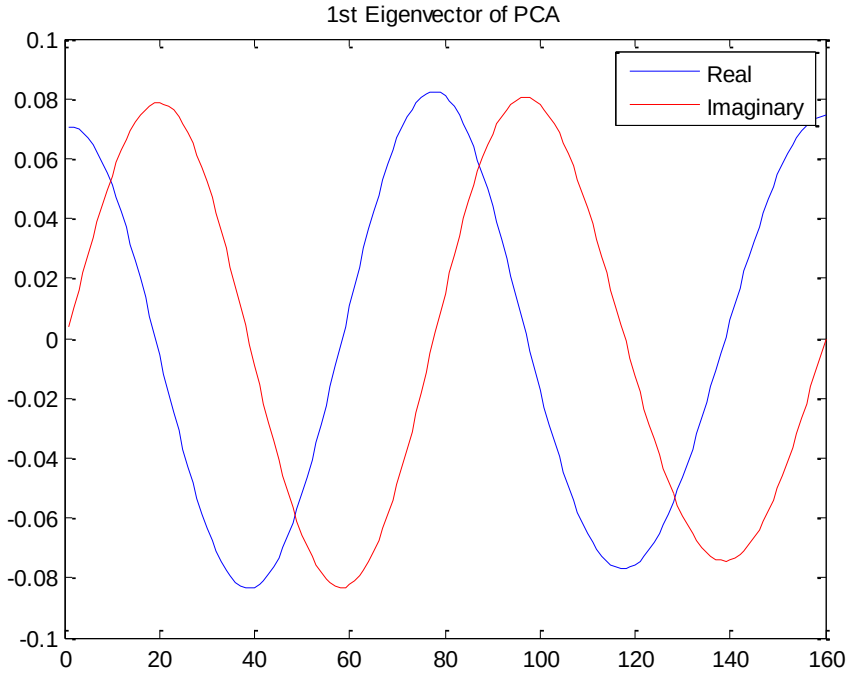

Figure 34: First basis vector of principal component analysis (time-domain)

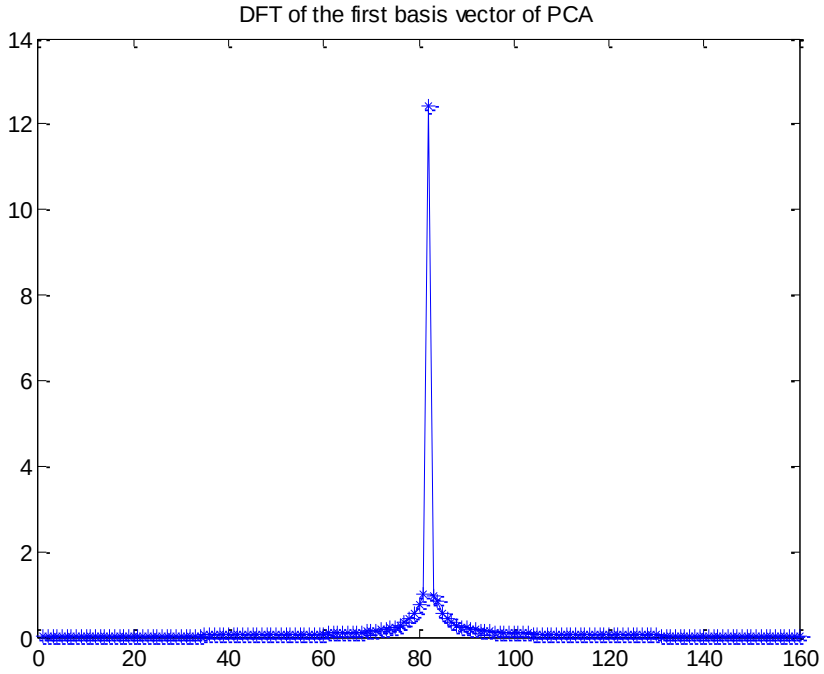

Figure 35: DFT of the first basis vector of principal component analysis

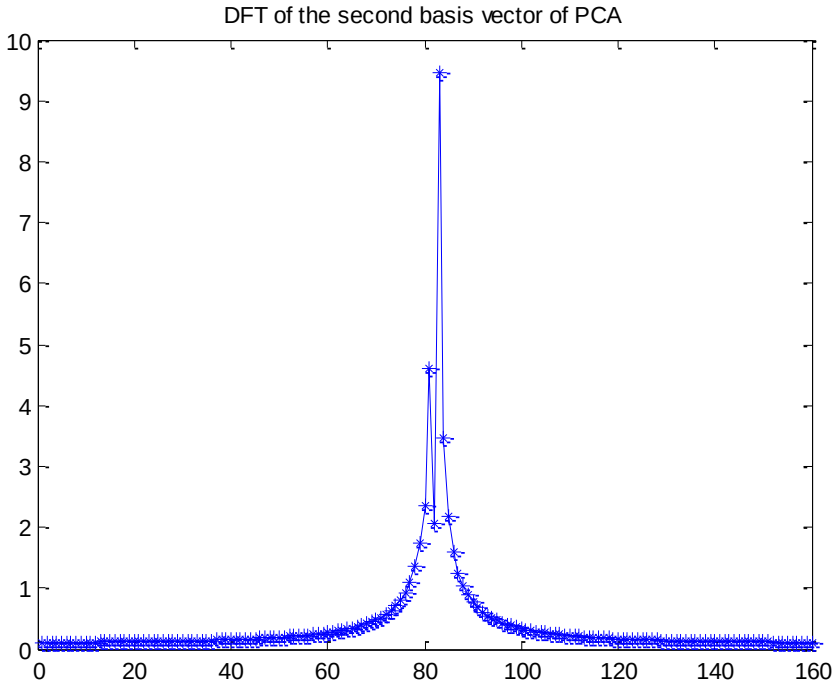

Figure 36: DFT of the second basis vector of principal component analysis

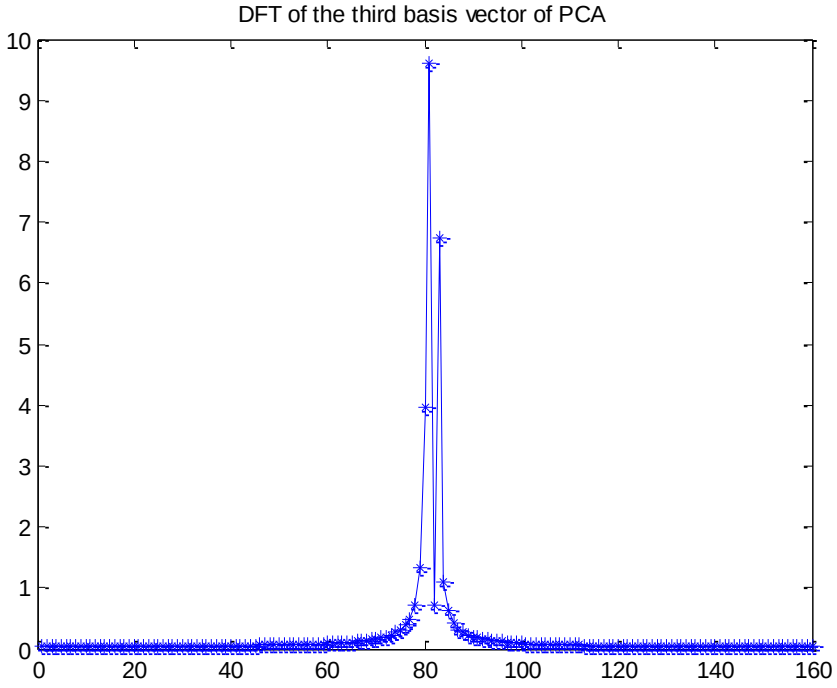

Figure 37: DFT of the third basis vector of principal component analysis

Since the extracted basis vectors with PCA cover 95% energy of the radar return signal, it is possible to reconstruct the original signal without significant loss. Figure 38 and Figure 39 show the spectrograms of original and reconstructed signal for human walking, respectively. Appendix C contains the spectrograms of reconstructed and original signals for other motions as well.

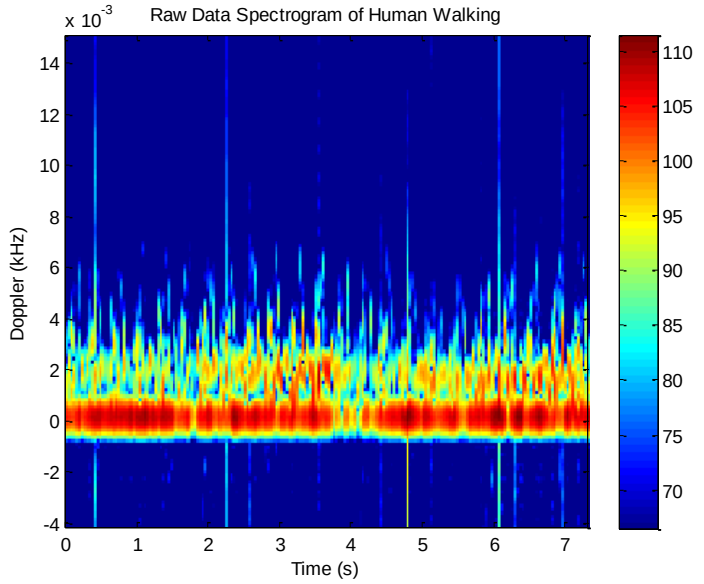

Figure 38: Original human walking signal

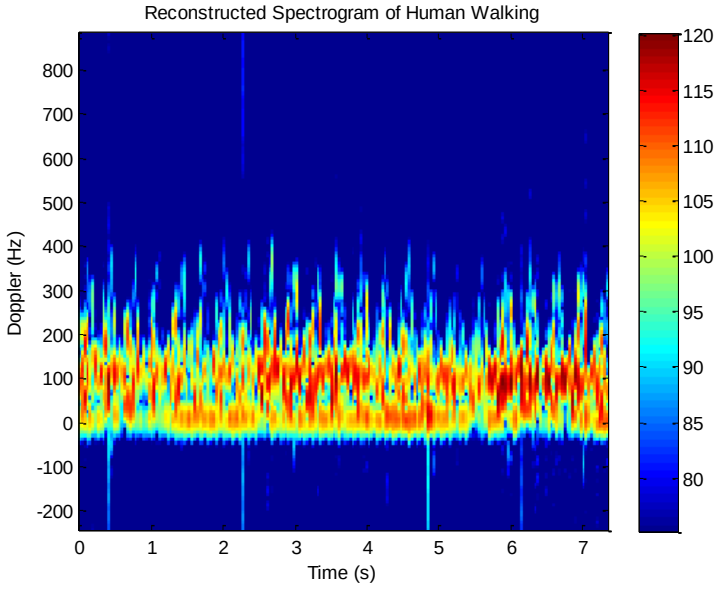

Figure 39: Reconstructed human walking signal

CHAPTER 5

CLASSIFICATION OF HUMAN MOTIONS USING HIDDEN MARKOV MODELS

Most human motions have cyclic nature, thus their micro-Doppler signatures are also expected to have periodic characteristics in time. As discussed in Chapter 2, a cycle of the motions can be considered as composed of a number of states. Although even same type of movement is slightly different for every single person, cycle of the same motion is similar in general. Therefore, cycle of the motions is desired to be modeled as states while variations of the movement both during the motion and from one person to another should be modeled as well. As hidden Markov models (HMM) are composed of non-observable states, and observations belonging to a state are modeled probabilistically, variations from one person to another can be modeled. Moreover, probabilistic modeling of state transitions gives the opportunity of modeling velocity difference caused by the movements of different people. Therefore, it is possible to model the human motions with hidden Markov models with states and transitions between states. In hidden Markov models, observations are assumed to be outcomes of a Markov process with hidden states [18].

This chapter presents background information about hidden Markov models and two classification experiments for human motions using micro-Doppler signatures. These two experiments provides insight about performance of the human dependent and human independent motion classification systems.

5.1 BACKGROUND INFORMATION ABOUT HIDDEN MARKOV MODELS

Hidden Markov model is a stochastic model that models the process as a number of non-observable states [18]. The model consists of initial state probabilities, transition

probabilities between the states and probabilities for observations belonging to a state. Every observation belongs to a state, and the next state for the next observation is determined by the multiplication of probability of transition between two states and probability of the next observation belonging to the next state. The models can also be used as classifiers when probability of the observation sequence given the model is calculated for each model, and the class whose model provides the largest probability is selected for the given input.

Through these properties, Hidden Markov models can model the variations inside the input signal and variations across different people. The parameters of the model for a particular class can be trained a signal for modeling and evaluation of model for a given input sequence can be implemented in real time [18]. A Hidden Markov model can be seen as a Markov model, except that the states cannot be observed directly. Instead, observations are statistically related to the states in the model [18].

It is defined in [18] that hidden Markov models is characterized by five basic elements;

1. N; number of states in the model. It is explained that although states are hidden, they are interconnected in a way that any state can be reached from any other state with a state transition probability (unless the transitions are restricted by forcing the state transition probability to zero).
2. M; number of different observations in each state. The observations are the physical outcomes of the system being modeled. It can be infinite for continuous observations.
3. $\boldsymbol{A} = \{a_{ij}\}$; the state transition probability from state i to state j. The matrix $\boldsymbol{A}$ involves all transition probabilities from one state to another.
4. $\boldsymbol{B} = \{b_j(k)\}$; probability of the observation belonging to the state j.
5. $\boldsymbol{\pi} = \{\pi_i\}$; initial state probability that the initial state is state i.

An example of a three state hidden Markov model is given in Figure 40.

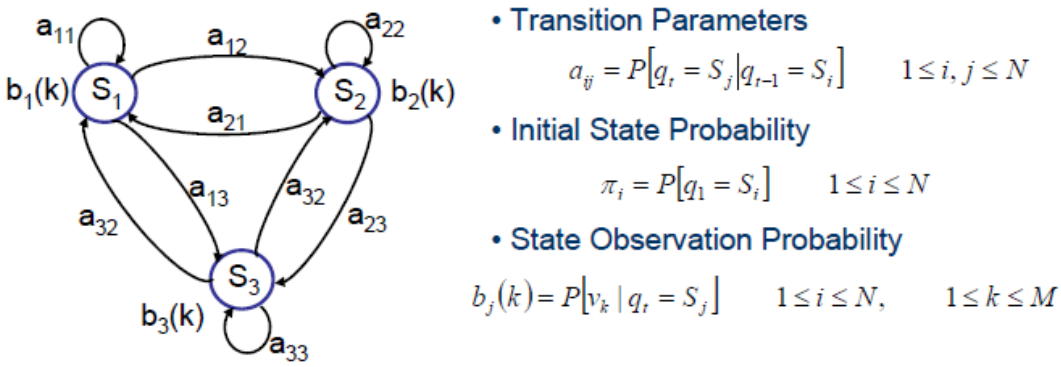

Figure 40: A three state HMM

Once suitable values for N, M, $\boldsymbol{A}$, $\boldsymbol{B}$ and $\boldsymbol{\pi}$ are chosen, hidden Markov models can be used to generate an appropriate observation sequence $\boldsymbol{O} = O_1 O_2 \dots O_T$.

The generation process for observation sequence is explained in [18] as five basic steps;

1. An initial state is chosen according to the initial state probability matrix $\boldsymbol{\pi}$.
2. Time is set as t = 1.
3. An observation O_t is chosen according to the observation probability $b_i(k)$ in state S_i.
4. A new state is chosen for $t = t + 1$ according to the state transition probabilities in matrix $\boldsymbol{A}$.
5. Time is set as $t = t + 1$ and iteration goes on from step 3 if $t < T$. Otherwise, the procedure is terminated and observation sequence is generated.

There are three basic problems that should be solved for hidden Markov models [18]. These are;

1. Evaluation problem: How can probability of observation sequence $P(\boldsymbol{O}|\boldsymbol{\lambda})$ be calculated given the model $\boldsymbol{\lambda} = (\boldsymbol{A}, \boldsymbol{B}, \boldsymbol{\pi})$?

2. State estimation problem: How can the state sequence $\boldsymbol{Q} = q_1 q_2 \dots q_t$ be chosen given the observation sequence $\boldsymbol{O} = O_1\, O_2 \dots O_T$ so that the sequence is the optimal one?
3. Training problem: How can the model parameters $\boldsymbol{\lambda} = (\boldsymbol{A}, \boldsymbol{B}, \boldsymbol{\pi})$ be adjusted to maximize $P(\boldsymbol{O}|\boldsymbol{\lambda})$?

Evaluation problem should be solved for HMM so that it can be used in real time solutions. Training problem and state estimation problem do not have to be solved in real time, but they should be solved for proper calculation of parameters.

5.1.1 EVALUATION PROBLEM

The first problem of HMM is the evaluation problem. It is desired to calculate the probability of observation sequence $\boldsymbol{O} = O_1\, O_2 \dots O_T$ given model $\boldsymbol{\lambda} = (\boldsymbol{A}, \boldsymbol{B}, \boldsymbol{\pi})$. The solutions for this problem are given as the straightforward method and forward-backward procedure [18].

5.1.1.1 THE STRAIGHTFORWARD METHOD

A state sequence is chosen where $\boldsymbol{Q} = q_1 q_2 \dots q_t$ and q_1 is the initial state and probability of the observation sequence $P(\boldsymbol{O}|\boldsymbol{Q}, \boldsymbol{\lambda})$ is calculated where;

$$P(\boldsymbol{O}|\boldsymbol{\lambda}) = \sum_{all\ Q}^{Q_t} P(\boldsymbol{O}|\boldsymbol{Q}, \boldsymbol{\lambda}) P(\boldsymbol{Q}|\boldsymbol{\lambda}) \tag{13}$$

$$= \sum_{all\ Q}^{Q_t} \pi_{q_1}\, b_{q_1}(O_1) a_{q_1 q_2} b_{q_2}(O_2) \dots\ a_{q_{T-1} q_T} b_{q_T}(Q_T)$$

For given observation sequence, probabilities of all possible state sequences are computed and most probable one is selected as the model states. The computational complexity of this method is $2TN^T$ where N is number of states and T is number of observations.

5.1.1.2 THE FORWARD-BACKWARD PROCEDURE

In this method, a forward variable $\alpha_t(i)$ is defined as the probability of the partial observation sequence $\boldsymbol{O} = O_1\, O_2 \ldots O_t$ until time t and state S_i at time t given the model $\boldsymbol{\lambda}$.

$$\alpha_t(i) = P(O_1\, O_2 \ldots O_t, q_t = S_i|\lambda) \tag{14}$$

The forward variable is solved inductively through three steps as initialization, induction and termination. The forward variable is computed until time T and probability of observation sequence is calculated as the following

$$Initialization: \alpha_1(i) = \pi_i b_i(O_1) \tag{15}$$

$$Induction: \alpha_{t+1}(j) = \left[\sum_{i=1}^{N} \alpha_t(i) a_{ij}\right] b_j(O_{t+1}) \tag{16}$$

$$Termination: P(O|\lambda) = \sum_{i=1}^{N} \alpha_T(i) \tag{17}$$

The backward procedure is applied in a similar manner with a backward variable starting from $t + 1$ as

$$\beta_t(i) = P(O_{t+1}\, O_{t+2} \ldots O_T |\, q_t = S_i|\lambda) \qquad t = T-1, T-2, ,1 \tag{18}$$

$$Initialization: \beta_T(i) = 1 \tag{19}$$

$$Induction: \beta_t(i) = \sum_{i=1}^{N} a_{ij}\, b_j(O_{t+1})\beta_{t+1}(j) \tag{20}$$

The computational cost of this method is $\boldsymbol{TN^2}$ where $\boldsymbol{N}$ is number of states and $\boldsymbol{T}$ is number of observations. Complexity of the first method increases exponentially according to the number of observations, which makes it non-feasible after a number of observations. However, computational cost of the second method increases

linearly with T, which makes it easier to compute. Therefore this method is preferable according to the first method in case of complexity.

5.1.2 STATE ESTIMATION PROBLEM

This problem interests in the solution of maximizing $P(\boldsymbol{O}, \boldsymbol{Q}|\boldsymbol{\lambda})$by finding the best state sequence $\boldsymbol{Q} = q_1 q_2 \dots q_t$. Viterbi algorithm can be used to find a tractable probable sequence formation.

5.1.2.1 VITERBI ALGORITHM

Viterbi algorithm is a recursive method to estimate the state sequence of Markov processes [31]. In general, this algorithm can be perceived as a solution to the problem of determining state sequence so that the probability of observation sequence of the Markov process becomes maximum. The algorithm flow can be expressed in three steps as in [32]. Probability of most probable path ending in state *j* at time t $(v_j(t))$ is calculated recursively using

$$v_j(t) = \max\left[v_i(t-1)a_{ij}\right]b_j(O_t) \qquad 1 \le i \le N \tag{21}$$

with the initialization

$$v_i(1) = \lambda_i b_i(O_1) \tag{22}$$

and termination

$$P = \max[v_i(T)] \qquad 1 \le i \le N \tag{23}$$

An example of the Viterbi algorithm for HMM is given in [32] for three states and three observations where $1 \le t \le 3$. There are three urns and two colors in each urn in the example. The purpose is to find the optimal state sequence given that the observation sequence is Red-Blue-Red. The probabilities for all paths are calculated and most probable path is selected as the state sequence. The purple path is the most probable path in the example with the highest probability as can be seen in Figure 41. As a difference in notation, w_j , p_{ij} and $e_j(O_t)$ represent the initial state probability,

transition probabilities and probability of observation belonging to a state respectively.

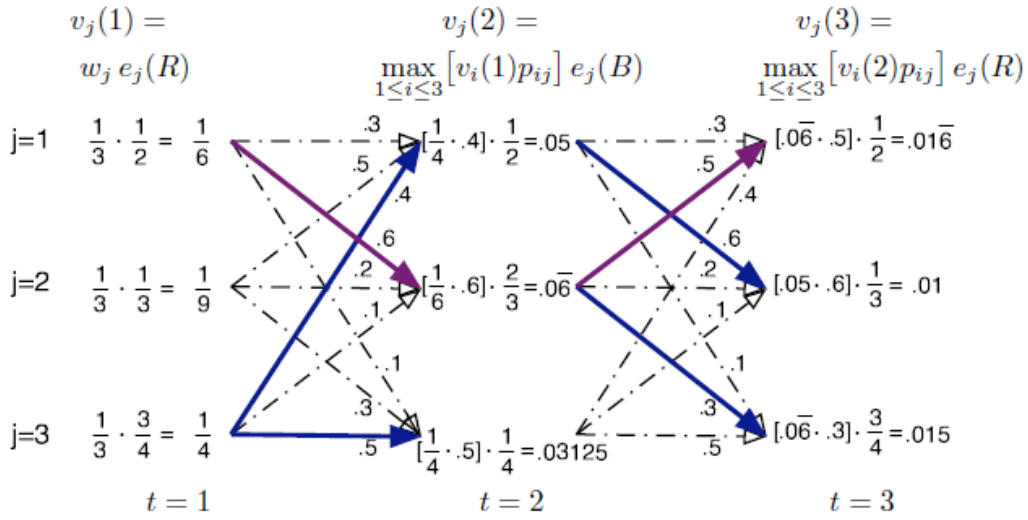

Figure 41: Viterbi algorithm example in [32]

5.1.3 TRAINING PROBLEM

The third problem of HMM is to adjust the model parameters $\boldsymbol{\lambda} = (\boldsymbol{A}, \boldsymbol{B}, \boldsymbol{\pi})$ so that $P(\boldsymbol{O}|\,\boldsymbol{\lambda})$ is maximized. Baum-Welch algorithm is used as an iterative method to determine the optimal model parameters as the solution to this problem.

5.1.3.1 BAUM-WELCH ALGORITHM

It is explained in [33] that Baum-Welch algorithm can be used train the parameters of the model. The algorithm is used to estimate the model parameters when the state sequence is not determined before. The parameters are chosen so that probability of the observation sequence given the model $P(\boldsymbol{O}|\,\boldsymbol{\lambda})$ is maximized. Flow of the algorithm is as the follows [33];

1. Initial values for the model are chosen randomly $\boldsymbol{\lambda} = (\boldsymbol{A}, \boldsymbol{B}, \boldsymbol{\pi})$.
2. Probable state paths are determined.
3. Model parameters are re-estimated according to the formulas below.

4. Convergence is checked (Either a threshold or numerical change in probability values between iterations can be controlled). If not converged, step 2, step 3 and step 4 are applied again until $P(\boldsymbol{O}|\,\boldsymbol{\lambda})$ is maximized.

As explained above, the algorithm starts working by randomly setting the parameters initially and continues by updating parameters until $P(\boldsymbol{O}|\,\boldsymbol{\lambda})$ is converged. In each iteration, model parameters are updated as follows [18]:

$$\pi' = number\ of\ times\ in\ state\ S_i at\ time\ t = 1 \tag{24}$$

$$a'_{ij} = \frac{number\ of\ transitions\ from\ state\ S_i to\ state\ S_j}{number\ of\ transitions\ from\ S_i} \tag{25}$$

$$b'_j(k) = \frac{number\ of\ times\ in\ state\ j\ and\ observing\ symbol\ v_k}{number\ of\ times\ in\ state\ j} \tag{26}$$

5.2 CLASSIFICATION EXPERIMENTS

In this study the data to be used with HMM is generated as follows: radar echo sequences are processed first on a frame-by-frame basis as explained in Chapter 3. Then, the signals are transformed onto another domain by using the eigenvectors as explained in Chapter 4 so that the features are uncorrelated and the dimension of input is reduced. The observation features are then concatenated from the successive frames in the whole sequence in order to form the observation sequence. After that, the observation sequence is used either for training or for testing purposes.

Kevin Murphy's HMM tool [19] is utilized in this study. The micro-dopplersignals extracted from the recorded data belong to one of the four different human motions; walking, running, creeping and crawling. Two classification experiments for human motions using micro-Doppler signatures are presented in this section. In the first experiment, recordings from five people are used for training and different recordings obtained from the same five people are used for testing. In the second

experiment, recordings from three people are used to train the models and recordings from two different people are used for testing purposes. These two experiments reveal the performance difference between the human dependent and human independent systems for this method of classification. Moreover, although it is expected that analysis window length of 20 milliseconds and 20 eigenvectors should give the best classification results, classification results for various different analysis window lengths and various different number of eigenvectors are also tested in both experiments. In addition, classification results for the cases where different feature vectors are used are presented for both experiments.

5.2.1 CLASSIFICATION EXPERIMENT 1

Human dependent experiment is performed using training and test sets formed by the recordings from the same people. The name "human dependent" is inspired from the “speaker-dependent speech recognition” systems. In this experiment, the HMM models are trained with 30 recordings from five different people in order to test the success rate of human dependent recognition system. The training set consists of 20 recordings for walking and running, 10 recordings for creeping and crawling. A separate hidden Markov model is trained for each of these four classes. After models are trained, feature sequences are extracted for each file in the test set. The classification is done by selecting the most likely model given the feature (observation) sequence. 10 recordings for walking and running, 10 recordings for creeping and crawling are reserved for testing purpose. Although the testing and training data are from the same people, different recordings are used for both. The experiment is repeated for four different combinations of the test and training sets.

As the first experiment, total number of states in an HMM model is investigated to best model the motions. Four different “number of states” configurations are tested for this purpose. Two and three state HMM are also tried; but they are not listed since the classification results were remarkably unsatisfactory. The classification results for four different “number of states” are given between Table 10 and Table 13. The tests with four, five, six and seven-state HMMs show that the four-state

HMM is the best choice for modeling and classification. Although both seven-state and four-state HMMs give the same classification performance, computational complexity of four state HMM is less. Table 14 shows the transition probabilities and initial state probabilities for the models with four states. The transition probability matrix includes the information about the probability of transition from one state to another in the model. Initial state probability vector represents the probability of the particular state to start the sequence.

Table 10: 7 state HMM classification results for classification experiment 1

Motion	Creeping	Crawling	Running	Walking
Creeping	20/20	0/20	0/20	0/20
Crawling	0/20	20/20	0/20	0/20
Running	0/20	0/20	20/20	0/20
Walking	0/20	0/20	0/20	20/20

Table 11: 6 state HMM classification results for classification experiment 1

Motion	Creeping	Crawling	Running	Walking
Creeping	20/20	0/20	0/20	0/20
Crawling	0/20	20/20	0/20	0/20
Running	0/20	0/20	19/20	1/20
Walking	0/20	0/20	1/20	19/20

Table 12: 5 state HMM classification results for classification experiment 1

Motion	Creeping	Crawling	Running	Walking
Creeping	20/20	0/20	0/20	0/20
Crawling	0/20	20/20	0/20	0/20
Running	0/20	0/20	19/20	1/20
Walking	0/20	0/20	1/20	19/20

Table 13: 4 state HMM classification results for classification experiment 1

Motion	Creeping	Crawling	Running	Walking
Creeping	20/20	0/20	0/20	0/20
Crawling	0/20	20/20	0/20	0/20
Running	0/20	0/20	20/20	0/20
Walking	0/20	0/20	0/20	20/20

Table 14: Transition matrices and initial state probabilities of 4 state HMM

Motion		Transition Matrix				Initial State Vector
		State 1	State 2	State 3	State 4	
Creeping	State 1	0.93	0.00	0.07	0.00	0.2
	State 2	0.00	0.76	0.12	0.12	0.2
	State 3	0.04	0.25	0.57	0.14	0.4
	State 4	0.08	0.10	0.01	0.81	0.2
Running	State 1	0.95	0.04	0.0	0.01	0.2
	State 2	0.02	0.78	0.01	0.19	0.4
	State 3	0.01	0.01	0.92	0.06	0.3
	State 4	0.01	0.20	0.04	0.75	0.1
Crawling	State 1	0.73	0.04	0.18	0.05	0.4
	State 2	0.02	0.81	0.17	0.00	0.4
	State 3	0.18	0.19	0.62	0.01	0
	State 4	0.05	0.00	0.04	0.91	0.2
Walking	State 1	0.77	0.02	0.17	0.04	0.4
	State 2	0.02	0.87	0.06	0.05	0.2
	State 3	0.14	0.05	0.78	0.03	0.1
	State 4	0.02	0.07	0.03	0.88	0.3

Some empirical observations can be stated on the state transition probabilities in Table 14. To illustrate, for the creeping, the first state does not communicate much with the others; but there is a communication between 2^{nd}, 3^{rd} and 4^{th} states. It seems that the first state does not carry much information about the creeping motion, and could be used to model the part of the recording before the motion begins. The same observation can be done for other motion types as well.

Classification is based on computing the log likelihood of the feature sequence belonging to models of four classes, and then, selecting the class with the largest log-likelihood. The classification outcomes for 20 test sequences for different analysis windows lengths and different number of eigenvectors used in transformation are given in Table 15 and Table 16. These results show that analysis window of 20 milliseconds and 20 eigenvectors used in transformation is the best choice for classification as expected. The classification results are worse when number of eigenvectors and/or length of analysis window change. When the number of eigenvectors are reduced, important information would be lost, which also affects classification performance. On the other hand, when window length changes, either signal within windows is more likely to be non-stationary (when the length of analysis window is increased) or frequency resolution becomes worse (when it is decreased). These changes worsen the classification results as seen on Table 15. Therefore, as it is expected, best results are obtained with analysis window length of 20 milliseconds and 20 eigenvectors to be used for feature extraction.

Table 15: Results of classification experiment 1 for various analysis window lengths

	Motion	Creeping	Crawling	Running	Walking
20ms Window 20 Eigenvectors	Creeping	20/20	0/20	0/20	0/20
	Crawling	0/20	20/20	0/20	0/20
	Running	0/20	0/20	20/20	0/20
	Walking	0/20	0/20	0/20	20/20
45ms Window 20 Eigenvectors	Creeping	18/20	2/20	0/20	0/20
	Crawling	2/20	18/20	0/20	0/20
	Running	0/20	0/20	19/20	1/20
	Walking	1/20	0/20	3/20	16/20
10ms Window 20 Eigenvectors	Creeping	15/20	3/20	0/20	2/20
	Crawling	1/20	19/20	0/20	0/20
	Running	0/20	0/20	18/20	2/20
	Walking	1/20	0/20	2/20	17/20

Table 16: Results of classification experiment 1 for various number of eigenvectors

	Motion	Creeping	Crawling	Running	Walking
20ms Window 20 Eigenvectors	Creeping	20/20	0/20	0/20	0/20
	Crawling	0/20	20/20	0/20	0/20
	Running	0/20	0/20	20/20	0/20
	Walking	0/20	0/20	0/20	20/20
20ms Window 5 Eigenvectors	Creeping	14/20	4/20	0/20	2/20
	Crawling	2/20	18/20	0/20	0/20
	Running	0/20	0/20	18/20	2/20
	Walking	1/20	0/20	3/20	16/20
20ms Window 10 Eigenvectors	Creeping	14/20	3/20	0/20	3/20
	Crawling	1/20	18/20	0/20	1/20
	Running	0/20	0/20	19/20	1/20
	Walking	0/20	0/20	1/20	19/20
20ms Window 25 Eigenvectors	Creeping	19/20	1/20	0/20	0/20
	Crawling	0/20	20/20	0/20	0/20
	Running	0/20	0/20	20/20	0/20
	Walking	0/20	0/20	0/20	20/20

The experiment is conducted with the features that are obtained after principal component analysis and transformation are applied to the input signal. The features are uncorrelated and they reduce the dimension from 160 samples to 20. In order to understand the effect of uncorrelated features on the final classification results, the features obtained by PCA are compared with the features obtained with an alternative orthogonal basis (obtained by multiplying the eigenvectors obtained by PCA with an orthogonal matrix which rotates the two successive PCA vectors by 15, 30 and 45 degrees as described below) and features calculated with the Fourier basis vectors, which are the rows of the DFT matrix which correspond to the low frequency terms.

It is well known that among all orthogonal bases, the PCA basis vectors are the only set of vectors decorrelating the input. In order have controlled experiments, we have used the rotated version of PCA vectors, which forms an alternate orthonormal basis without the decorrelated property. The rotated vectors are generated by Givens rotation matrices. The Givens rotations matrices are defined as;

$$\boldsymbol{G}(i,j,\theta) = \begin{bmatrix} 1 & \cdots & 0 & \cdots & 0 & \cdots & 0 \\ \vdots & \ddots & \vdots & \ddots & \vdots & \ddots & \vdots \\ 0 & \cdots & c & \cdots & s & \cdots & 0 \\ \vdots & \ddots & \vdots & \ddots & \vdots & \ddots & \vdots \\ 0 & \cdots & -s & \cdots & c & \cdots & 0 \\ \vdots & \ddots & \vdots & \ddots & \vdots & \ddots & \vdots \\ 0 & \cdots & 0 & \cdots & 0 & \cdots & 1 \end{bmatrix} \tag{27}$$

Here $c = \cos(\theta)$, $s = \sin(\theta)$ and $\boldsymbol{G}(i,j,\theta)\boldsymbol{M}$ results in the rotation of i'th and j'th columns vectors of $\boldsymbol{M}$ with θ degrees. The rotation operation is in the plane of i'th and j'th columns vectors. It is easy to see that $\boldsymbol{G}(i,j,\theta)^T\boldsymbol{G}(i,j,\theta) = \boldsymbol{I}$, hence $\boldsymbol{G}(i,j,\theta)$ is an orthogonal matrix.

The rotated PCA vectors are generated as follows:

$$\widehat{\boldsymbol{M}}(\theta) = \prod_{k=1}^{k=N-1} \boldsymbol{G}(k,k+1,\theta)\boldsymbol{M} \tag{28}$$

Here the columns of matrix $\boldsymbol{M}$ are the first N eigenvectors of the autocorrelation matrix (PCA vectors) and $\widehat{\boldsymbol{M}}(\theta)$ is an alternate basis formed implementing rotations in the plane of consecutive eigenvectors through $\boldsymbol{G}(k,k+1,\theta)$ matrix. We have chosen to have rotations in the plane of eigenvectors whose eigenvalues are similar to each other. This choice is made in order to generate an orthonormal basis, which is in some sense similar to the PCA basis.

It is intuitively clear that as the rotation degree increases, the columns of $\widehat{\boldsymbol{M}}(\theta)$, which is the alternative orthogonal basis, deviates from the columns $\boldsymbol{M}$, which is the PCA basis. To quantify the amount of deviation; we use the Hellinger distance. The

Hellinger distance is defined for the multivariate Normal distributions. The squared Hellinger distance between the distribution $P \sim N(\mu_1, \Sigma_1)$ and $Q \sim N(\mu_2, \Sigma_2)$ is defined as

$$H^2(P,Q) = 1 - \frac{|\boldsymbol{\Sigma_1}|^{\frac{1}{4}} \, |\boldsymbol{\Sigma_2}|^{\frac{1}{4}}}{\left|\frac{\boldsymbol{\Sigma_1} + \boldsymbol{\Sigma_2}}{2}\right|^{\frac{1}{2}}} \exp\{-\frac{1}{8}(\mu_1 - \mu_2)^T \left(\frac{\boldsymbol{\Sigma_1} + \boldsymbol{\Sigma_2}}{2}\right)^{-1} (\mu_1 - \mu_2)\} \quad (29)$$

For our case, $\boldsymbol{\Sigma_1}$ is the resultant correlation matrix for the vector $\boldsymbol{M^H x}$ (which is a diagonal matrix with N most dominant eigenvalues) and , Σ_2 is the resultant correlation matrix for the vector $\boldsymbol{\widehat{M}^H x}$, which is not a diagonal matrix as mentioned before.

The classification results are presented in Table 17. Results show that classification success rate gets worse when the features used in HMM are correlated as seen on the tables. Average success rate of FT coefficients, correlated PCA features for 45, 30, 15 degrees rotation of PCA basis vectors and uncorrelated PCA features are 85%, 94%, 96%, 96% and 100% respectively. The results are expected since probability density functions of the states and observations can be calculated more reliably with uncorrelated features as modeling is done with a small number of finite data set.

Table 17: Results of classification experiment 1 with non-orthogonal PCA vectors and Fourier transform coefficients

	Motion	Creeping	Crawling	Running	Walking	Success Rate
Orthogonal PCA Vectors	Creeping	20/20	0/20	0/20	0/20	
	Crawling	0/20	20/20	0/20	0/20	
	Running	0/20	0/20	20/20	0/20	
	Walking	0/20	0/20	0/20	20/20	100%
Alternative PCA Vectors (15 degrees rotation and Hellinger Dist: 0.7614)	Creeping	19/20	1/20	0/20	0/20	
	Crawling	0/20	20/20	0/20	0/20	
	Running	0/20	0/20	19/20	1/20	
	Walking	1/20	0/20	0/20	19/20	96%
Alternative PCA Vectors (30 degrees rotation and Hellinger Dist: 0.7930)	Creeping	19/20	0/20	0/20	0/20	
	Crawling	1/20	19/20	0/20	0/20	
	Running	0/20	0/20	19/20	1/20	
	Walking	0/20	0/20	0/20	20/20	96%
Alternative PCA Vectors (45 degrees rotation and Hellinger Dist: 0.8345)	Creeping	18/20	2/20	0/20	0/20	
	Crawling	1/20	19/20	0/20	0/20	
	Running	0/20	0/20	19/20	2/20	
	Walking	0/20	0/20	1/20	19/20	94%
FT Coefficients	Creeping	15/20	3/20	0/20	2/20	
	Crawling	3/20	17/20	0/20	0/20	
	Running	0/20	0/20	19/20	1/20	
	Walking	2/20	0/20	1/20	17/20	85%

5.2.2 CLASSIFICATION EXPERIMENT 2

Human independent experiment is perceived as both training and test sets are the recordings of different people. The name "human independent" is inspired from the speaker dependent speech recognition phenomenon in speech processing as in the first experiment. This experiment is more important since a classification system in real life would use micro-Doppler data obtained from anyone and the training would always be done with limited data. In this experiment, the system is trained with 30 recordings from three people in order to test the success rate of human independent recognition system. The training set consists of 18 recordings for walking and running, and 12 recordings for creeping and crawling. As in case for experiment 1, a

separate hidden Markov model is trained for each of these four classes. After modeling, features sequences obtained from the test sets are used for classification. The classification is done by selecting the most likely model according to the observation sequence. There are twelve recordings for walking and running, eight recordings for creeping and crawling for testing purpose. The test data are obtained from different two people. In experiment 1, training and test sets are formed from different recordings of five people. However in experiment 2, recordings for training and testing are obtained from different people. Through this way, how successful the system can generalize the four different movements is tested. The experiment is repeated for four different combinations of the test and training sets.

As in the first experiment, total number of states in an HMM model is examined to find the best choice for modeling. Four different "number of states" configurations are tested for this purpose. Two and three state HMM are also tried; but they are not listed since the classification results were remarkably unsatisfactory. The classification results for four different "number of states" are given between Tables 18 and 21. It is concluded from the results that a four state HMM is still the best choice for modeling four types of human movements on the average, although seven-state HMM gives better results only for running. A "four-state" model also reduces the computational complexity of the system. The result is expected from the outcome of the first experiment, since even if the data is changed, same types of movements are modeled. Therefore, it can be concluded that optimal state number for a movement is not data dependent. Table 22 shows the transition probabilities and initial state probabilities for the models with four states.

Table 18: 7 state HMM classification results for classification experiment 2

Motion	Creeping	Crawling	Running	Walking
Creeping	13/16	2/16	0/16	1/16
Crawling	2/16	14/16	0/16	0/16
Running	0/24	0/24	21/24	3/24
Walking	0/24	0/24	2/24	22/24

Table 19: 6 state HMM classification results for classification experiment 2

Motion	Creeping	Crawling	Running	Walking
Creeping	11/16	4/16	0/16	1/16
Crawling	4/16	15/16	0/16	0/16
Running	0/24	0/24	21/24	3/24
Walking	0/24	0/24	1/24	23/24

Table 20: 5 state HMM classification results for classification experiment 2

Motion	Creeping	Crawling	Running	Walking
Creeping	10/16	6/16	0/16	4/16
Crawling	0/16	16/16	0/16	0/16
Running	0/24	0/24	20/24	4/24
Walking	0/24	0/24	0/24	24/24

Table 21: 4 state HMM classification results for classification experiment 2

Motion	Creeping	Crawling	Running	Walking
Creeping	12/16	3/16	0/16	1/16
Crawling	0/16	16/16	0/16	0/16
Running	0/24	0/24	20/24	4/24
Walking	0/24	0/24	0/24	24/24

Table 22: Transition matrices and initial state probabilities of 4 state HMM

Motion		Transition Matrix State 1	State 2	State 3	State 4	Initial State Vector
Creeping	State 1	0.56	0.14	0.28	0.02	0.16
	State 2	0.01	0.87	0.00	0.12	0.16
	State 3	0.08	0.00	0.68	0.24	0
	State 4	0.27	0.09	0.06	0.58	0.68
Running	State 1	0.80	0.03	0.10	0.07	0.55
	State 2	0.12	0.79	0.02	0.07	0.11
	State 3	0.04	0.08	0.85	0.03	0
	State 4	0.03	0.05	0.03	0.89	0.34
Crawling	State 1	0.62	0.05	0.18	0.15	0.71
	State 2	0.07	0.76	0.11	0.06	0.16
	State 3	0.24	0.07	0.62	0.07	0.13
	State 4	0.08	0.01	0.18	0.73	0
Walking	State 1	0.75	0.07	0.1	0.07	0.45
	State 2	0.04	0.90	0.00	0.06	0.11
	State 3	0.09	0.00	0.89	0.02	0.11
	State 4	0.04	0.05	0.03	0.88	0.33

Some empirical observations can be stated on the state transition probabilities in Table 22. To illustrate, for crawling, every state has communication with each other. This is expected since human motion has a cyclic nature in time and the transitions between states show that HMM can model the motion well.

As in the first experiment, a four state HMM is used for classification purpose. Classification results can be seen on Table 23 and Table 24. Similarto the first experiment, analysis window length of 20 milliseconds and 20 eigenvectors configuration gives the best classification results. Change in number of eigenvectors and analysis window length makes the classification results worse. Moreover, the

rate of success decreases in this experiment compared to the first experiment in general. This is expected, since it is very hard to capture all variations of a motion with the recordings from only three people. Still, even if the training data is very limited, it is possible to capture enough variation especially for walking and crawling. On the other hand, it is expected that classification results for running and creeping can be improved if the amount of training data is increased with data from more people so that the variations are captured properly.

Table 23: Results of classification experiment 2 for various analysis window length

	Motion	Creeping	Crawling	Running	Walking
20ms Window 20 Eigenvectors	Creeping	12/16	3/16	0/16	1/16
	Crawling	0/16	16/16	0/16	0/16
	Running	0/24	0/24	20/24	4/24
	Walking	0/24	0/24	0/24	24/24
45ms Window 20 Eigenvectors	Creeping	8/16	4/16	0/16	4/16
	Crawling	1/16	15/16	0/16	0/16
	Running	0/24	0/24	20/24	4/24
	Walking	1/24	0/24	3/24	20/24
10ms Window 20 Eigenvectors	Creeping	1/16	8/16	0/16	7/16
	Crawling	1/16	15/16	0/16	0/16
	Running	0/24	0/24	23/24	1/24
	Walking	1/24	0/24	3/24	20/24

Table 24: Results of classification experiment 2 for various number of eigenvectors

	Motion	Creeping	Crawling	Running	Walking
20ms Window 20 Eigenvectors	Creeping	12/16	3/16	0/16	1/16
	Crawling	0/16	16/16	0/16	0/16
	Running	0/24	0/24	20/24	4/24
	Walking	0/24	0/24	0/24	24/24
20ms Window 5 Eigenvectors	Creeping	0/16	8/16	0/16	8/16
	Crawling	2/16	14/16	0/16	0/16
	Running	1/24	0/24	15/24	8/24
	Walking	1/24	0/24	4/24	19/24
20ms Window 10 Eigenvectors	Creeping	9/16	3/16	0/16	4/16
	Crawling	2/16	14/16	0/16	0/16
	Running	0/24	0/24	20/24	4/24
	Walking	0/24	0/24	1/24	23/24
20ms Window 25 Eigenvectors	Creeping	13/16	2/16	0/16	1/16
	Crawling	0/16	16/16	0/16	0/16
	Running	0/24	0/24	20/24	4/24
	Walking	0/24	0/24	1/24	23/24

Effectiveness of the uncorrelated features is also investigated as in the first experiment. Correlated features in the second experiment are obtained through the same way as in the first experiment. The results when correlated feature vectors are modeled are given in Table 25. Classification success rate gets worse when the features used in HMM are correlated as in the first experiment. Average success rate of FT coefficients, correlated PCA features for 45, 30, 15 degrees rotation of PCA basis vectors, and uncorrelated PCA features are 74%, 83%, 83%, 88% and 90%, respectively. The results are expected since probability density functions of the states and observations can be calculated reliably with uncorrelated features, and as model parameters are trained with a small number of training data.

Table 25: Results of classification experiment 2 with non-orthogonal PCA vectors and Fourier transform coefficients

	Motion	Creeping	Crawling	Running	Walking	Success Rate
Orthogonal PCA Vectors	Creeping	12/16	3/16	0/16	1/16	
	Crawling	0/16	16/16	0/16	0/16	
	Running	0/24	0/24	20/24	4/24	
	Walking	0/24	0/24	0/24	24/24	90%
Alternative PCA Vectors (15 degrees rotation and Hellinger Dist: 0.7614)	Creeping	12/16	2/16	0/16	2/16	
	Crawling	1/16	15/16	0/16	0/16	
	Running	0/24	0/24	20/24	4/24	
	Walking	0/24	0/24	1/24	23/24	88%
Alternative PCA Vectors (30 degrees rotation and Hellinger Dist: 0.7930)	Creeping	11/16	3/16	0/16	2/16	
	Crawling	2/16	14/16	0/16	0/16	
	Running	0/24	0/24	20/24	4/24	
	Walking	1/24	0/24	2/24	21/24	83%
Alternative PCA Vectors (45 degrees rotation and Hellinger Dist: 0.8345)	Creeping	11/16	3/16	0/16	2/16	
	Crawling	3/16	13/16	0/16	0/16	
	Running	0/24	0/24	19/24	5/24	
	Walking	0/24	0/24	1/24	23/24	83%
FT Coefficients	Creeping	10/16	5/16	0/16	1/16	
	Crawling	5/16	11/16	0/16	0/16	
	Running	0/24	0/24	18/24	6/24	
	Walking	1/24	0/24	3/24	20/24	74%

5.2.3 CONCLUSION FROM THE EXPERIMENTS

It is concluded from the experiments that selection of 20 milliseconds analysis window length and transformation of the signal with 20 eigenvectors give the best classification results as expected. Four-state HMM is also found to be the best among other HMMs especially in terms of computational complexity. The experiments show that the test sequences can be classified perfectly when training set and test sequences are takes from the same people. Although success rate decreases slightly for human independent case, the results are still very promising. It is expected that the success rate would be increased for this case when training set can be enlarged to model all the variations of the movements. These results also show that uncorrelated

feature can provide better classification accuracy although only slightly. However, the experiments also show that the more the features are correlated, the worse the classification accuracy gets. Therefore, it is always best to use uncorrelated feature in HMM.

CHAPTER 6

CONCLUSIONS

This study shows that typical human motions can be classified by using the micro-Doppler signatures. The following gives the conclusions obtained from the study.

- Each human motion has distinct micro-Doppler signatures. The difference between different motions can be visually observed in the spectrogram of Doppler signals of the radar returns.
- The selection of analysis window length is important when processing a time domain signal on a frame-by-frame basis. Analysis window length is desired to be as long as possible for better frequency resolution, but a long analysis window may result in frequency smearing inside the analysis window, especially when a single frequency component makes a large change inside the window. A poor analysis window choice is shown to affect the classification performance.
- Based on the analysis of human walking simulation, an analysis window length of 20 milliseconds is determined to be the best selection for the investigation of the time domain Doppler return signal for human walking, running, creeping and crawling.
- After reviewing the literature, it is observed that most of the micro-Doppler studies are based on investigation of micro-Doppler spectrograms obtained by periodic application of Fourier transformation on a frame-by-frame basis. Use of all FFT basis vectors is needed in FFT based experiments as all frequency components may carry information. Therefore, dimension of the workspace can not be reduced, and therefore, it is difficult to capture vital statistics of the signal from limited training data.

- Eigenvectors obtained by PCA can be used for transformation of the time-domain signal so that uncorrelated features of the instantaneous properties of the radar echo can be obtained. Hence, PCA based dimensionality reduction has the advantage of capturing the vital signal characteristics at the lowest dimension possible.
- It is observed that all four type of human motions can be represented with 20 eigenvectors while preserving at least 95% energy of signal space by principal component analysis (PCA). It is also observed that the resulting eigenvectors with relatively large eigenvalues usually cover multiple frequency components on the frequency domain at the same time, which indicates heavy correlation between individual frequency components.
- Experiments with hidden Markov model (HMM) proved that human motions can be classified efficiently with a HMM based classifier. Experiments show that a four-state HMM is found to successfully model all variations within the motions. According to the results of the experiments, it is possible to differentiate between four different human motions with high accuracy both for human dependent and human independent cases. The experiments show that human motions can be classified with an accuracy of 100% for human dependent case (i.e. training and testing set contains data from same people) and 90% for human independent case (i.e. training and testing set contains data from different people). This result shows that it is possible to generalize the human motions with training data obtained from a small number of people. This is one of the most important findings in this thesis since a classifier to be used in an actual radar system can not be trained with data from everyone.
- It is observed from the experiments that classification success rate increases when the system is trained and tested with uncorrelated features.
- When trained with a true and rich training set, hidden Markov model (HMM) is expected to be an excellent classifier for differentiating the human motions.

Future Research Directions:

- The study can be extended with the inclusion of some other operational scenario dependent parameters, such as SNR, clutter, etc.
- The success of proposed method can be examined for walking, running, creeping and crawling motions at different aspect angles and speed.
- This study can be extended for other types of motions such as boxing, jogging, walking carrying an object with one or two hands, etc.
- Robustness of the feature extraction through PCA can be investigated with low SNR data.
- The success of HMM based classifier can be investigated further by examining the sequence of state transitions for a specific motion in order to attach a physical attribute the state definitions.
- As human motions are cyclic and HMM models the human motions with a number of states, imposing cyclic transition constraint on HMM model through limiting the transitions between the states can be investigated.
- For the human independent case, effect of using a larger training set on classification performance can be investigated. It is expected that a larger training database would capture more variations in the motions, and hence, would improve the classification results.

REFERENCES

[1] Skolnik Merrill I., Introduction to Radar Systems, McGraw-Hill Book Company, 1981

[2] Chen V.C., "The Micro Doppler Effect in Radar", Artech House, 2011

[3] Chen V.C., Li F., Ho S., Wechsler H., "MicroDoppler Effect in Radar Phenomenon Model and Simulation Study", IEEE Transactions on Aerospace and Electronic Systems, 2006

[4] Chen V.C., "Analysis of Radar Micro-Doppler signature with Time Frequency Transform", Proc of the Tenth IEEE Workshop on Statistical Signal and Array Processing, 2000

[5] Thayaparan T., Abrol S., Riseborough E., Stankovic L., Lamothe D., Duff G., "Analysis of Radar MicroDoppler Signatures from Experimental Helicopter and Human Data", IET Radar, Sonar & Navigation, pp. 289-299, 2007

[6] Tahmoush D., Silvious J., "Radar Micro-Doppler for Long Range Front-View Gait Recognition", IEEE 3rd International Conference on Biometrics: Theory, Applications and Systems, 2009

[7] Otero M., "Application of a continuous wave radar for human gait recognition," SPIE, vol. 5809, pp. 538-548, 2005

[8] Vignaud L., Ghaleb A., Kernee J. L., "Radar high resolution range & micro-Doppler analysis of human motions," International Radar Conference, pp. 1-6, 2009

[9] Youngwook K., Hao L., "Human Activity Classification Based on Micro-Doppler Signatures Using an Artificial Neural Network," IEEE Antennas and

Propagation Society International Symposium, 2008

[10] Dorp P.v., Groen F. C. A., “Feature-Based Human Motion Parameter Estimation with Radar,” IET, vol. 2, pp. 135-145, 2008

[11] Pan F., Wang J., Lin X., “Feature Extraction Algorithm Based on K Nearest Neighbor Local Margin”, Chineese Conference on Pattern Recognition , CCPR 2009

[12] Xiao B., “Principal Component Analysis for Feature Extraction of Image Sequence”, International Conference on Computer and Telecommunication Technologies in Agriculture Engineering (CCTAE), 2010

[13] Smith L.I. “A Tutorial on Principal Component Analysis”, 2002

[14] Youngwook K., Hao L., “Human Activity Classification Based on Micro-Doppler Signatures Using a SVM,” IEEE Transactions on Geoscience and Remote Sensing, 2009

[15] Lei J., Lu C, “Target Classification Based on Micro-Doppler Signatures,” IEEE Radar Conference, pp. 179-183, 2005

[16] Smith G. E., Woodbridge K., Baker C. J., “Micro-Doppler Signature Classification,” International Conference on Radar, CIE’06, pp. 1-4, 2006

[17] Li J., Phung S.L., Tivive F.H.C., Bouzerdoum A. “Automatic Classification of Human Motions using Doppler Radar”, The 2012 International Joint Conference on Neural Networks (IJCNN), 2012

[18] Rabiner L.R. “A Tutorial on Hidden Markov Models and Selected Applications in Speech Recognition”, Proc of the IEEE, v:77, issue:2, 1989

[19] Murphy K., “Hidden Markov Model (HMM) Toolbox for MATLAB”,

https://www.cs.ubc.ca/~murphyk/Software/HMM/hmm.html, 2005

[20] Alemdaroğlu Topuz Ö., Candan Ç., Koç S., "The Radar Application of Micro Doppler Features from Human Motions", IEEE Radar Conference, 2015

[21] Tahmoush D., “Review of Micro-Doppler Signatures”, IET Radar, Sonar & Navigation, 2015

[22] Björklund S., Petersson H., Hendeby G., "Features for micro-Doppler based activity classification", IET Radar, Sonar & Navigation, 2015

[23] Balleri A., Chetty K., Woodbridge K., "Classification of personnel targets by acoustic micro-Doppler signatures", IET Radar, Sonar & Navigation, 2011

[24] Liu L., Popescu M., Skubic M., Yardibi T., Cuddihy P., "Automatic Fall Detection Based on Doppler Radar Motion Signature", IEEE 5th International Conference on Pervasive Computing Technologies for Healthcare (Pervasive Health), 2011

[25] Harmanny R., Wit J.J.M., Cabic G.P., "Radar Micro-Doppler Feature Extraction Using the Spectrogram and Cepstrogram", European Radar Conference, 2014

[26] Molchanov P., Astola J., Egiazarian K., Totsky A., "Classification of ground moving radar targets by using joint time-frequency analysis", IEEE Radar Conference, 2012

[27] McDonald M., "Discrimination of human targets for radar surveillance via micro-Doppler characteristics", IET Radar, Sonar & Navigation, 2015

[28] Bilik I., Tabrikian J., Cohen A., "GMM-Based Target Classification for Ground Surveillance Doppler Radar", IEEE Transactions on Aerospace and Electronic Systems, 2006

[29] University of Illinois at Urbana-Champaign, “Principal Component Analysis”, CS 498 Lecture Notes

[30] Roweis S., “EM Algorithms for PCA and SPCA”, Neural Information Processing Systems, 1998

[31] Forney G., "The Viterbi Algorithm", Proc. of the IEEE, v.61, No. 3, 1973

[32] Cornell University, "Hidden Markov Models and the Viterbi algorithm", CS 295 Lecture Notes

[33] Hoberman R., "HMM Lecture Notes", Carnegie Mellon University Computational Genomics and Molecular Biology lecture notes, 2006

[34] Padar M.O., Ertan A.E., Candan Ç., "Classification of Human Motion Using Radar Micro-Doppler Signatures With Hidden Markov Models", IEEE Radar Conference, 2016

[35] G. Güvensen, C. Candan, S. Koç, U. Orguner, "On Generalized Eigenvector Space For Target Detection in Reduced Dimensions," IEEE Radar Conference, 2015

[36] Bar-Shalom Y., Osborne R., Willett P., Daum F., “Robust PCA micro-Doppler classification using SVM on embedded systems”, IEEE Transactions on Aerospace and Electronic Systems, 2014

[37] Fioranelli F., Ritchie M., Griffiths H., “Classification of Unarmed/Armed Personnel Using the NetRAD Multistatic Radar for Micro-Doppler and Singular Value Decomposition Features”, IEEE Geoscience and Remote Sensing Letters, 2015

APPENDIX A

Appendix A includes the graphs of spectrograms of simulated CW radar signals obtained from human body parts during walking motion, and Doppler frequency graphs of the limbs during a walking cycle.

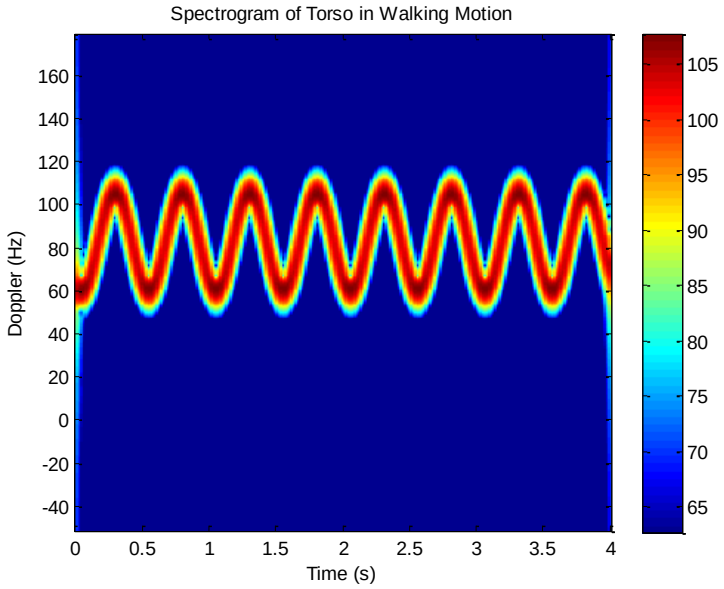

Figure 42: Spectrogram of simulated Doppler shift of torso

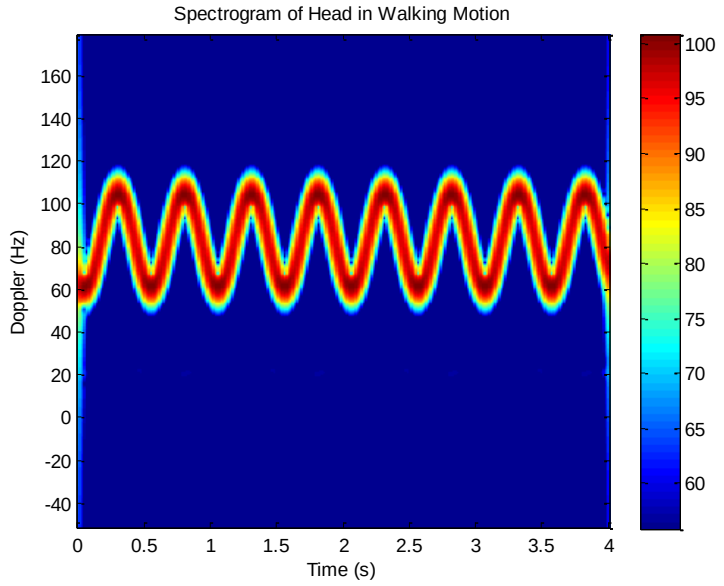

Figure 43: Spectrogram of simulated Doppler shift of head

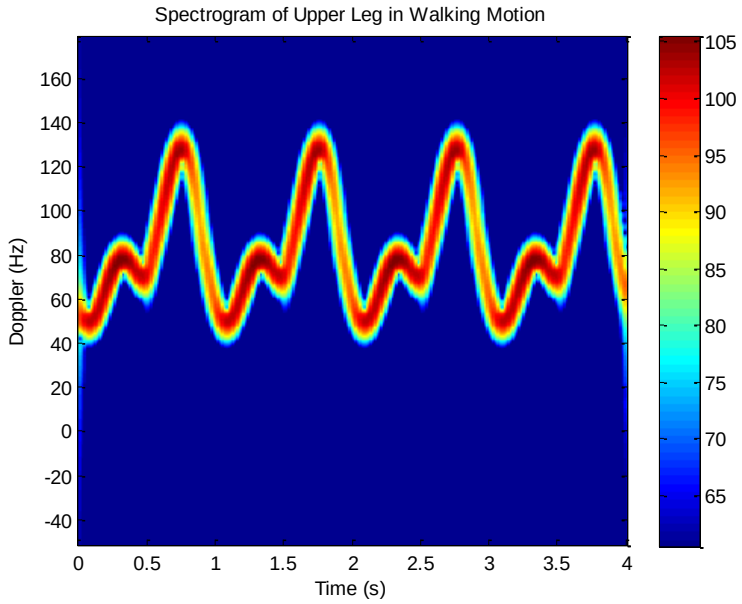

Figure 44: Spectrogram of simulated Doppler shift of upper leg

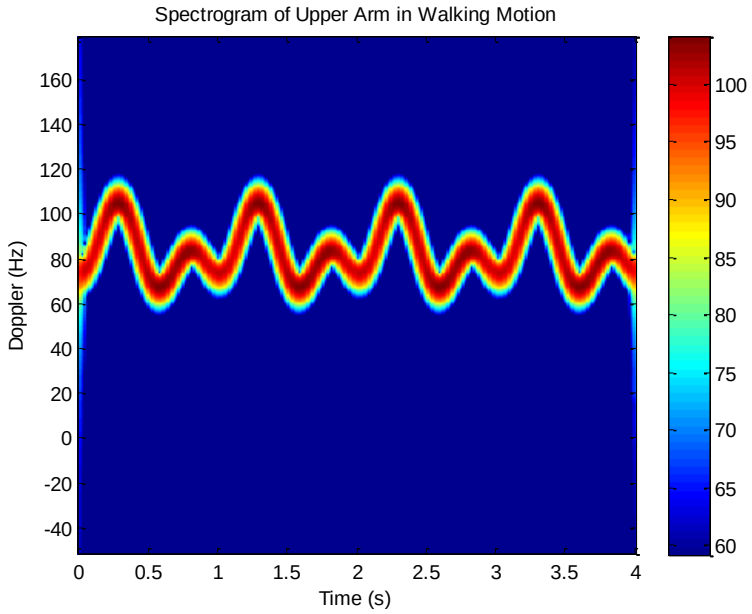

Figure 45: Spectrogram of simulated Doppler shift of upper arm

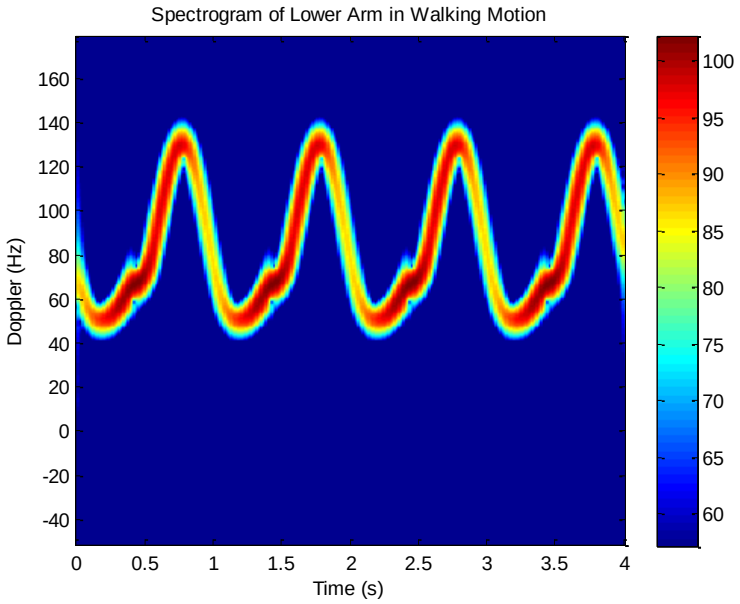

Figure 46: Spectrogram of simulated Doppler shift of lower arm

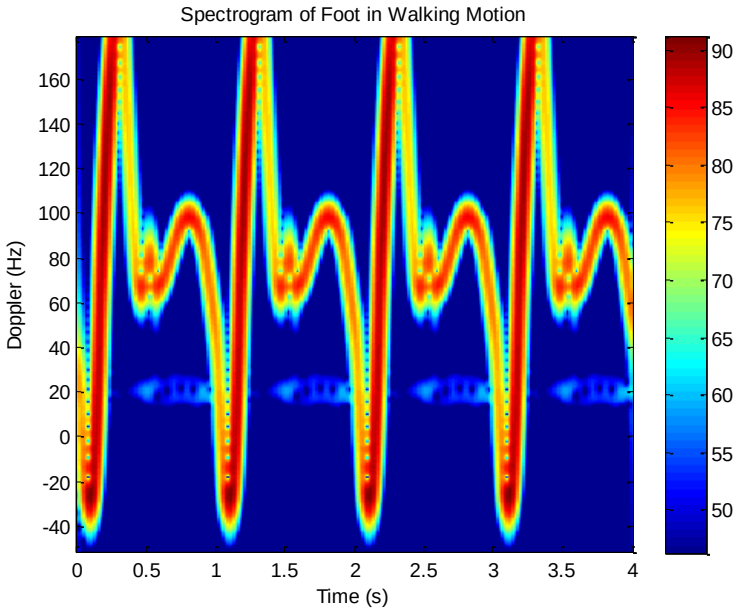

Figure 47: Spectrogram of simulated Doppler shift of foot

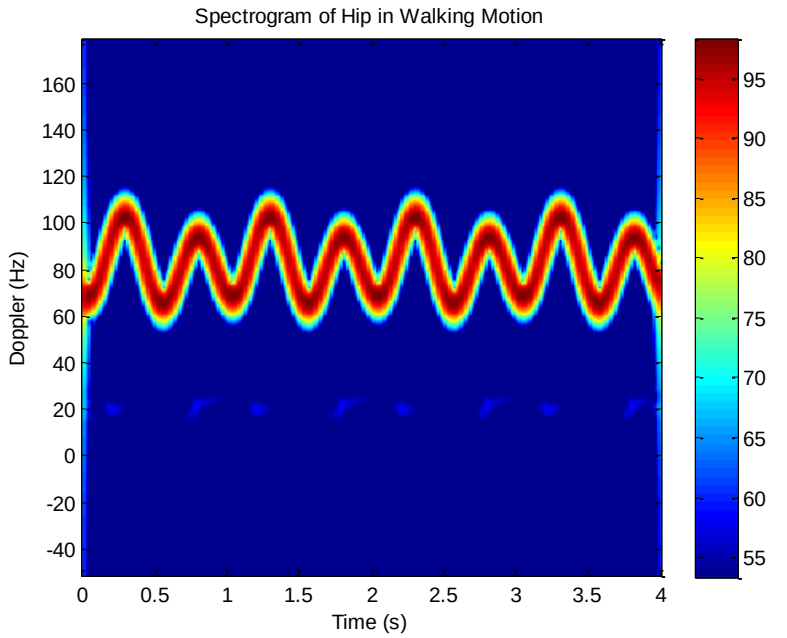

Figure 48: Spectrogram of simulated Doppler shift of hip

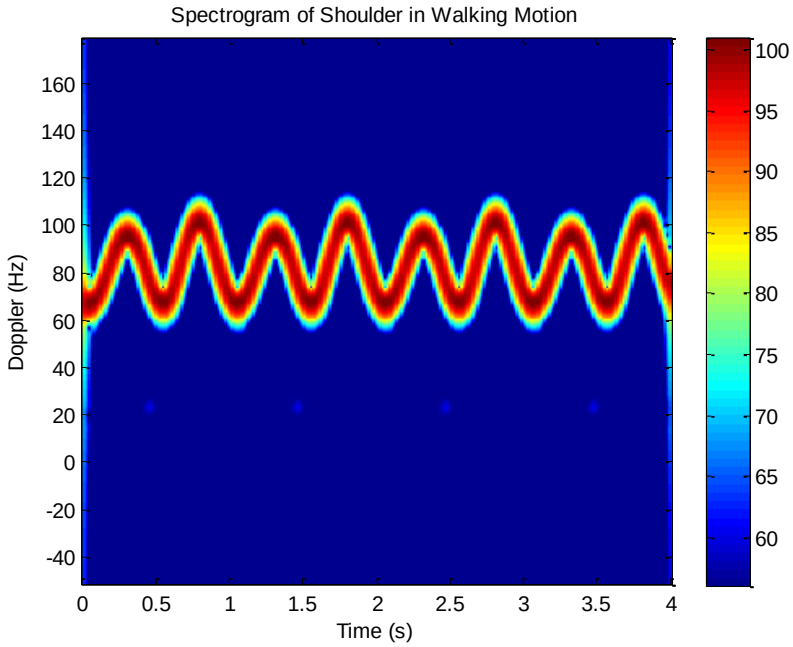

Figure 49: Spectrogram of simulated Doppler shift of shoulder

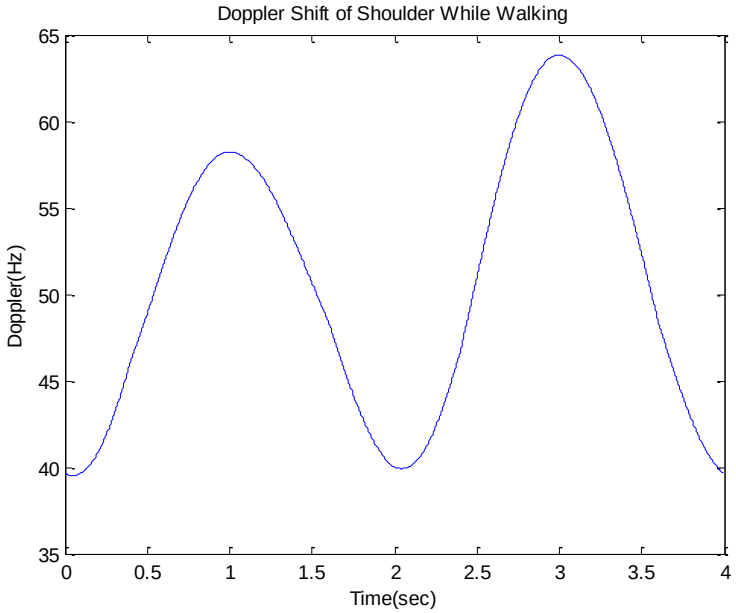

Figure 50: Simulated Doppler shift of shoulder for a single cycle of human walking

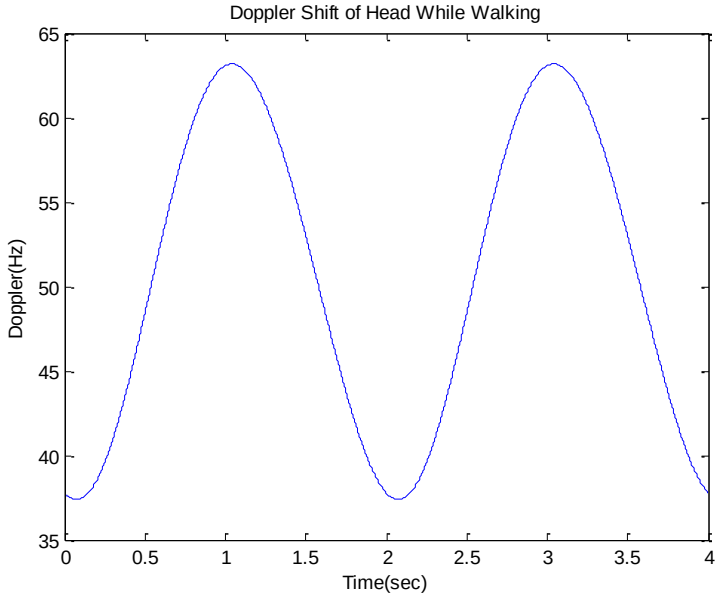

Figure 51: Simulated Doppler shift of head for a single cycle of human walking

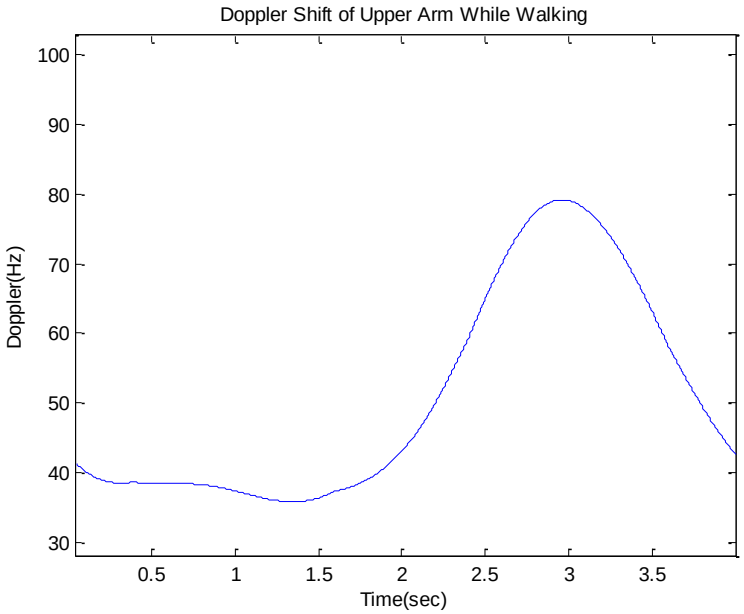

Figure 52: Simulated Doppler shift of upper arm for a single cycle of human walking

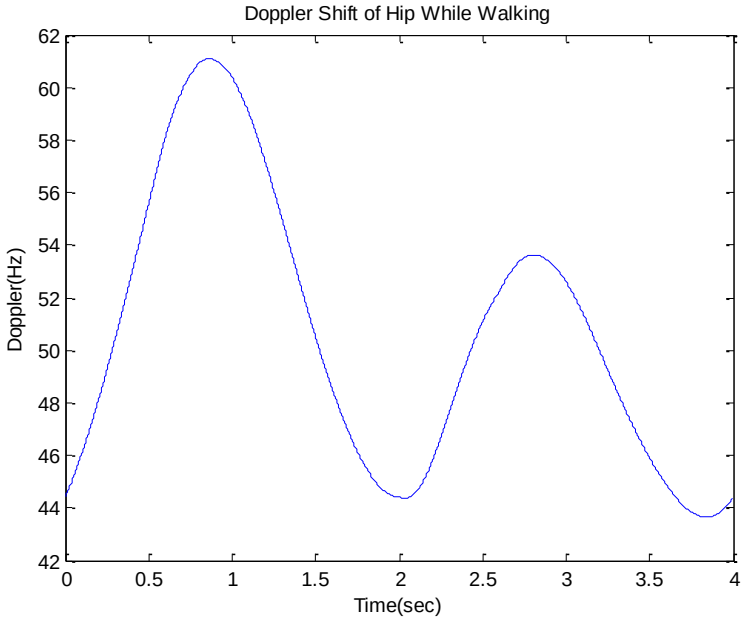

Figure 53: Simulated Doppler shift of hip for a single cycle of human walking

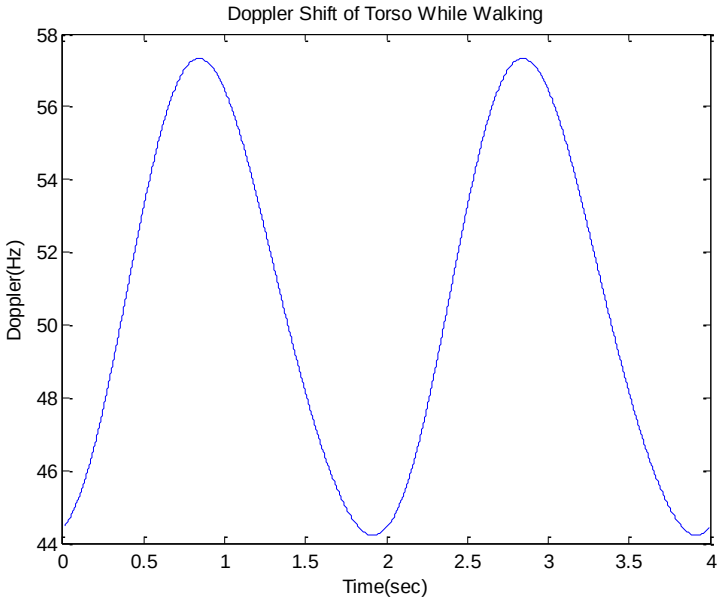

Figure 54: Simulated Doppler shift of torso for a single cycle of human walking

APPENDIX B

Appendix B presents the original and resampled raw data spectrograms of running, creeping and crawling.

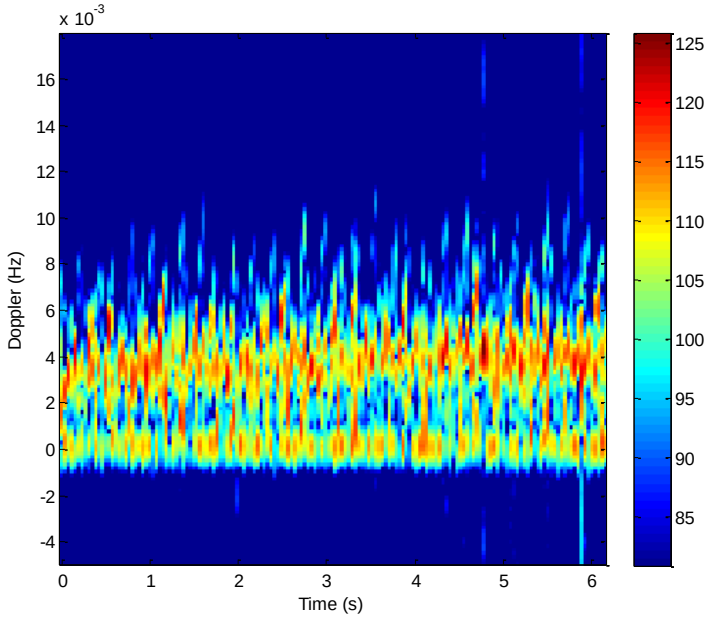

Figure 55: Original raw data spectrogram of running

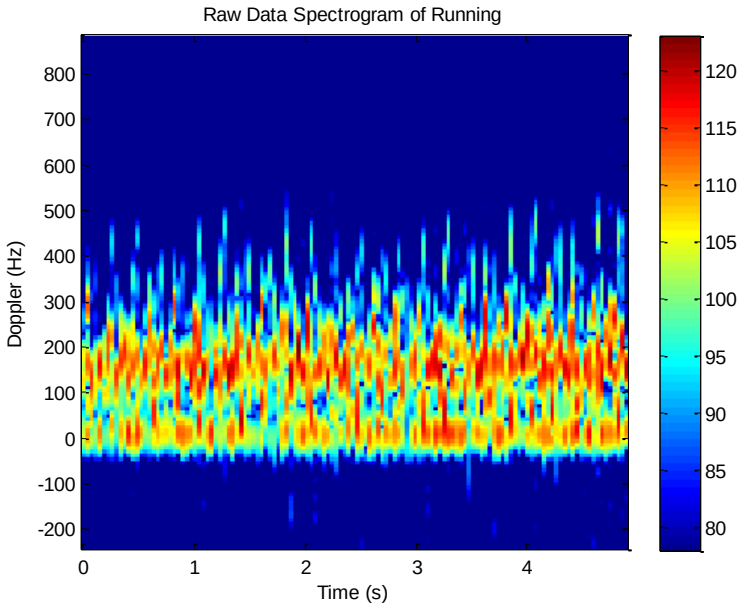

Figure 56: Resampled raw data spectrogram of running

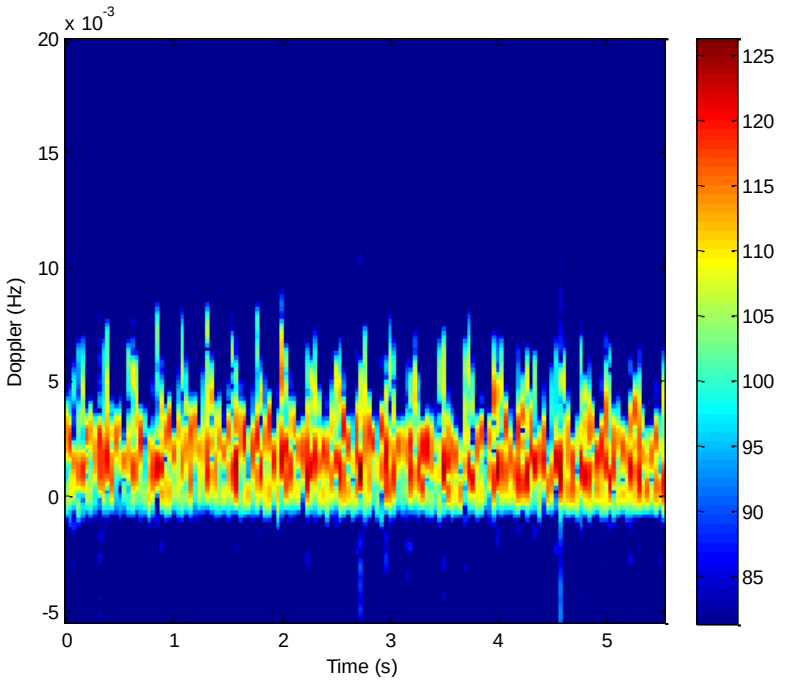

Figure 57: Original raw data spectrogram of creeping

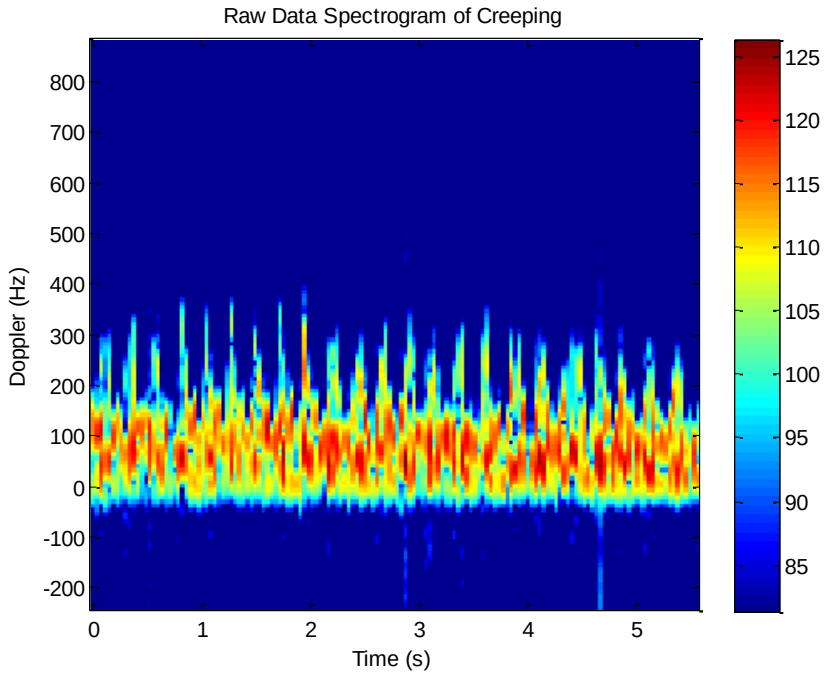

Figure 58: Resampled raw data spectrogram of creeping

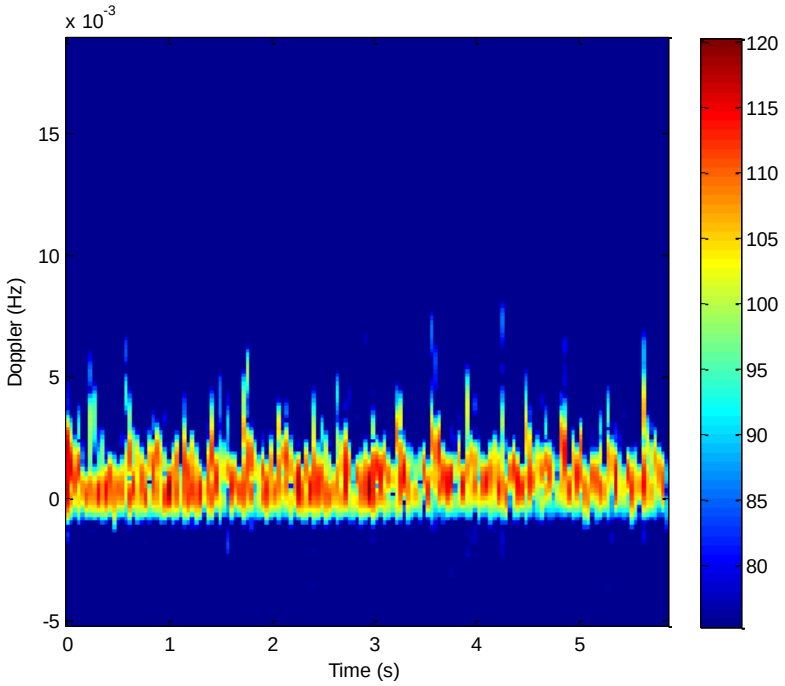

Figure 59: Original raw data spectrogram of crawling

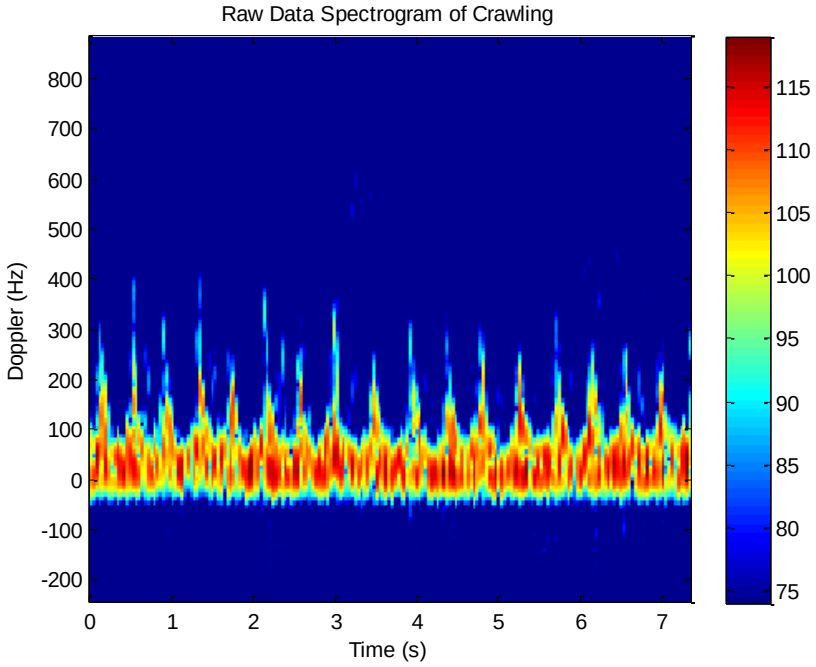

Figure 60: Resampled raw data spectrogram of crawling

APPENDIX C

Appendix C includes the time domain representation and DFT of second, third, fourth and fifth Fourier transform coefficients, time domain representation and DFT of fourth and fifth PCA vectors and original and reconstructed signal spectrograms for running, creeping and crawling.

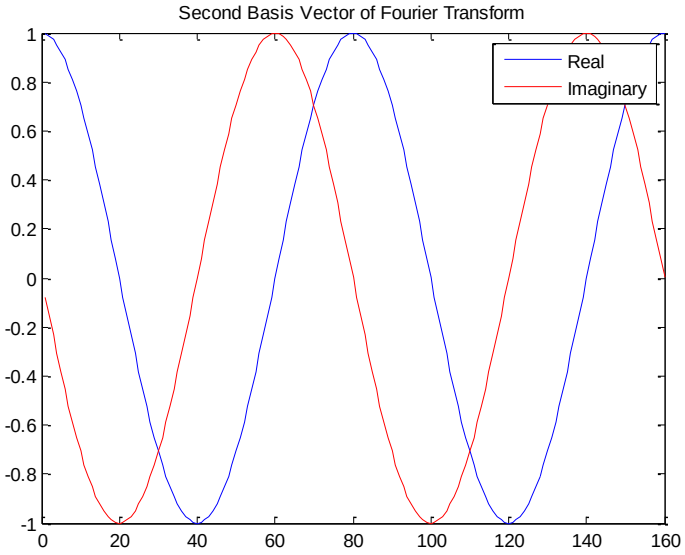

Figure 61: Second basis vector of Fourier transform

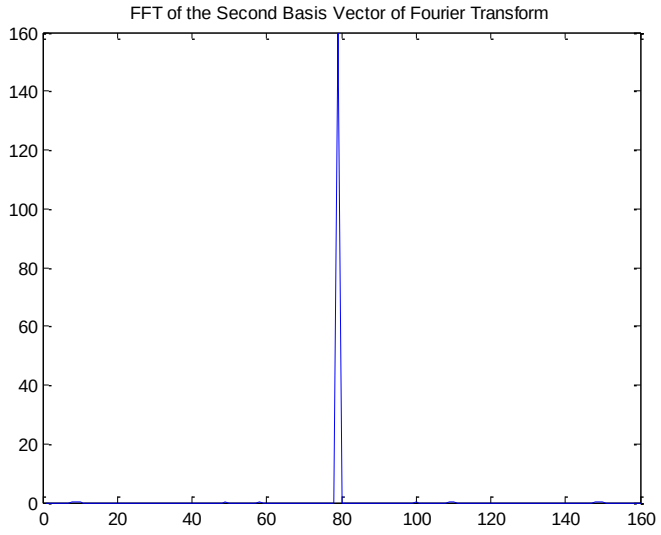

Figure 62: DFT of the second basis vector of Fourier transform

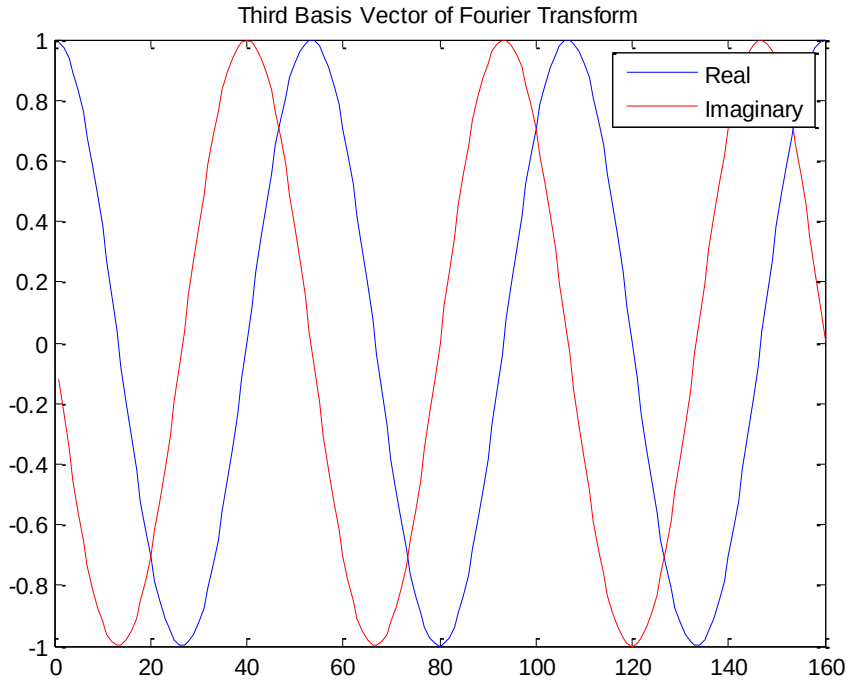

Figure 63: Third basis vector of Fourier transform

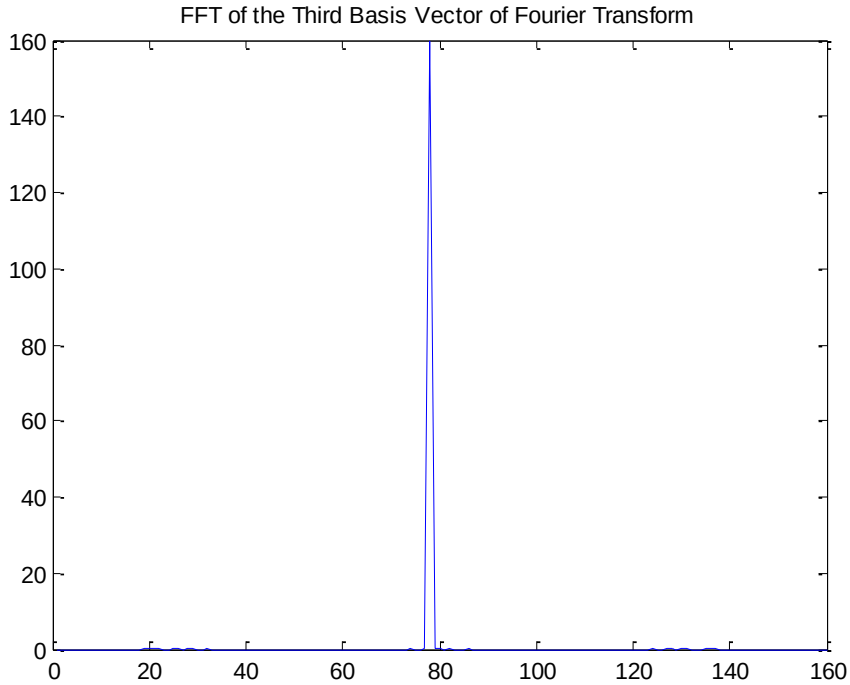

Figure 64: DFT of the third basis vector of Fourier transform

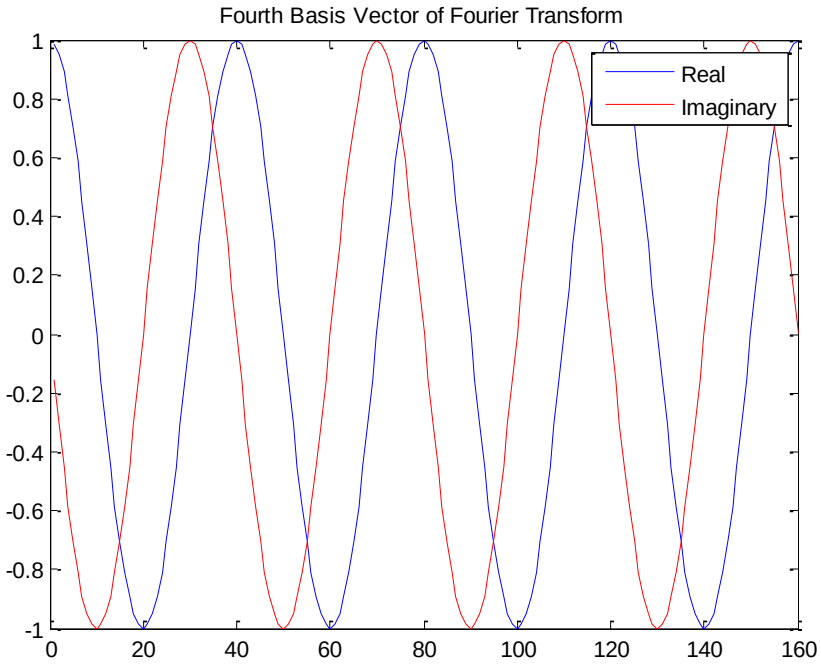

Figure 65: Fourth basis vector of Fourier transform

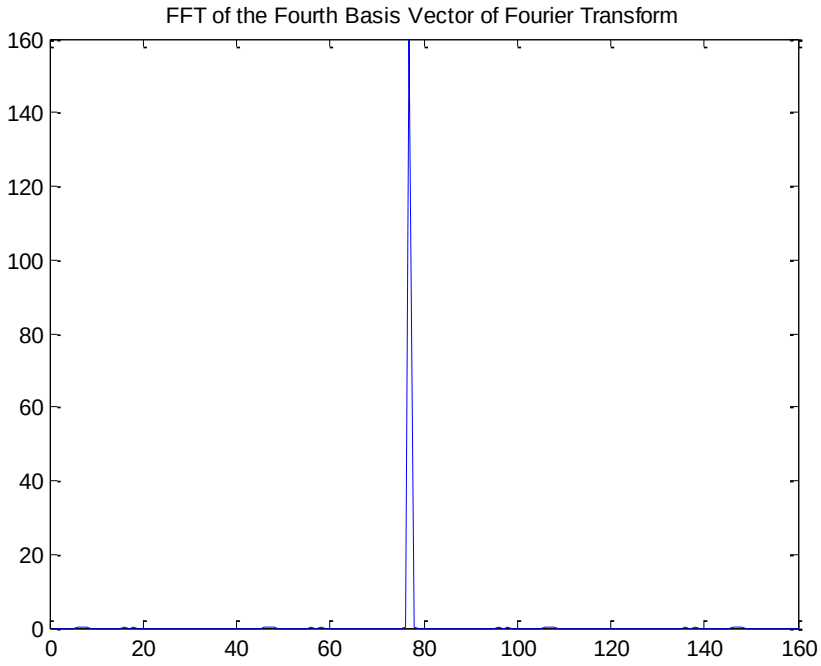

Figure 66: DFT of the fourth basis vector of Fourier transform

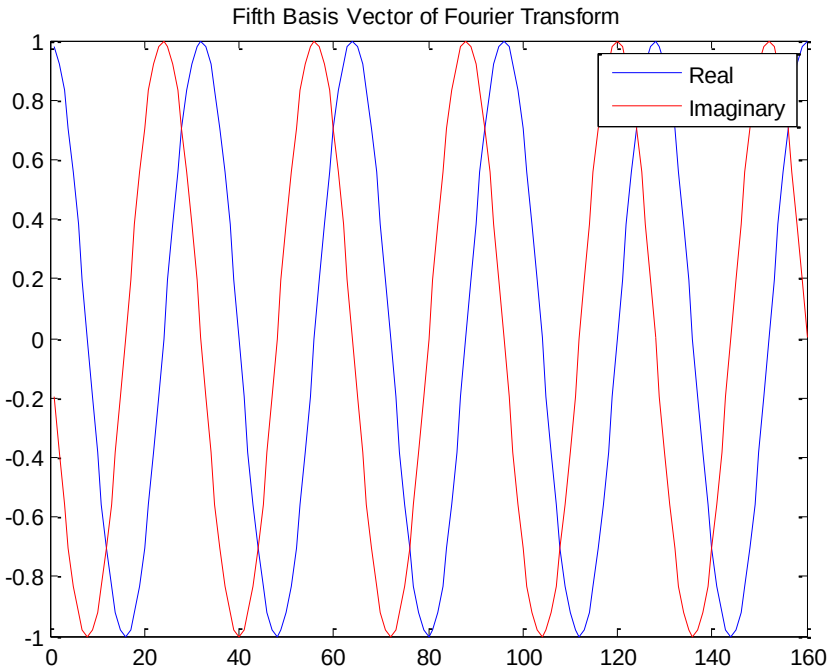

Figure 67: Fifth basis vector of Fourier transform

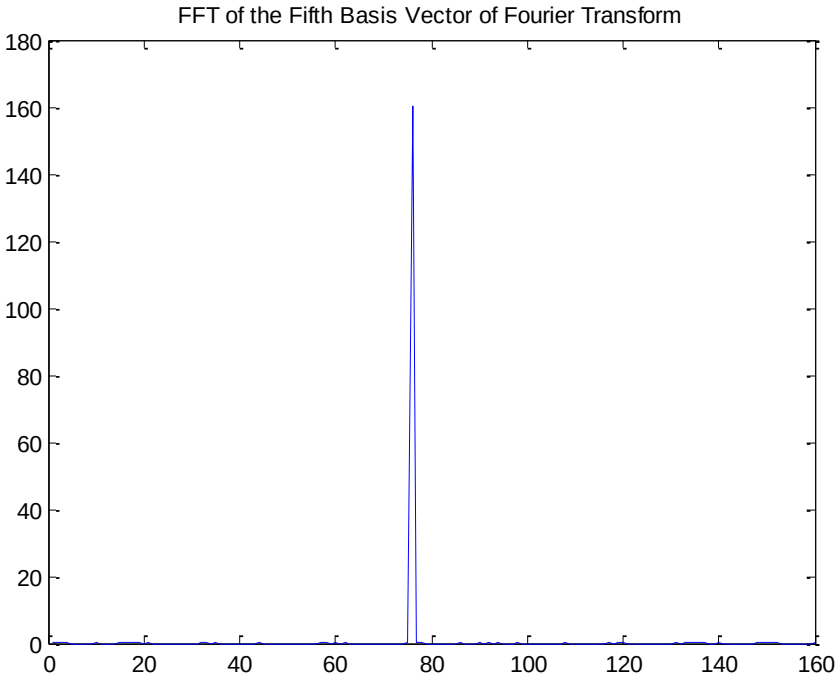

Figure 68: DFT of the fifth basis vector of Fourier transform

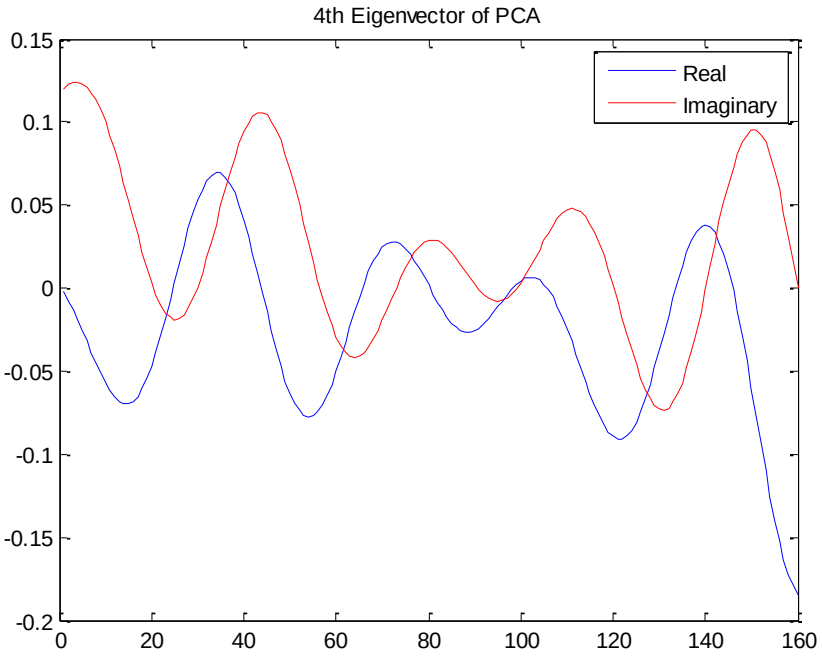

Figure 69: Fourth basis vector of principal component analysis

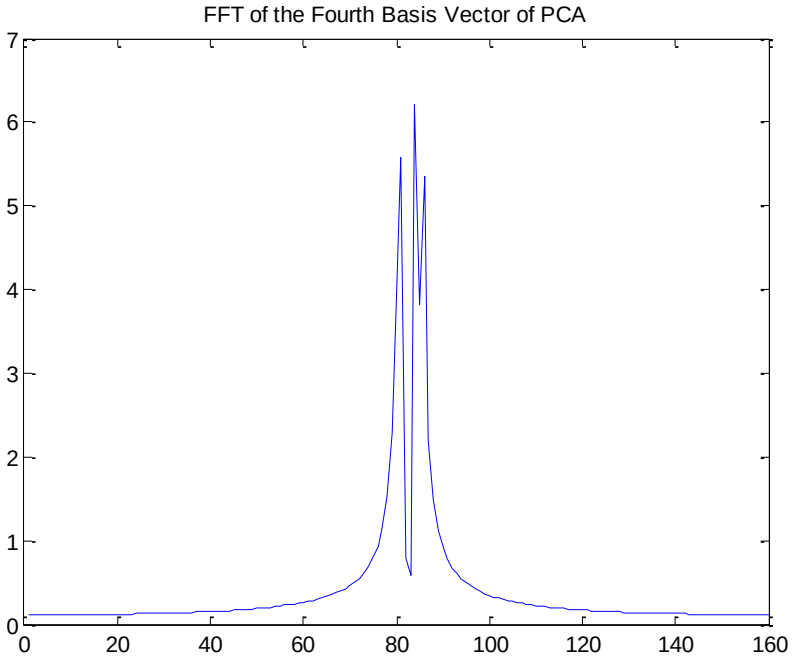

Figure 70: DFT of the fourth basis vector of principal component analysis

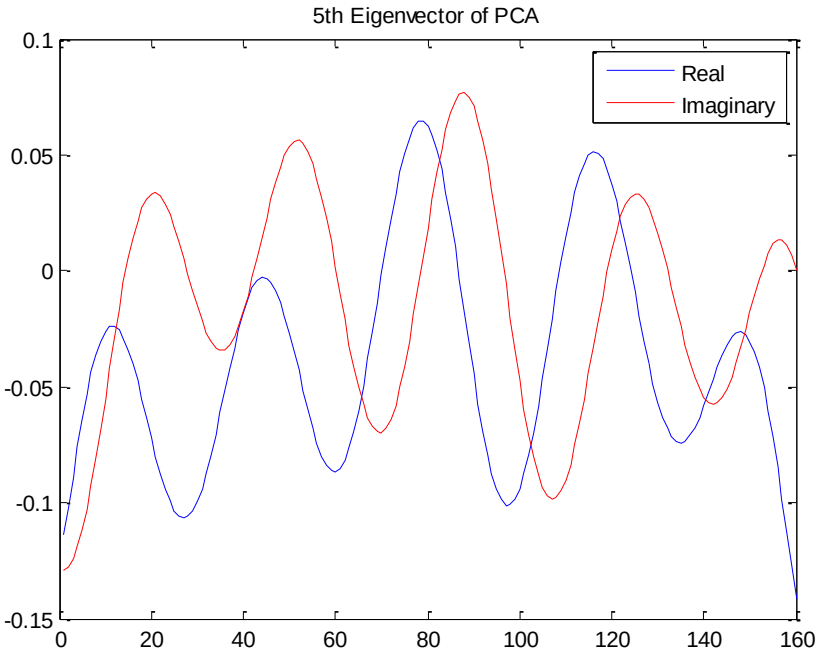

Figure 71: Fifth basis vector of principal component analysis

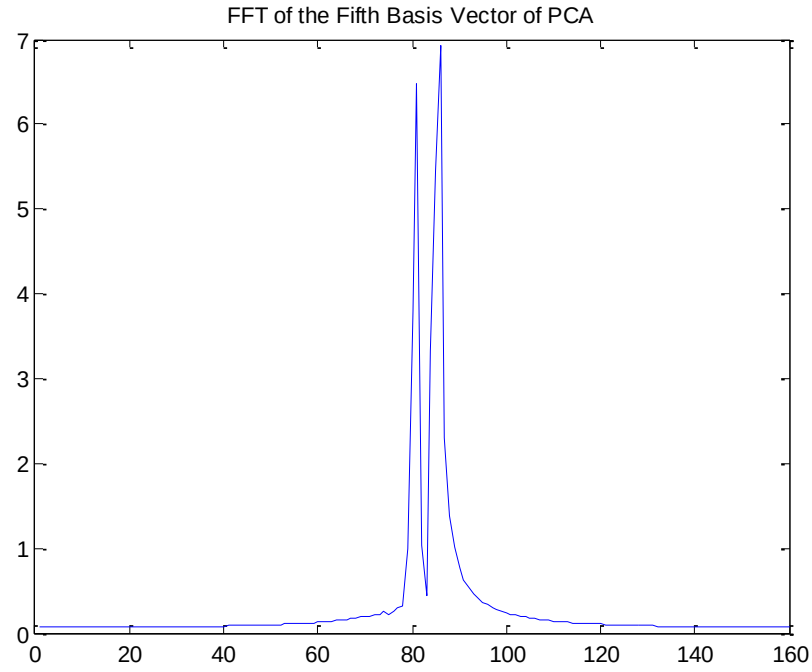

Figure 72: DFT of the fifth basis vector of principal component analysis

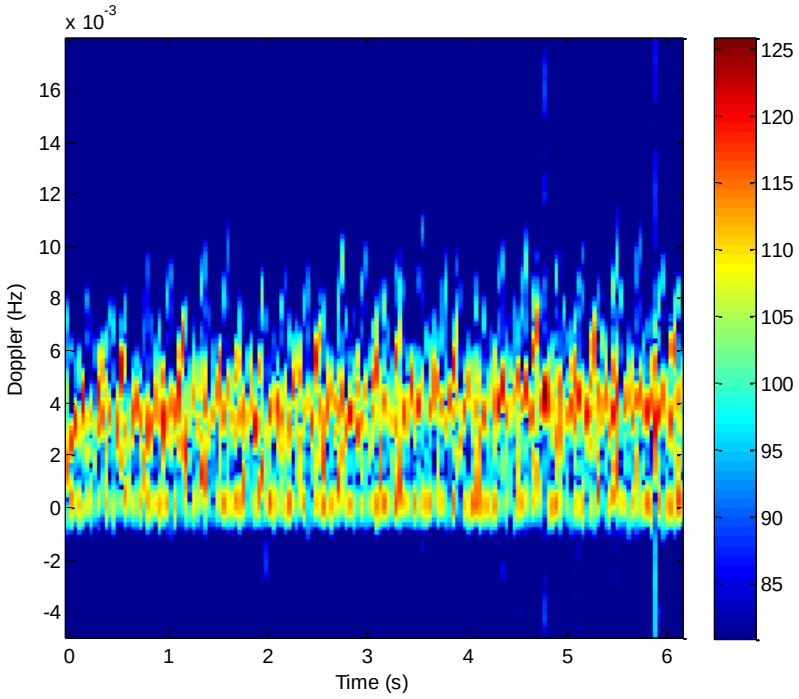

Figure 73: Original human running signal

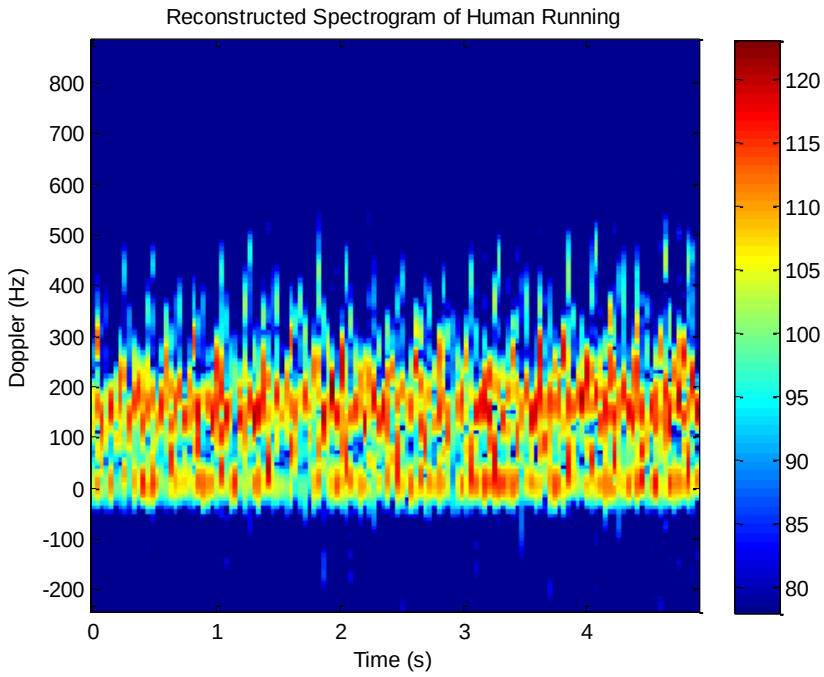

Figure 74: Reconstructed human running signal

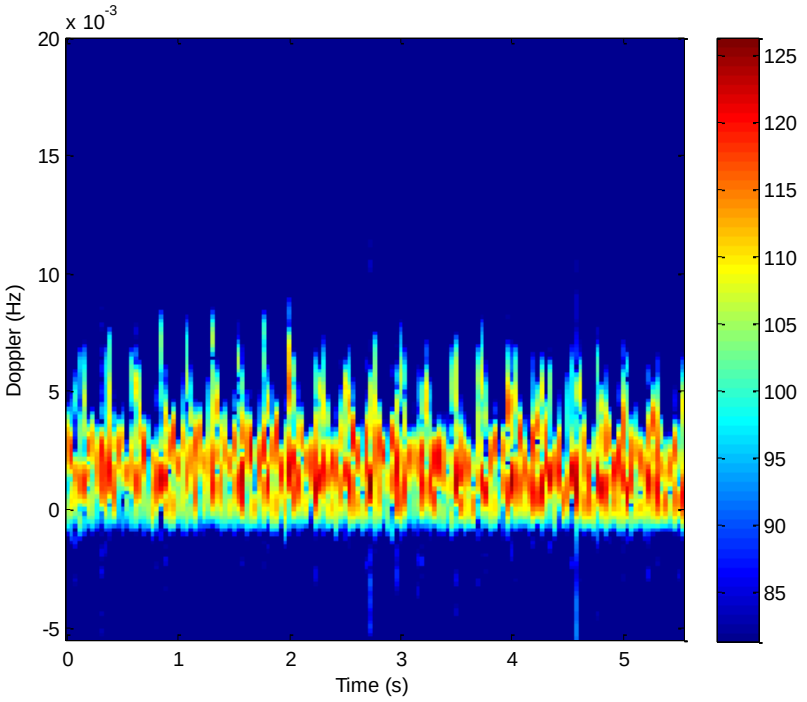

Figure 75: Original human creeping signal

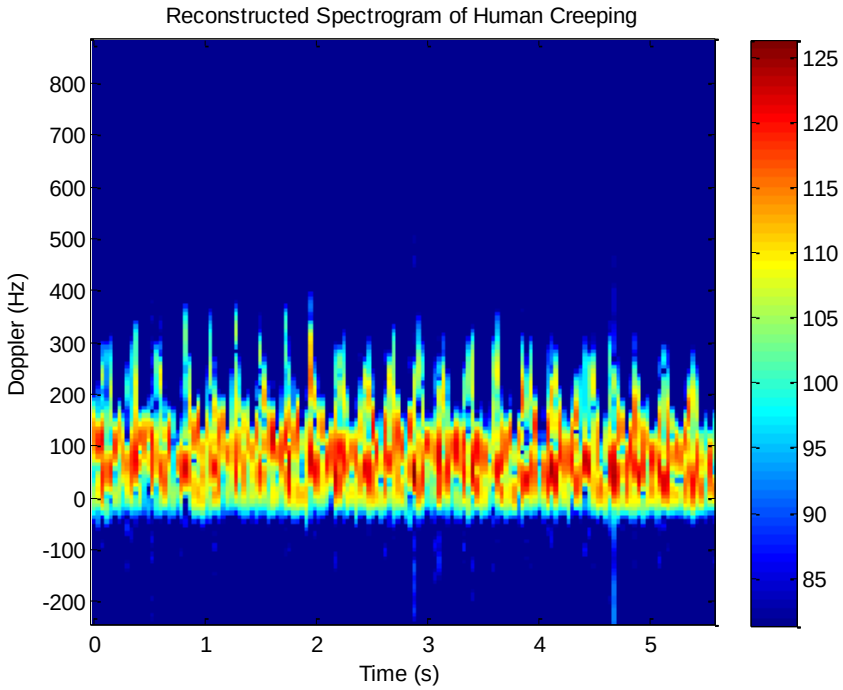

Figure 76: Reconstructed human creeping signal

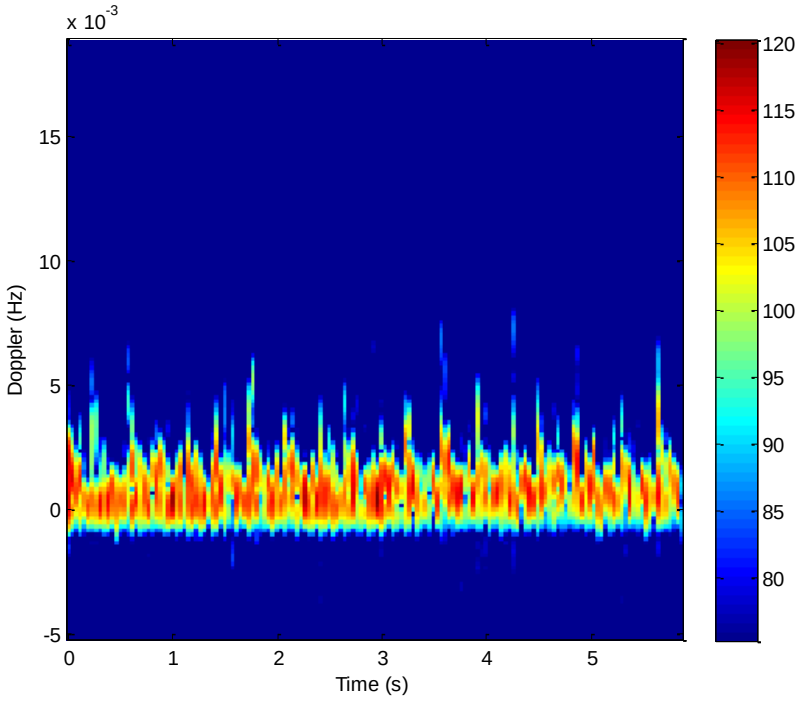

Figure 77: Original human crawling signal

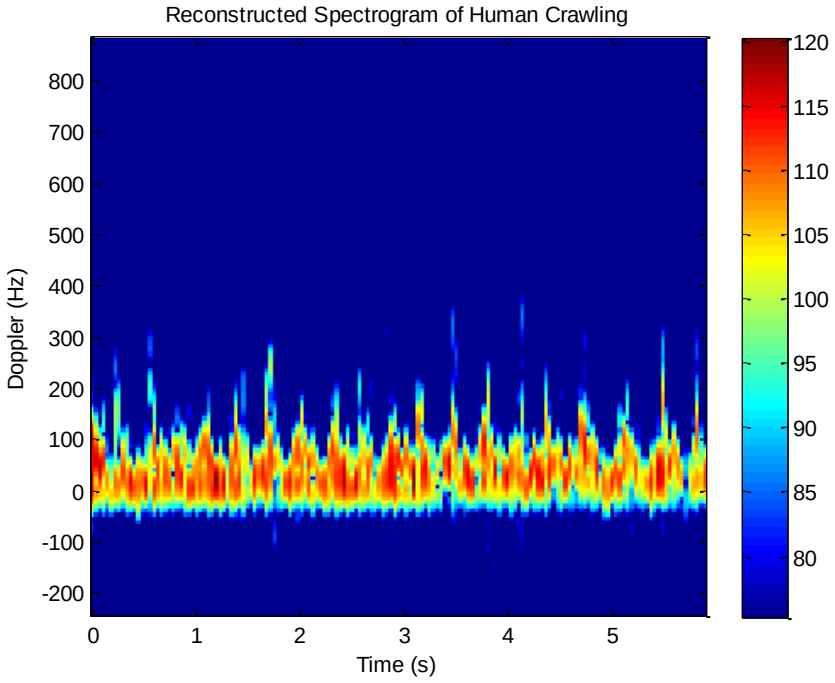

Figure 78: Reconstructed human crawling signal